博士学位論文

Mechanistic insights into tRNA thiolation catalyzed by iron-sulfur enzymes

(鉄硫黄クラスター含有酵素が触媒する tRNA 硫黄修飾の反応機構解析)

石坂優人

北海道大学大学院生命科学院

2023 年 3 月

Index

Major abbreviations

AA	Amino acid
AdetRNA	Activated tRNA: Adenylated tRNA
AF2	AlphaFold version 2
AMPPNP	ATP analog: Adenylyl-imidodiphosphate
APM	[(*N*-Acryloylamino) phenyl]mercuric chloride
APM-PAGE	APM-polyacrylamide gel electrophoresis
ATP	Adenosine triphosphate
B. subtilis	*Bacillus subtilis*
*Bsu*MnmA	MnmA from *Bacillus subtilis* strain 168
Cα RMSD	Root-mean-square deviation of the alpha carbon
CBB	Coomassie brilliant blue
$cmnm^5s^2U$	5-carboxymethylaminomethyl-2-thiouridine
CV	Column volume
DT	Reductant: Dithionite
DTT	Reductant: Dithiothreitol
E. coli	*Escherichia coli*
*Eco*MnmA	MnmA from *Escherichia coli* strain K12
*Eco*ThiI	ThiI from *Escherichia coli* strain K12
*Eco*TtcA	TtcA from *Escherichia coli* strain K12
EPR	Electron paramagnetic resonance
Fe-S	Iron-sulfur
Gm	2'-*O*-methylguanosine
H. sapiens	Human: *Homo sapiens*
HPLC	High-performance liquid chromatography
*Hsa*Ncs6	Ncs6 from *Homo sapiens*
*Hsa*Urm1	Urm1 from *Homo sapiens*
I34	Inosine at position 34 of tRNA (the wobble position)
IPTG	Isopropyl β-D-1-thiogalactopyranoside
KO	Knockout
LB	Lysogeny broth

m^5s^2U	5-methyl-2-thiouridine
m^5s^2U54	5-methyl-2-thiouridine at position 54 of tRNA
m^5U	5-methyluridine
m^5U54	5-methyluridine at position 54 of tRNA
M. maripaludis	*Methanococcus maripaludis* strain S2
MALDI-TOF MS	Matrix-assisted laser desorption/ionization-time-of-flight mass spectrometry
mcm^5s^2U	5-methoxycarbonylmethyl-2-thiouridine
mcm^5s^2U34	5-methoxycarbonylmethyl-2-thiouridine at position 34 of tRNA
MERRF	Mitochondrial disease: Myoclonic epilepsy with ragged-red fibers
mnm^5s^2U	5-methylaminomethyl-2-thiouridine
*Mma*Ncs6	Ncs6 from *Methanococcus maripaludis* strain S2
*Mma*ThiI	ThiI from *Methanococcus maripaludis* strain S2
mRNA	Messenger ribonucleic acid
ms^2A	2-methylthioadenosine
ms^2ct^6A	2-methylthio-cyclic-N^6-threonylcarbamoyladenosine
ms^2i^6A	2-methylthio-N^6-isopentenyladenosine
ms^2t^6A	2-methylthio-N^6-threonylcarbamoyladenosine
ms^2x^6A37	Modified 2-methylthioadenosine at position 37 of tRNA
MT	Mutant
mt-tRNA	Mitochondrial tRNA
Mw	Molecular weight
m/z	Mass-to-charge ratio
NiAC	Ni-affinity chromatography
OD_{600}	Absorption at 600 nm
P. horikoshii	*Pyrococcus horikoshii*
PDB	Protein Data Bank
*Pho*TtuA	TtuA from *Pyrococcus horikoshii* strain OT-3
P_i	Inorganic phosphate: PO_4^{3-}
pLDDT	Predicted local-distance difference test
PPase	Pyrophosphatase
PP_i	Pyrophosphate: $P_2O_7^{4-}$

R^2	Coefficient of determination
RT	Room temperature: 25°C
s^2C	2-thiocytidine
s^2C32	2-thiocytidine at position 32 of tRNA
s^2U	2-thiouridine
s^2U34	2-thiouridine at position 34 of tRNA (the wobble position)
s^4U	4-thiouridine
s^4U8	4-thiouridine at position 8 of tRNA
S. cerevisiae	Budding yeast: *Saccharomyces cerevisiae*
SAM	*S*-adenosyl methionine
SD	Standard deviation
SDS	Sodium dodecyl sulfate
SDS-PAGE	Sodium dodecyl sulfate-polyacrylamide gel electrophoresis
SEC	Size exclusion chromatography
T. thermophilus	*Thermus thermophilus*
Tm	Melting temperature
*Tma*ThiI	ThiI from *Thermotoga maritima* strain MSB8
tRNA	Transfer ribonucleic acid
$tRNA^{AA(NNN)}$	tRNA that carry AA with anticodon of NNN
*Tth*MnmA	MnmA from *Thermus thermophilus* strain HB27
*Tth*TtuA	TtuA from *Thermus thermophilus* strain HB27
TtuB-COOH	Non-sulfur donor TtuB with carboxyl group at the C-terminus
TtuB-COSH	Sulfur donor TtuB with thiocarboxyl group at the C-terminus
UV-Vis	Ultra violet and visible light
UV280	Ultra violet at wavelength of 280 nm
v/v	Volume/Volume
WT	Wild type
xm^5s^2U34	Modified 2-thiouridine at position 34 of tRNA (the wobble position)
τm^5s^2U	5-taurinomethyl-2-thiouridine
Ψ	Pseudouridine

*Abbreviations of standard amino acids and bases comply with international rules.

Abstract

tRNA transfers amino acids to ribosomes to translate genetic information into proteins. However, immature tRNA does not function immediately after transcription. Hence, tRNA undergoes post-transcriptional processes such as base/ribose modifications for maturation. To date, more than 110 base/ribose modifications have been discovered in tRNA. Particularly, thiolation (sulfur modification) is a universal and essential enzymatic reaction that improves the thermal stability and translational accuracy of tRNA.

My target is thiolation at position 54 of tRNA (5-methyl-2-thiouridine, m^5s^2U54), which is essential for thermophiles to survive above 70℃. m^5s^2U54 modification is catalyzed by 2-thiouridine synthetase TtuA with sulfur donor protein TtuB in *Thermus thermophilus*. Our recent structural analysis of the TtuA-TtuB complex showed that an oxygen-sensitive [4Fe-4S] cluster is required for the enzymatic activity of TtuA. Interestingly, a non-cysteine coordinated Fe (the unique Fe) of the [4Fe-4S] bound to the C-terminus of TtuB. This structure suggested that the unique Fe in TtuA relates to the sulfur transition from TtuB to tRNA, which is a novel reaction mechanism of m^5s^2U54 biosynthesis involving the unique Fe. On the other hand, TtuA homolog enzyme Ncs6 catalyzes thiolation at position 34 of tRNA (mcm^5s^2U34) with sulfur donor Urm1, which is similar to TtuA. However, a spectroscopic study indicated that Ncs6 contains [3Fe-4S], whereas crystallography supported [4Fe-4S]. Therefore, it was unclear whether the active form of tRNA-thiolation enzymes only require [4Fe-4S] or both [4Fe-4S] and [3Fe-4S].

In this study, I analyzed the structural change of Fe-S clusters in TtuA in time-course and evaluate their enzymatic activity. As a result, [3Fe-4S] spontaneously transformed into [4Fe-4S] even without the additional iron source, and the activity of TtuA gradually recovered corresponding to an increase in [4Fe-4S]. I also revealed that [3Fe-4S]-TtuA cannot bind to the C-terminus of TtuB, indicating that only [4Fe-4S]-TtuA is an active form. Furthermore, I found that TtuB does not release sulfur until tRNA is activated by ATP, and identified the critical residues of TtuA. Considering the similarity, I proposed that [4Fe-4S] is generally an active form in tRNA-thiolation enzymes and the detailed tRNA-thiolation mechanism catalyzed by TtuA. These findings showed that the time-course analysis of the structure and activity under strictly anaerobic conditions is necessary to elucidate the reaction mechanism of enzymes containing Fe-S clusters.

Chapter 1. Introduction

1-1. Post-transcriptional modifications of RNA

In protein biosynthesis, various ribonucleic acids (RNA) are involved such as transfer RNA (tRNA), messenger RNA (mRNA), and ribosomal RNA (rRNA). These RNAs do not function immediately after transcription *in vivo*. Thus, immature RNA undergoes enzymatic reactions called post-transcriptional processes including splicing and modifications for maturation. Among these processes, more than 150 kinds of base/ribose modifications have been discovered in RNA, and these modifications are the most diverse in tRNA[1]. Recently, the relationship between abnormalities in tRNA modifications and diseases has been reported[2,3]. Therefore, it is significant to understand the molecular mechanisms of tRNA maturation.

1-2. tRNA modifications

During translation, tRNA transfers amino acids to ribosomes according to their anticodon for protein biosynthesis. Immature tRNA undergoes post-transcriptional processes such as splicing, CCA addition, ribose/base modification, and aminoacylation (Fig. 1-1)[4]. For the ribose/base modification, more than 110 kinds of tRNA modifications have been identified such as methylation, acetylation, and thiolation[1]. In particular, diverse base modifications are found at position 1 of tRNA anticodon (position 3 of the codon), and loss of these modifications reduces the translation rate, causing ribosomal arrest and protein misfolding/aggregation[5].

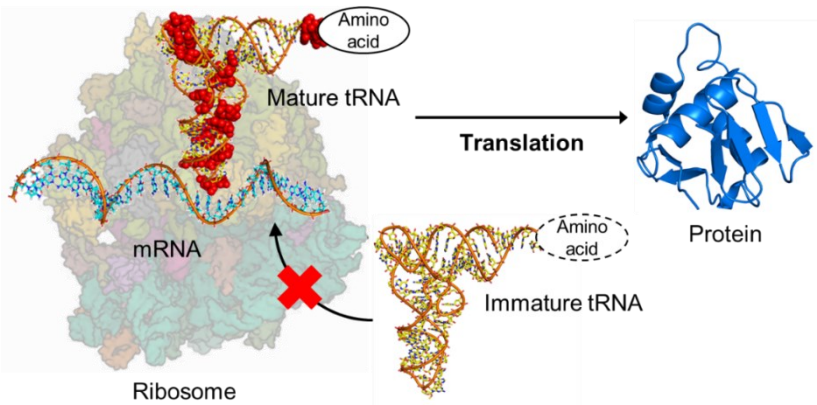

Fig. 1-1 The role of tRNA modifications in protein synthesis.
Red balls show modification sites on tRNA.

1-3. tRNA thiolation (sulfur modification)

tRNA thiolations are enzymatic modifications that replace the oxygen atom with a sulfur atom in the specific site in tRNA, which have been roughly classified into four types: 2-thiouridine (s^2U), 4-thiouridine (s^4U), 2-thiocytidine (s^2C), and 2-methylthioadenosine (ms^2A)[6]. These modifications are found in a specific position of tRNA and play universal roles in bacteria, archaea, and eukaryotes (Fig. 1-2, 1-3). tRNA thiolation improves the thermal stability of tRNA[7,8], translational speed and accuracy[9–11], and is responsible for near-UV sensing[12,13] depending on its modification site.

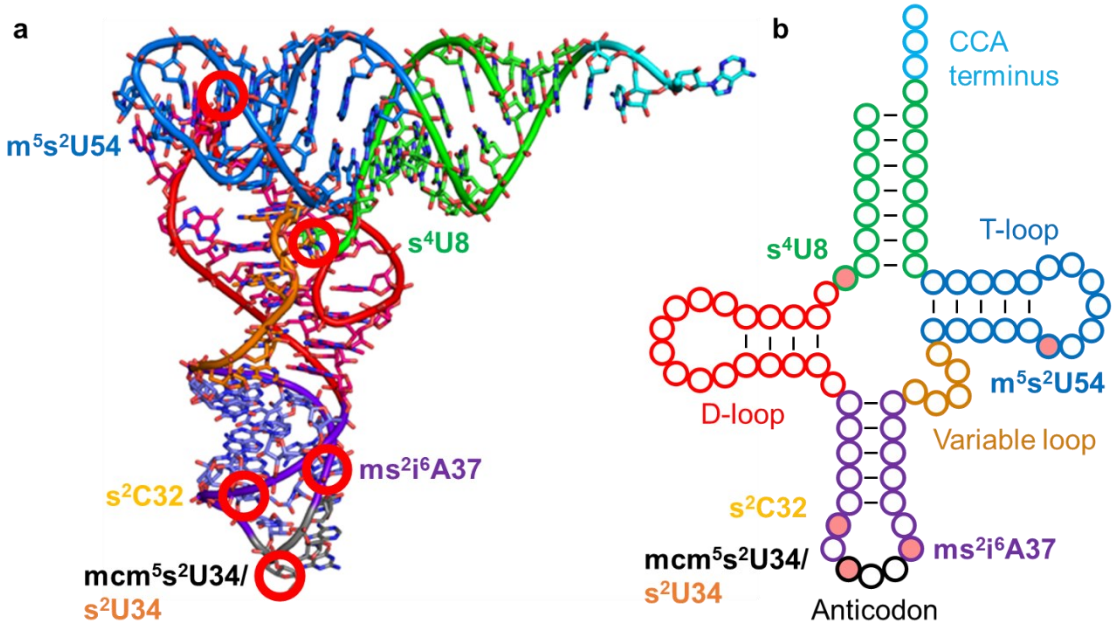

Fig. 1-2 Structures of tRNA.

(**a**) L-shaped 3D structure of tRNA (PDB ID: 1EHZ). The thiolation sites are indicated with red circles and the names of typical tRNA thiolation; 5-methoxycarbonylmethyl-2-thiouridine (mcm^5s^2U), 2-methylthio-N^6-isopentenyladenosine (ms^2i^6A), and 5-methyl-2-thiouridine (m^5s^2U). The numbers following the name of the thiolated base are the base number counted from the 5' end of tRNA. (**b**) The clover-leaf model of the 2D structure of tRNA. The length of the variable loop varies depending on the species and type of tRNA. The color code is the same as the 3D structure.

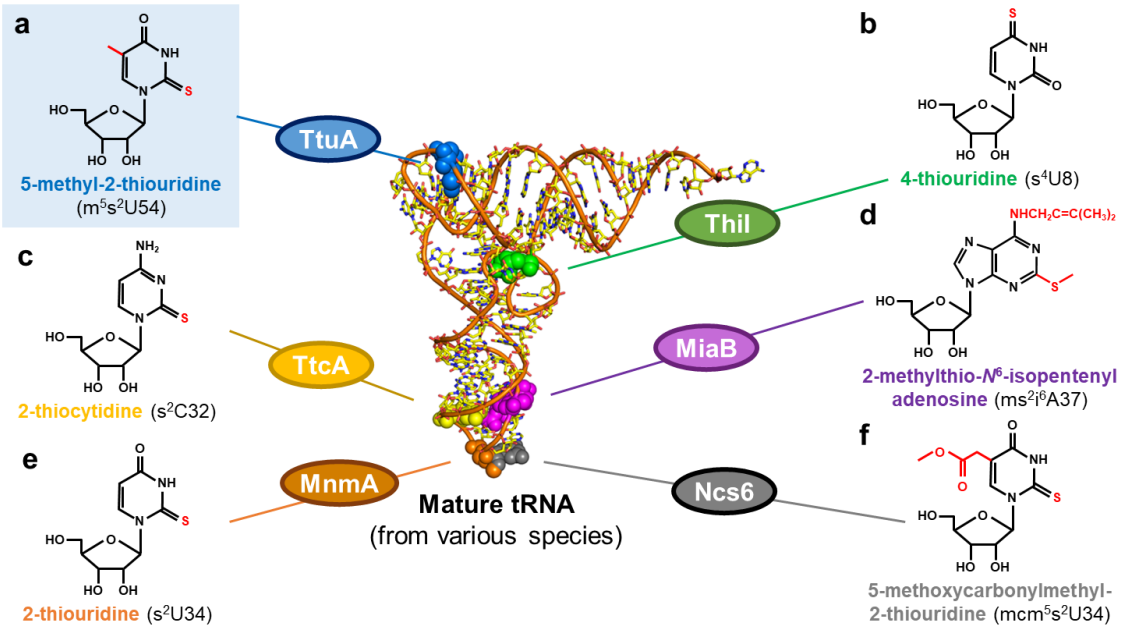

Fig. 1-3 Typical tRNA thiolations at the specific sites of tRNA, and their enzymes. TtuA, ThiI, TtcA, MiaB, MnmA, and Ncs6 catalyze m^5s^2U54, s^4U8, s^2C32, ms^2i^6A37, s^2U34, and mcm^5s^2U34 synthesis, respectively. My target, m^5s^2U54 is highlighted in blue.

1-3-1. Thermal stability of tRNA

Thermophilic prokaryotes have 5-methyl-2-thiouridine modifications at position 54 of tRNA (m^5s^2U54, s^2T54). Thermal adaption using m^5s^2U54 is found in a wide variety of substrate tRNAs[14], unlike other tRNA thiolations. Since the longer van der Waals radius of sulfur (1.80 Å) than that of oxygen (1.52 Å)[15], steric repulsion between a 2-thiocarbonyl group and a 2'-hydroxyl group of m^5s^2U54 induces the conformational change of the ribose from the unstable C2'-*endo* to the stable C3'-*endo* (Fig. 1-4a)[16]. This conformational change triggers the formation of base pairing between m^5s^2U54 and 1-methyladenine at position 58 of tRNA (m^1A58), which stacks between base pairs G53-C61 and pseudouridine (Ψ55)-2'-*O*-methylguanosine (Gm18) (Fig.1-4b)[16,17]. The local stabilization around m^5s^2U54 contributes interloop base pairs across T-loop (Ψ55) and D-loop (Gm18), resulting in high thermostability of tRNA. The melting temperature (Tm) of $tRNA^{Met}$ with m^5s^2U54 modification is 89°C[14], allowing thermophiles to survive in high-temperature environments of more than 80°C[8]. Note that m^5s^2U54 synthesis is catalyzed by 2-thiouridine synthetase (TtuA)[18].

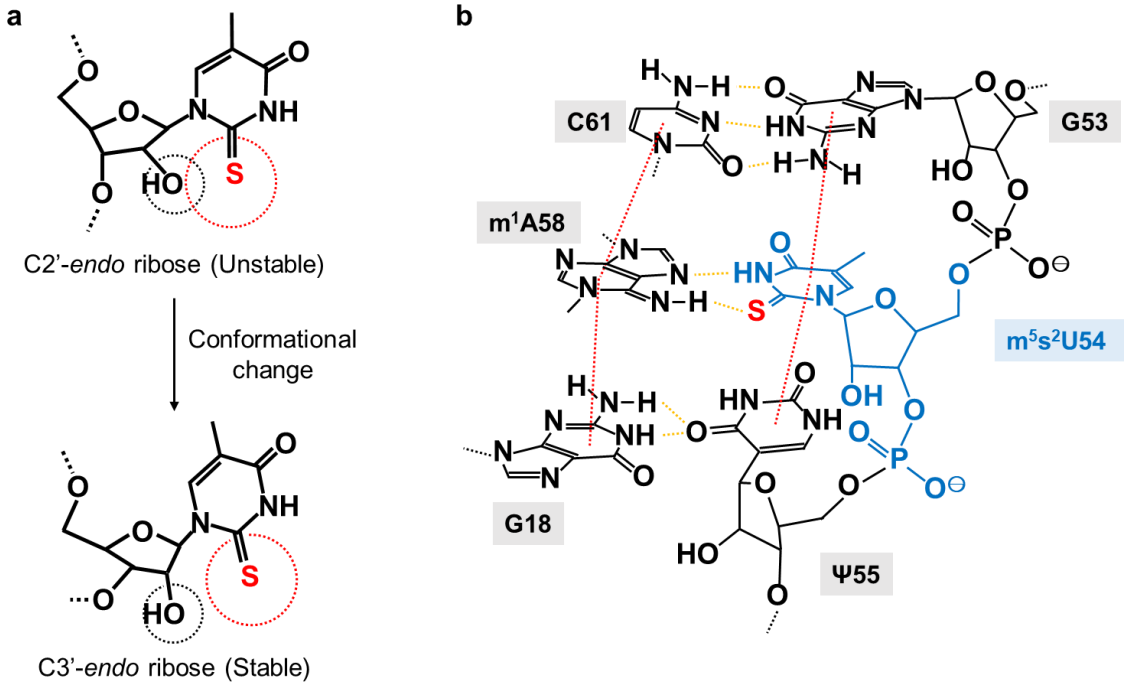

Fig. 1-4 Molecular mechanism of thermal adaption regulated by 5-methyl-2-thiouridine at position 54 of tRNA (m^5s^2U54)[16].

(**a**) Conformational change of the ribose in m^5s^2U54. The red and black dotted lines represent the van der Waals surface of the sulfur and oxygen atoms, respectively. (**b**) Base pairing across the T and D-loops of thermophilic tRNA. The dashed red and yellow lines represent π-π stacking interactions and hydrogen bonds, respectively. m^5s^2U54 is indicated in blue.

1-3-2. Translational fidelity regulated by thiolation at the wobble position

Accurate translation from genetic information into amino acids is critical for all organisms. To ensure this validation, modified 2-thiouridines (xm^5s^2U34) are universally found at position 34 (the wobble position) of $tRNA^{Glu}$, $tRNA^{Gln}$, and $tRNA^{Lys}$ such as 5-methylaminomethyl-2-thiouridine (mnm^5s^2U) or 5-carboxymethylaminomethyl-2-thiouridine ($cmnm^5s^2U$) in bacterial tRNA[19], 5-methoxycarbonylmethyl-2-thiouridine (mcm^5s^2U) in eukaryotic cytosolic tRNA[2], and 5-taurinomethyl-2-thiouridine (τm^5s^2U) or 5-carboxymethylaminomethyl-2-thiouridine ($cmnm^5s^2U$) in mitochondrial tRNA (Fig. 1-5)[20]. xm^5U34 alone facilitates base pairing between the oxygen atom at position 2 of the wobble uridine and mRNA guanosine as well as mRNA adenosine (Fig. 1-6a)[21].

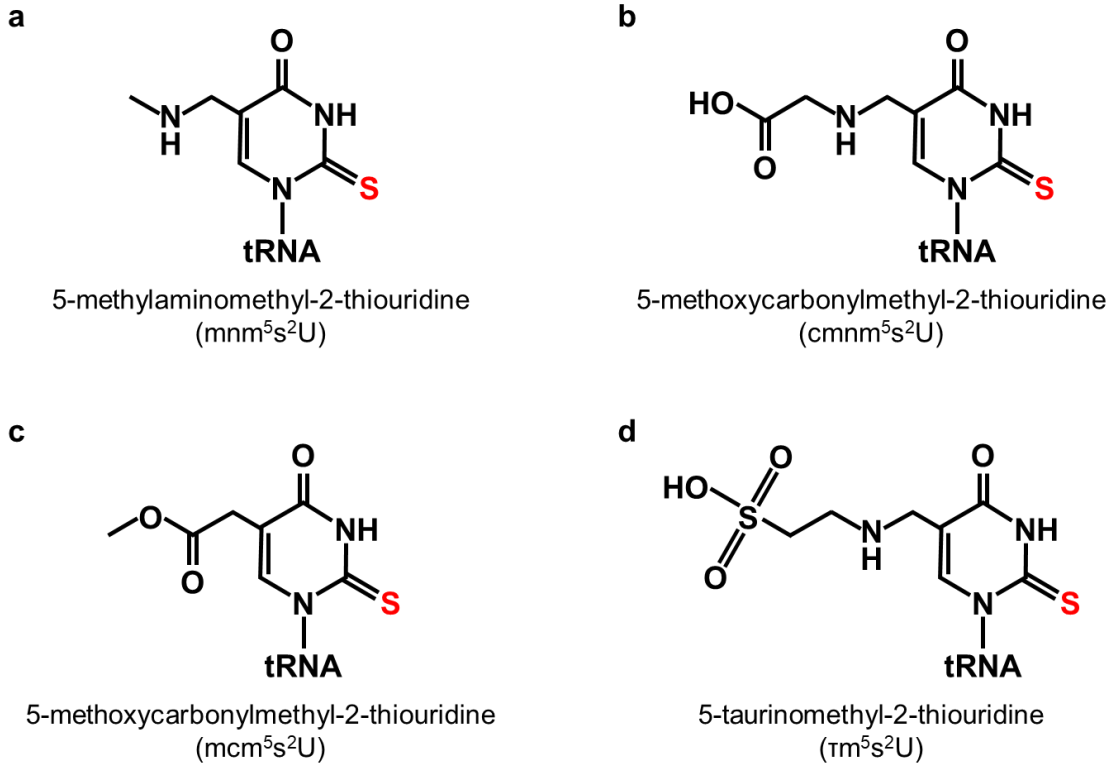

Fig. 1-5 Hypermodified uridines at position 34 of tRNA

(**a**) 5-methylaminomethyl-2-thiouridine. (**b**) 5-methoxycarbonylmethyl-2-thiouridine. (**c**) 5-methoxycarbonylmethyl-2-thiouridine. (**d**) 5-taurinomethyl-2-thiouridine.

On the other hand, xm^5s^2U34 promotes the formation of C3'-*endo* ribose due to steric effects similar to m^5s^2U54, which stabilizes base pairing with purine bases in mRNA[21]. Furthermore, the electronegativity of sulfur (2.58) is lower than that of oxygen (3.44)[22], making hydrogen bonds between sulfur and hydrogen weaker than those between oxygen and hydrogen[23]. Thus, xm^5s^2U34 interacts more weakly with guanosine (Fig. 1-6b) than with adenosine in the third letter of the codon (Fig. 1-6c)[21]. As a result, $tRNA^{Glu(UUC)}$, $tRNA^{Gln(UUG)}$, and $tRNA^{Lys(UUU)}$ with xm^5s^2U34 modification preferentially translate Glu (GAA), Gln (CCA), and Lys (AAA), respectively.

Notably, it has been reported that the abnormalities in human tRNA thiolations are related to various diseases. For example, defects in the τm^5s^2U34 modification in mitochondrial $tRNA^{Lys}$ (mt-$tRNA^{Lys}$) are associated with an incurable mitochondrial diseases (MERRF) with muscle weakness and stroke-like symptoms[24,25]. On the other

hand, excessive mcm^{5}s^{2}U34 modification of cytoplasmic tRNAs also promotes the translation of hypoxia-induced factor 1α (HIF1α) mRNA and glycolysis in melanoma cells[2,26]. The mcm^{5}s^{2}U34 synthetase complex Ncs6-Ncs2 (also known as Ctu1 and Ctu2 in eukaryotes) are overexpressed in breast cancer, which sustains metastasis[27,28]. Therefore, understanding the molecular mechanisms of tRNA thiolation is important for biology and medicine.

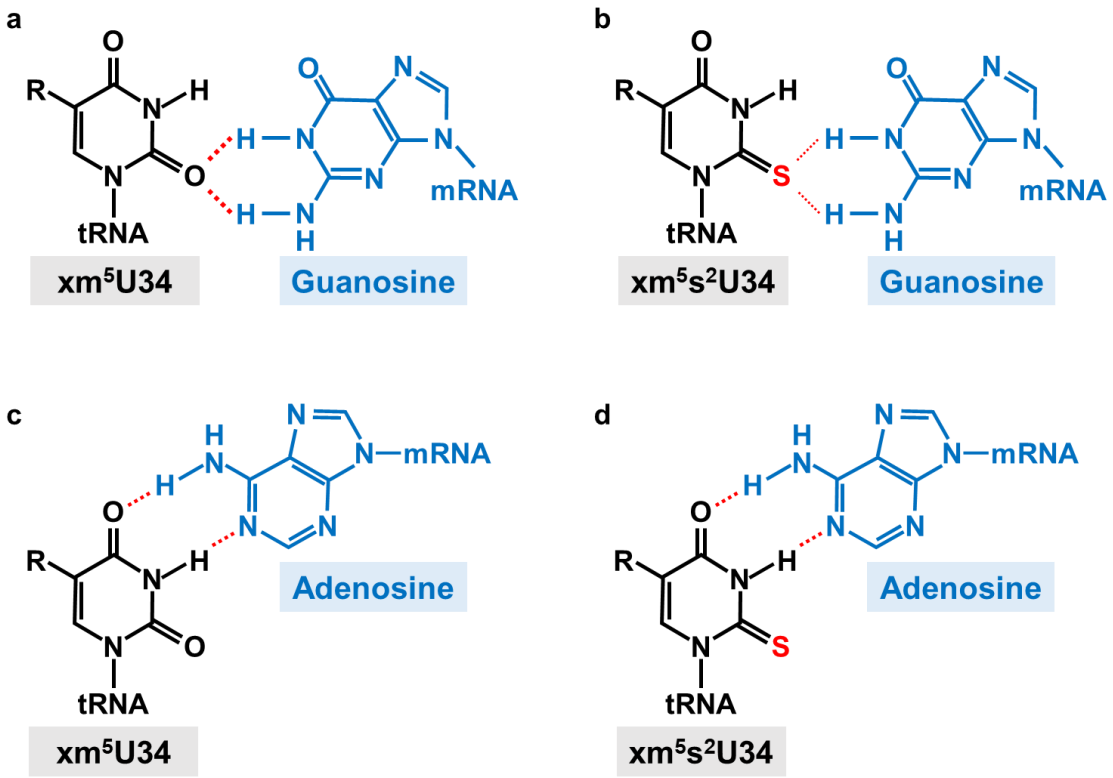

Fig. 1-6 Molecular mechanism of translational fidelity of tRNA with thiolated wobble uridine (xm^{5}s^{2}U34).

Wobble base pairing between (**a**) xm^{5}U34 or (**b**) xm^{5}s^{2}U34 of tRNA and mRNA guanosine. The red dotted lines in the non-thiolated state indicate stronger hydrogen bonds than those in the thiolated state. Base pairing between (**c**) xm^{5}U34 or (**d**) xm^{5}s^{2}U34 of tRNA and mRNA adenosine. The binding force does not change regardless of the sulfurization state of tRNA.

1-3-3. Translational fidelity regulated by other thiolation

tRNA thiolation responsible for the accuracy of translation is not only wobble uridines, but also 2-thiocytidine at position 32 of tRNA (s^2C32) and modified 2-methylthioadenosine at position 37 of tRNA (ms^2x^6A37). s^2C32 is found in bacterial and archaeal $tRNA^{Arg1(ICG)}$ with inosine at the wobble position (I34)[29]. $tRNA^{Arg1(ICG)}$ can decode CGC, CGU, and CGA codons using I34 (Fig. 1-7)[30]. However, the frequency of CGA codon usage in *E. coli* is only 0.43%[31], meaning the decoding of adenosine in the third letter of the codon by I34 is inefficient[32]. Although s^2C32 weakens the hydrogen bond with A38, s^2C32 stabilizes π-π stacking interactions at positions 31-33 of tRNA because sulfur has higher polarizability than oxygen[33]. Furthermore, s^2C32 destabilizes the structure of the tRNA anticodon, inhibiting the base pairing between I34 at the wobble position and adenosine at position three of the codon[29]. Thus, $tRNA^{Arg1(ICG)}$ can efficiently translate only CGC and CGU codons. Note that s^2C32 synthesis is catalyzed by 2-thiocytidine synthetase (TtcA)[33].

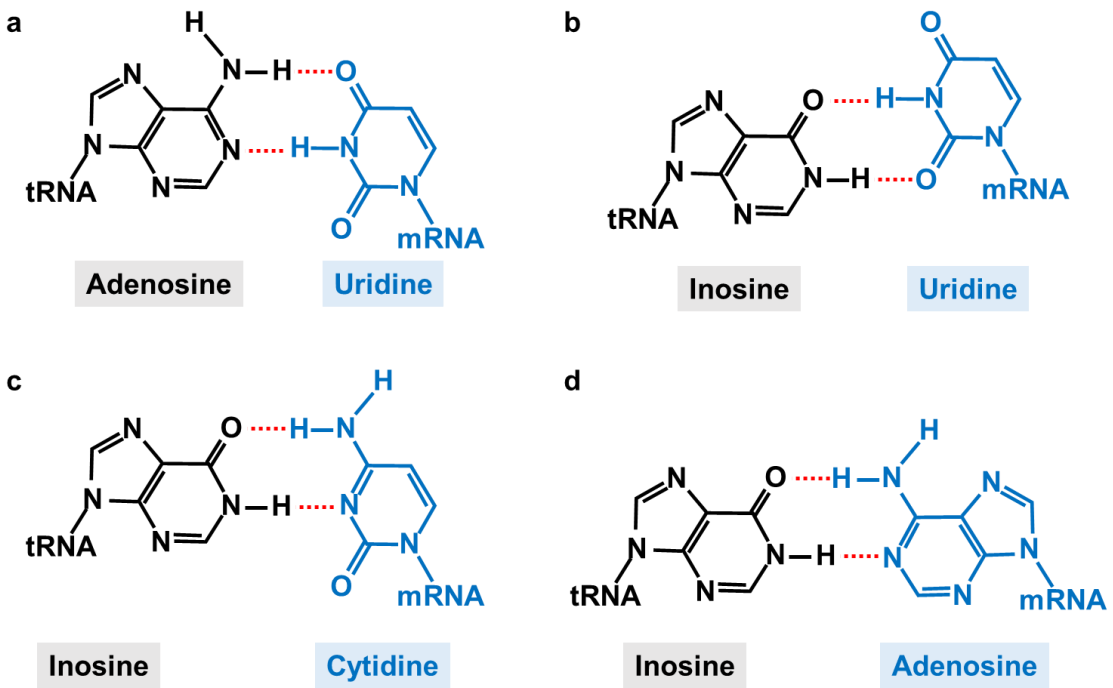

Fig. 1-7 Base pairs expanded by inosine at position 34 of tRNA (I34).

(**a**) Canonical Watson-Crick base pairing between A34 and mRNA uridine. (**b**) Base pairing between I34 and mRNA uridine. (**c**) Major wobble base pairing between I34 and mRNA cytidine. (**d**) Minor wobble base pairing between I34 and mRNA adenosine.

The ms^2x^6A37 modification is found at $tRNA^{(NNA)}$ decoding the UNN codon. The sulfur atom of the methylthio group of ms^2x^6A37 stacks with the uridine at position 1 of the codon (Fig. 1-8)[34]. This stacking strengthens the base pairing between U of mRNA (position 3 of the codon) and A of tRNA (position 1 of the anticodon), preventing slippage of the peptidyl-tRNA in the ribosomal P site[35]. As a result, ms^2x^6A37 contributes to maintaining the reading frame. Position 6 of the ms^2x^6A37 modification is diverse, with 2-methylthio-N^6-isopentenyladenosine (ms^2i^6A37, Fig. 1-9a) in $tRNA^{Lys(UUU)}$ from *E. coli*[36], 2-methylthio-N^6-threonylcarbamoyladenosine (ms^2t^6A37, Fig. 1-9b) in $tRNA^{Lys(UUU)}$ from *Bacillus subtilis*[37]. Recently, 2-methylthio-cyclic-N^6-threonylcarbamoyladenosine (ms^2ct^6A37, Fig. 1-9c) has also been discovered at position 37 of $tRNA^{Lys(UUU)}$ in *B. subtilis*, plants, and *Trypanosoma brucei*[38]. In mammals, ms^2t^6A37 is found at position 37 of cytoplasmic $tRNA^{Lys\ (UUU)}$[39], and ms^2i^6A37 at position 37 of mitochondrial $tRNA^{Phe}$, $tRNA^{Tyr}$, $tRNA^{Trp}$, and $tRNA^{Ser(UCN)}$[40].

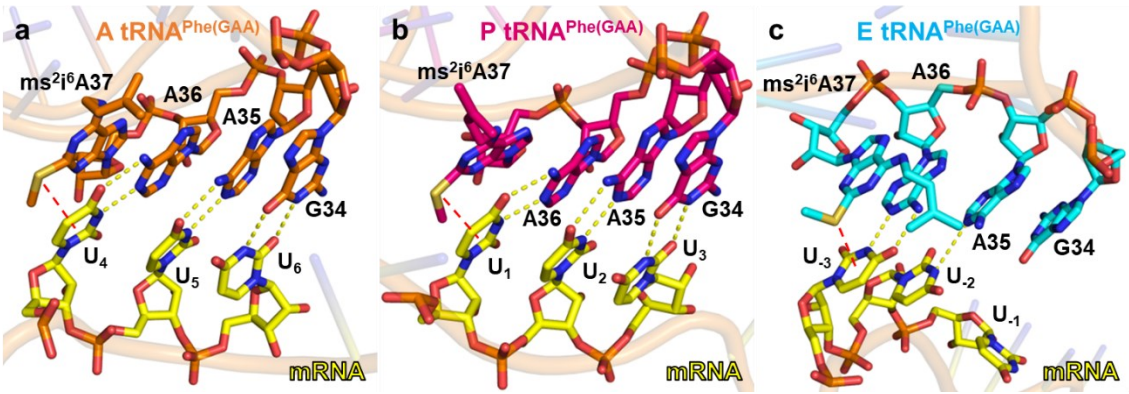

Fig. 1-8 Codon-anticodon interactions stabilized by 2-methylthio-N^6-isopentenyl adenosine at position 37 of tRNA (ms^2i^6A37)[34].

Base pairing between mRNA codon and $tRNA^{Phe}$ anticodon (**a**) at the ribosomal A site, (**b**) P site, and (**c**) E site (PDB ID: 4V6F). The red and yellow dashed lines indicate stacking and hydrogen bond, respectively.

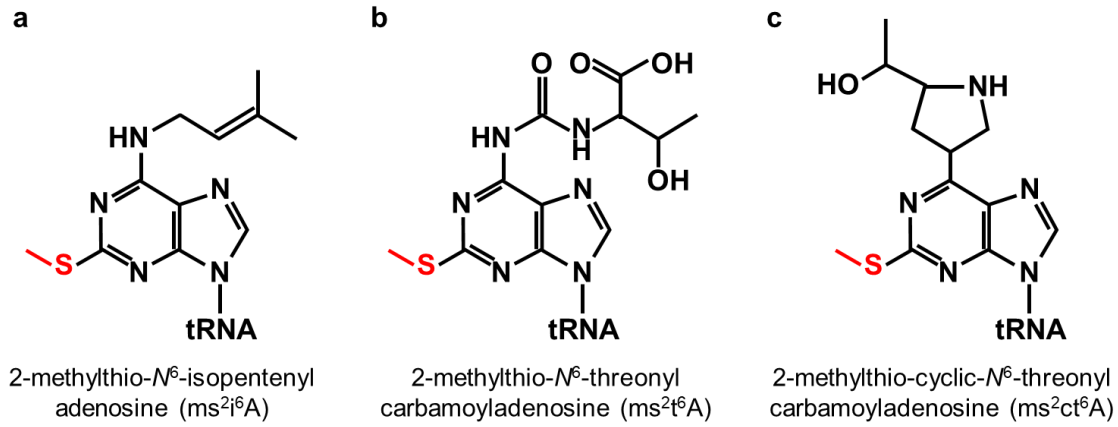

Fig. 1-9 Hypermodified adenosines at position 37 of tRNA

(**a**) 2-methylthio-N^6-isopentenyladenosine. (**b**) 2-methylthio-N^6-threonylcarbamoyl adenosine. (**c**) 2-methylthio-cyclic-N^6-threonylcarbamoyladenosine.

Bacterial ms^2i^6A37 and ms^2t^6A37 synthesis is catalyzed by MiaB[36] and MtaB[37], respectively. ms^2ct^6A37 synthesis is catalyzed by TcdA[38], but the detailed mechanism of biosynthesis is not clear. Mammalian cytoplasmic ms^2t^6A37 synthesis is catalyzed by MtaB homolog CDKAL1[37], and mitochondrial ms^2i^6A37 is synthesized by Cdk5rap1[41]. Notably, CDKAL1 KO mice showed a deficit of ms^2t^6A37, a decrease in insulin secretion, and lost blood glucose control[39]. Thus, ms^2t^6A37 is considered to be involved in insulin maturation and the development of type II diabetes[42]. It is also reported that ms^2t^6A37 is potentially linked to the development of neurodegenerative diseases[40,43].

1-3-4. Near-UV sensing

s^4U8 (or s^4U9 in some tRNAs) is found in many kinds of prokaryotic tRNA such as $tRNA^{Ala}$, $tRNA^{Met}$, and $tRNA^{Phe}$, which contain C13 (Fig. 1-10)[44,45]. When s^4U8 is exposed to near UV light (wavelengths: 310 nm-400 nm), it undergoes intramolecular cross-linking with C13 because sulfur is more reactive than oxygen (Fig. 1-11)[46]. As a result, the cross-linked tRNA changes its conformation and reduces its affinity for aminoacyl-tRNA synthetases, inhibiting aminoacylation, translation[45], and cellular growth[47,48]. In addition, s^4U8 stabilizes the structure of tRNA and prevents its degradation by RNase *in vivo*[49]. Interestingly, biosynthesis of s^4U8 and thiamine (vitamin B1) are catalyzed by the same enzyme, 4-thiouridine synthetase (ThiI)[50].

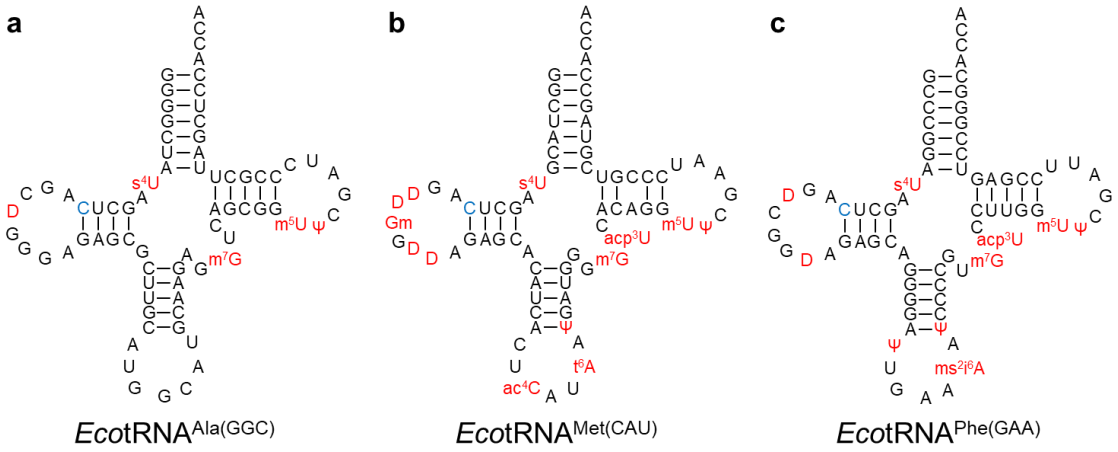

Fig. 1-10 Example of tRNA from *E. coli* which contain s^{4}U8 modification and C13. Secondary structures of (**a**) tRNA$^{Ala(GGC)}$[51]. (**b**) tRNA$^{Met(CAU)}$[52]. (**c**) tRNA$^{Phe(GAA)}$[53]. Modified nucleotides and C13 are colored in red and blue, respectively. The full name of modified nucleotides are as follows: Dihydrouridine (D), 7-methylguanosine (m^{7}G), 5-methyluridine (m^{5}U), pseudouridine (Ψ), 2'-*O*-methylguanosine (Gm), *N*^{4}-acetylcytidine (ac^{4}C), *N*^{6}-threonylcarbamoyladenosine (t^{6}A), 3-(3-amino-3-carboxypropyl)uridine (acp^{3}U), and 2-methylthio-*N*^{6}-isopentenyladenosine (ms^{2}i^{6}A).

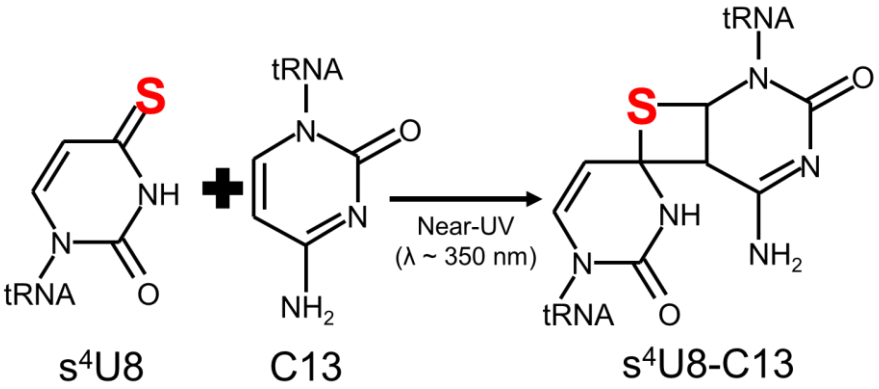

Fig. 1-11 Molecular mechanism of UV sensing regulated by 4-thiouridine at position 8 of tRNA (s^{4}U8).

1-4. Iron-sulfur clusters

To date, various thiolated nucleotides are discovered in tRNA, and their biosynthesis is catalyzed by tRNA-thiolation enzymes with an oxygen-sensitive cofactor, iron-sulfur (Fe-S) cluster[54]. Fe-S clusters are readily decayed in the air[55], but they are one of the most widely used as cofactors in proteins (Fe-S proteins) from ancient organisms to humans[56,57]. The fundamental functions of Fe-S clusters are electron transition, protein stabilization, and ligand binding, which are essential for cellular processes such as photosynthesis, respiration, nitrogen fixation, and oxygen sensing[56,58]. In addition, recent studies show that some Fe-S proteins regulate DNA replication and repair[59,60], RNA replication and function[61,62], and their dysfunction is linked to diseases[63–65].

These broad functions of Fe-S clusters are derived from the vide variety of the type of Fe-S clusters such as [2Fe-2S], [3Fe-4S], [4Fe-4S], and [8Fe-7S] (Fig. 1-12). Notably, [4Fe-4S] clusters can be classified into two groups: ferredoxin-type which is coordinated by four amino acids (typically by cysteine residues, Fig. 1-12c) and aconitase-type which is coordinated by three residues (Fig. 1-12d). Exceptionally, there is a unique [4Fe-4S] coordinated by five cysteine residues (Fig. 1-12f)[66], but not adopted in tRNA-thiolation enzymes[67].

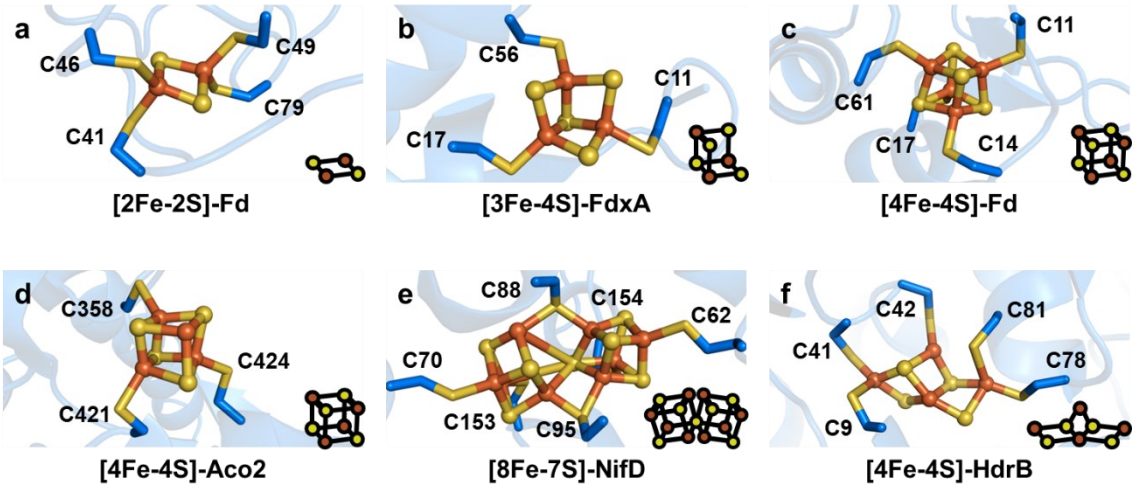

Fig. 1-12 Biological iron-sulfur clusters.

(**a**) [2Fe-2S] in ferredoxin (PDB ID: 4FXC). (**b**) [3Fe-4S] in ferredoxin (PDB ID: 1SIZ). (**c**) [4Fe-4S] in ferredoxin (PDB ID: 1IQZ). (**d**) [4Fe-4S] in aconitase (PDB ID: 1C96). (**e**) [8Fe-7S] in nitrogenase (PDB ID: 2MIN). (**g**) Non-cubane [4Fe-4S] in heterodisulfide reductase (PDB ID: 5ODC). The brown and yellow balls represent Fe and S, respectively.

1-5. tRNA-thiolation enzymes

Studies have identified several tRNA-thiolation enzymes, such as TtuA, TtcA, and Ncs6 of the TtuA/Ncs6 family; MnmA; ThiI; and MiaB. These enzymes are sulfurtransferases that share a PP-loop (SGGXD[S/T]) motif in the pyrophosphatase (PPase) domain and a CXXC…C motif in the binding site of the Fe-S cluster except for the MiaB (methylthiotransferases) (Fig. 1-13)[67]. As discussed below, I will skip the detailed explanations on MiaB-type enzymes in this paper because their properties are significantly different from those of other tRNA-thiolation enzymes.

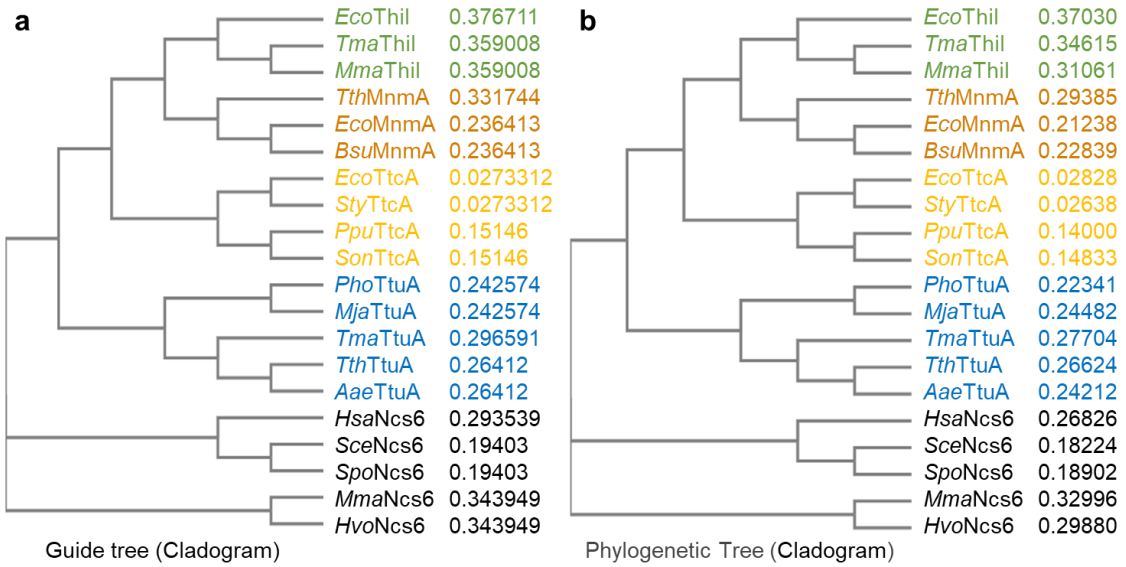

Fig. 1-13 Relevance of tRNA-thiolation enzymes discussed in this paper.

(**a**) Guide tree. (**b**) Phylogenetic tree. These Neighbour-joining trees without distance corrections are built by Clustal Omega (https://www.ebi.ac.uk/Tools/msa/clustalo/)[68]. ThiI from *Escherichia coli* K12 (*Eco*ThiI), *Thermotoga maritima* MSB8 (*Tma*ThiI), and *Methanococcus maripaludis* S2 (*Mma*ThiI)[69,67]. MnmA from *Thermus thermophilus* HB27 (*Tth*MnmA), *E. coli* K12 (*Eco*MnmA), and *Bacillus subtilis* 168 (*Bsu*MnmA)[70]. TtcA from *E. coli* K12 (*Eco*TtcA), *Salmonella typhimurium* LT2 (*Sty*TtcA), *Pseudomonas putida* W619 (*Ppu*TtcA), and *Shewanella oneidensis* MR-1 (*Son*TtcA)[71]. TtuA from *Pyrococcus horikoshii* OT-3 (*Pho*TtuA), *Methanocaldococcus jannaschii* ATCC 43067 (*Mja*TtuA), *T. maritima MSB8* (*Tma*TtuA), *T. thermophilus* HB27 (*Tth*TtuA), and *Aquifex aeolicus* VF5 (*Aae*TtuA)[18,72]. Ncs6 from *Homo sapiens* (*Hsa*Ncs6), *Saccharomyces cerevisiae* ATCC 204508 (*Sce*Ncs6), *Schizosaccharomyces pombe* 972 strain (*Spo*Ncs6), *M. maripaludis* S2 (*Mma*Ncs6), and *Haloferax volcanii* ATCC 29605 (*Hvo*Ncs6)[67,73].

From the early 2000s until around 2014, tRNA-thiolation enzymes were roughly classified into two groups: Fe-S-dependent enzymes (for s^2C32 and ms^2x^6A synthesis) and Fe-S-independent enzymes (for s^4U8 and x^5s^2U synthesis) (Fig. 1-14a)[19,74,75]. Then, it was reported that s^2C32 synthetase TtcA depends on a [4Fe-4S] cluster[71], which triggered the discoveries of the presence of [3Fe-4S] cluster in archaeal s^4U8 synthetases ThiI (also known as TtuI) and mcm^5s^2U synthase Ncs6 (also known as NcsA) and the eukaryotic mcm^5s^2U synthetase Ncs6 (also known as Ctu1)[69]. Furthermore, structural and functional analyses of the m^5s^2U54 synthetase TtuA showed that TtuA has a [4Fe-4S] cluster[72,76]. Around 2018, these results enabled us to suggest a new classification that tRNA-thiolation enzymes can be classified into three types: the MnmA/ThiI type which is independent of Fe-S clusters; the TtuA/Ncs6/TtcA type which is dependent on Fe-S clusters and adenosine triphosphate (ATP); and the MiaB type which is dependent on Fe-S clusters and *S*-adenosyl methionine (SAM) (Fig. 1-14b)[6].

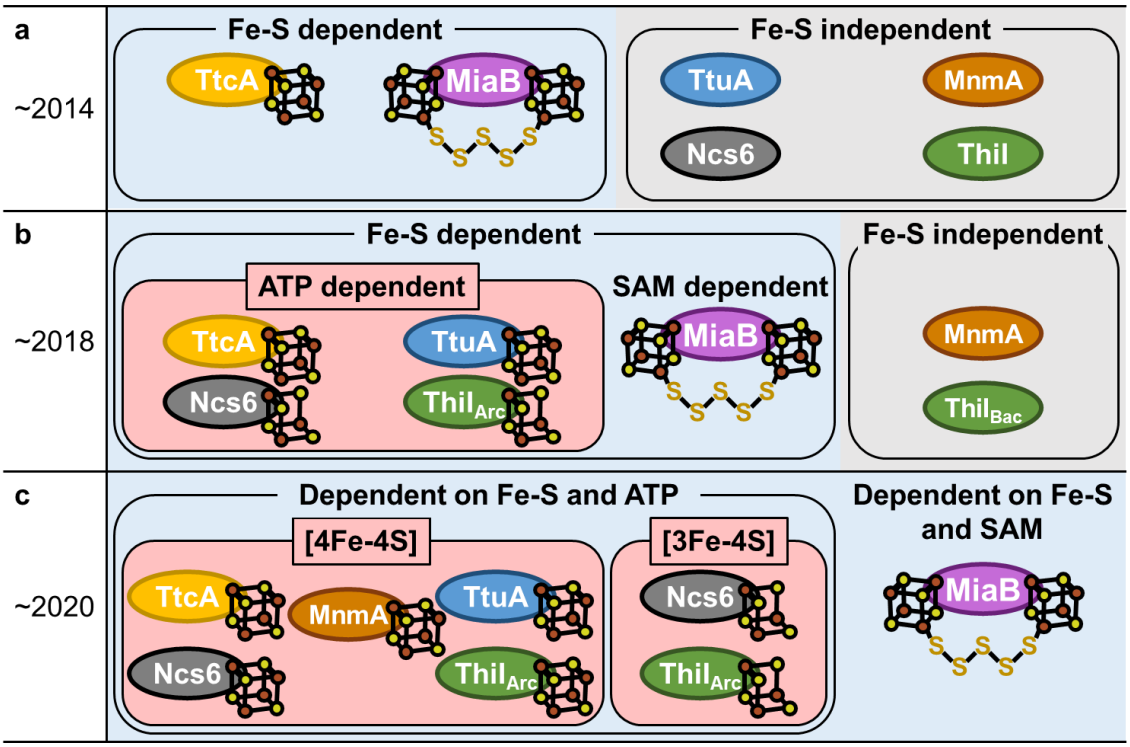

Fig. 1-14 Changes in the classification of typical tRNA-thiolation enzymes.
(**a**) Two major groups depending on the Fe-S clusters until 2014. (**b**) Three major groups depending on the Fe-S clusters and other cofactors. (**c**) Three major groups depending on the type of Fe-S clusters. Note that bacterial ThiI ($ThiI_{Bac}$) is independent of Fe-S clusters whereas archaeal ThiI ($ThiI_{Arc}$) is dependent on Fe-S clusters.

In the 2020s, spectroscopic and biochemical experiments revealed that the enzymatic active form of MnmA is [4Fe-4S] cluster[70,77]. Furthermore, [4Fe-4S] cluster is required for the enzymatic activity of bacterial ThiI under strict anaerobic conditions[67]. Interestingly, some research groups proposed that Ncs6 and ThiI have [4Fe-4S], but others proposed [3Fe-4S] despite the sequence similarity of these enzymes (Table 1-1). It is now proposed that tRNA-thiolation enzymes are generally dependent on Fe-S clusters and can be classified into two types: TtuA/Ncs6 and MiaB (Fig. 1-14c)[54,67].

	Tth TtuA	*Aae* TtuA	*Tma* TtuA	*Pho* TtuA	*Mja* TtuA	*Eco* TtcA	*Ppu* TtcA	*Son* TtcA	*Sty* TtcA	*Has* Ncs6	*Sce* Ncs6	*Spo* Ncs6	*Mma* Ncs6	*Hvo* Ncs6	*Eco* MnmA	*Bsu* MnmA	*Tth* MnmA	*Eco* ThiI	*Tma* ThiI	*Mma* ThiI
Tth TtuA		45.5 (74.0)	37.0 (71.6)	39.6 (72.9)	33.5 (67.7)	17.4 (52.6)	18.5 (48.0)	17.4 (50.0)	16.6 (52.6)	27.1 (52.9)	23.6 (56.1)	22.6 (59.8)	23.4 (57.8)	23.8 (54.7)	13.2 (44.6)	11.3 (40.2)	15.6 (40.9)	13.7 (37.9)	13.9 (46.2)	12.8 (47.3)
Aae TtuA			47.3 (76.1)	44.3 (75.5)	39.1 (71.7)	19.2 (52.9)	20.4 (54.9)	17.2 (50.6)	18.3 (52.3)	22.5 (49.3)	23.4 (51.3)	22.6 (54.8)	26.9 (60.9)	29.0 (63.3	12.1 (41.2)	11.3 (42.1)	13.1 (39.1)	13.1 (37.8)	14.8 (45.7)	12.8 (44.7)
Tma TtuA				41.1 (76.1)	41.3 (74.8)	18.0 (50.2)	17.7 (51.5)	16.8 (51.1)	18.1 (51.5)	20.7 (50.3)	23.4 (53.8)	22.7 (59.1)	26.0 (60.2)	30.3 (59.6)	10.5 (30.9)	10.2 (39.1)	11.8 (40.6)	11.0 (36.5)	14.3 (42.5)	14.8 (46.2)
Pho TtuA					50.6 (80.6	17.5 (51.4)	18.0 (49.8)	16.7 (51.1)	18.3 (51.9)	25.1 (52.3)	27.3 (55.2)	25.7 (58.8)	30.2 (62.2)	27.5 (59.7)	12.4 (41.2)	13.2 (44.0)	12.5 (40.9)	13.0 (38.5)	13.4 (43.8)	12.8 (43.6)
Mja TtuA						18.9 (50.9)	19.9 (51.3)	19.2 (51.4)	18.4 (50.5)	21.7 (50.6)	23.4 (55.4)	24.1 (60.7)	27.1 (62.5)	26.7 (61.5)	12.8 (42.9)	12.3 (43.2)	11.7 (42.0)	11.8 (39)	12.6 (45.9)	15.6 (45.1)
Eco TtcA							59.5 (78.5	60.8 (85.7)	94.5 (99.7)	17.7 (47.6)	16.9 (54.7)	17.7 (52.7)	19.8 (53.0)	20.4 (51.4)	10.8 (41.5)	13.6 (44.1)	10.5 (38.1)	11.0 (38.0)	13.6 (44.2)	12.5 (47.4)
Ppu TtcA								63.8 (80.7)	59.2 (78.8)	19.9 (49.0)	17.2 (49.2)	17.8 (49.9)	21.1 (53.8)	21.6 (54.6)	12.0 (39.7)	14.0 (39.4)	14.5 (41.1)	10.6 (36.7)	12.5 (42.5)	12.7 (40.9)
Son TtcA									61.5 (85.0)	19.1 (49.0)	18.7 (52.4)	18.2 (52.4)	18.5 (50.5)	20.9 (51.6)	11.7 (42.6)	12.7 (42.6)	14.0 (44.7)	13.2 (37.8)	12.3 (40.8)	12.5 (45.7)
Sty TtcA										18.8 (48.7)	18.9 (53.9)	17.7 (51.5)	20.1 (52.1)	20.4 (49.0)	12.7 (45.4)	13.6 (43.3)	10.8 (38.8)	10.4 (38.6)	15.9 (44.3)	12.5 (44.8)
Has Ncs6											43.6 (72.2)	42.9 (74.2)	26.9 (58.2)	29.5 (56.8)	11.8 (44.0)	13.3 (44.7)	15.0 (41.0)	11.0 (38.4)	11.4 (43.2)	11.6 (39.3)
Sce Ncs6												58.3 (80.0)	25.6 (59.2)	29.3 (57.8)	11.6 (44.2)	12.6 (42.4)	12.8 (42.4)	10.6 (43.0)	12.9 (50.1)	11.3 (47.7)
Spo Ncs6													28.0 (62.8)	28.3 (59.1)	10.2 (44.7)	8.3 (44.8)	10.3 (44.1)	13.0 (38.9)	12.2 (50.1)	13.0 (44.4)
Mma Ncs6														33.7 (68.1)	11.7 (39.6)	10.7 (42.9)	12.7 (44.1)	9.1 (38.6)	12.1 (45.5)	14.3 (43.9)
Hvo Ncs6															13.3 (46.2)	13.5 (44.3)	12.8 (42.7)	11.6 (41.0)	11.0 (44.4)	12.0 (42.1)
Eco MnmA																54.3 (79.5)	37.7 (65.4)	12.0 (41.7)	12.4 (44.7)	10.2 (43.0)
Bsu MnmA																	36.6 (66.5)	12.9 (41.5)	12.3 (46.9)	11.3 (45.5)
Tth MnmA																		11.6 (42.5)	12.2 (42.5)	9.3 (43.8)
Eco ThiI																			21.8 (52.1)	23.1 (51.2)
Tma ThiI																				31.9 (66.1)

Table 1-1 Sequence identity of tRNA-thiolation enzymes. The upper value indicates identity (%) and the lower value indicates similarity (%) of the amino acid sequence evaluated using ClustalW available on the NPS@ server (https://npsa-prabi.ibcp.fr/cgi-bin/npsa_automat.pl?page=/NPSA/npsa_clustalw.html)[78]. Identity values ≥40%; ≥30% but <40%; and ≥20% but <30% are highlighted in red, yellow, and green, respectively.

1-5-1. 2-thiouridine synthetase TtuA

TtuA catalyzes m^5s^2U54 biosynthesis with ATP and sulfur donor protein TtuB (Fig. 1-15), and these proteins were identified in the thermophilic bacterium *T. thermophilus* in 2006[18]. TtuB is a ubiquitin-like protein with a conserved GG motif at the thiocarboxyl C-terminus (R-COSH), like other sulfur donors (Fig. 1-16)[79]. The substrate tRNA of TtuA is modified with 5-methyluridine (m^5U54) by the methyltransferase TrmFO[80], and it is suggested that m^1A58 modification also promotes m^5s^2U54 formation[81].

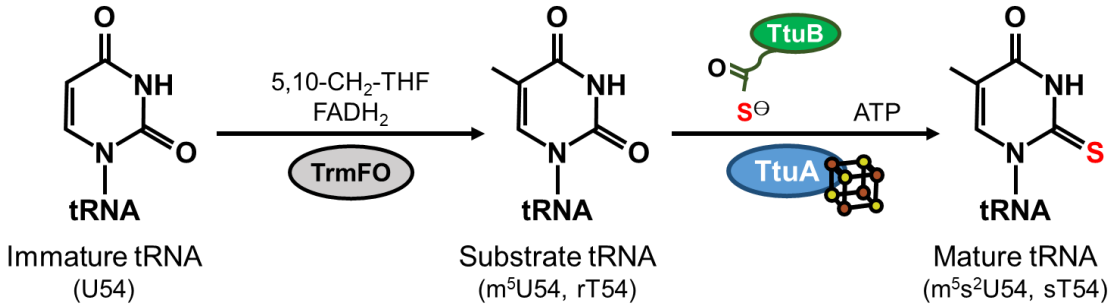

Fig. 1-15 Scheme of 5-methyl-2-thiouridine biosynthesis.

TrmFO catalyzes m^5U54 biosynthesis with N^5,N^{10}-methylenetetrahydroforate (CH_2THF) and reduced flavin adenine dinucleotide ($FADH_2$). TtuA transfers sulfur from the C-terminus of TtuB to substrate tRNA with ATP. Note that some organisms without *ttub* gene catalyze m^5s^2U54 biosynthesis using inorganic sulfur from the environment.

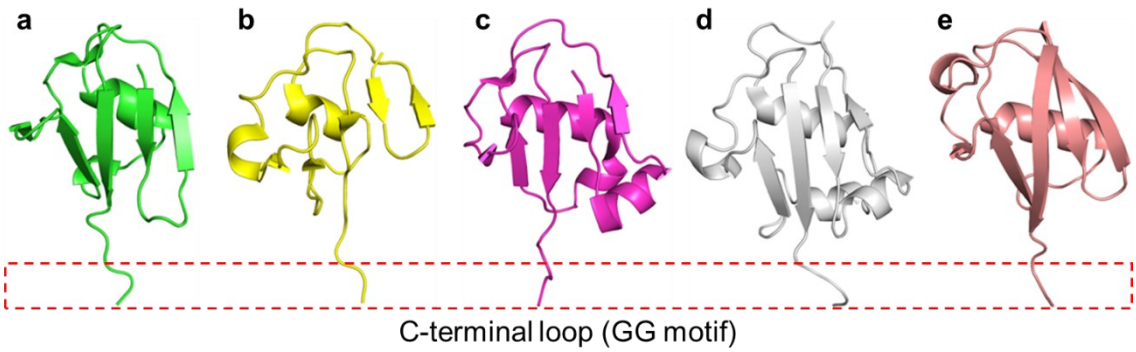

Fig. 1-16 Ubiquitin-like sulfur donor proteins.

(**a**) TtuB is a sulfur donor of m^5s^2U54 (PDB ID: 5ZTB). (**b**) ThiS is a sulfur donor of thiamine (PDB ID: 1TYG). (**c**) MoaD is a sulfur donor of molybdopterin (PDB ID: 2QIE). (**d**) Urm1 is a sulfur donor of mcm^5s^2U34 (PDB ID: 2AX5). (**e**) Ubiquitin is not a sulfur donor, but responsible for the degradation of proteins in eukaryotes (PDB ID: 1UBQ).

The crystal structure of apo-TtuA from *Pyrococcus horikoshii* (*Pho*TtuA) was determined and the critical residues were also identified in 2013[82], then it was revealed that *Pho*TtuA and TtuA from *T. thermophilus* (*Tth*TtuA) contain a [4Fe-4S] cluster in their catalytic site in 2017[72,76]. Interestingly, whereas three of the four Fe atoms in the [4Fe-4S] were coordinated to the CXXC...C motif, the remaining one bare Fe (the unique Fe) was exposed to the solution[72]. Furthermore, we have recently determined the crystal structure of the [4Fe-4S]-TtuA-TtuB-ATP complex, showing that the unique Fe binds to the C-terminus of TtuB (Fig. 1-17)[83]. Based on these structures, we proposed a novel reaction mechanism of tRNA thiolation in which the unique Fe receives sulfur from TtuB, then transfers sulfur to the adenylated tRNA (AdetRNA)[83]. However, the reaction mechanism of tRNA activation potentially involved in [4Fe-4S] has not been elucidated because the TtuA-tRNA complex structure is unknown.

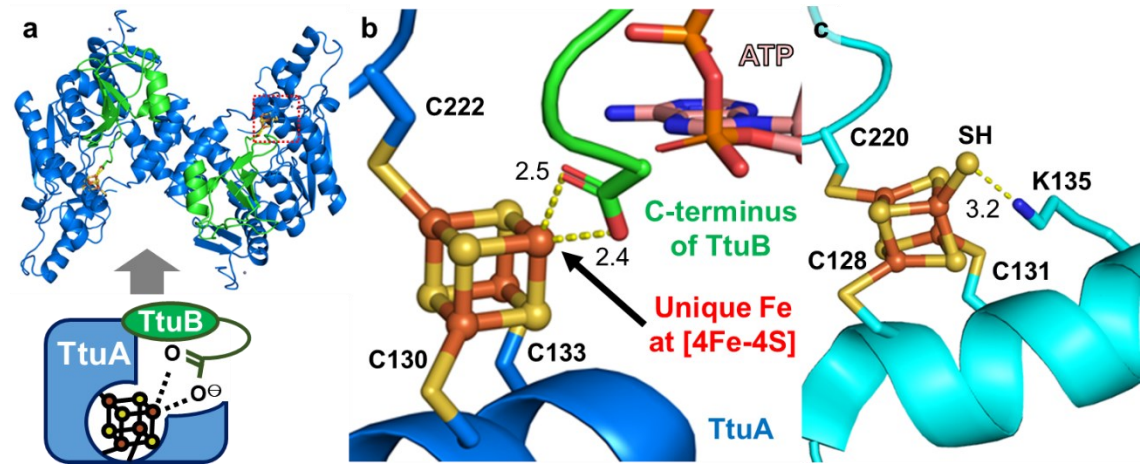

Fig. 1-17 Crystal structure of the [4Fe-4S]-TtuA complex.

(**a**) Overall structure of the [4Fe-4S]-*Tth*TtuA-*Tth*TtuB-ATP complex dimer (PDB ID: 5ZTB). TtuA and TtuB are colored blue and green, respectively as indicated in the illustration. The catalytic site is marked by the red dotted frame. (**b**) Close-up view of the catalytic center of *Tth*TtuA. The brown and yellow balls represent Fe and S, respectively. [4Fe-4S] is coordinated by Cys130, Cys133, and Cys222. The yellow dotted lines indicate coordination bonds between the unique Fe and O atoms at the C-terminus of TtuB with distance in angstrom units. (**c**) Close-up view of the catalytic site of *Pho*TtuA (PDB ID: 5MKP). [4Fe-4S] is coordinated by Cys128, Cys131, and Cys220. The unique Fe captures inorganic sulfur and forms the [4Fe-5S]-TtuA intermediate stabilized by Lys135.

1-5-2. 2-thiouridine synthetase Ncs6

Ncs6 catalyzes mcm^5s^2U34 biosynthesis in eukaryotic $tRNA^{Glu}$, $tRNA^{Gln}$, and $tRNA^{Lys}$ with ATP, Ncs2, and sulfur donor protein Urm1 (Fig. 1-18), and Ncs6/Ncs2 and Urm1 were identified in *S. cerevisiae* in 2003 and 2000, respectively[84,85]. Urm1 is a ubiquitin-like sulfur donor similar to TtuB (Fig. 1-16d)[86]. The substrate tRNA of Ncs6 has mcm^5U34 modification involving more than 10 genes including the methyltransferase Trm9[87]. The previous reports that Ncs6 recruits Ncs2, indicating the formation of the Ncs6-Ncs2 complex, but the detailed role of Ncs2 is still unclear[73,87].

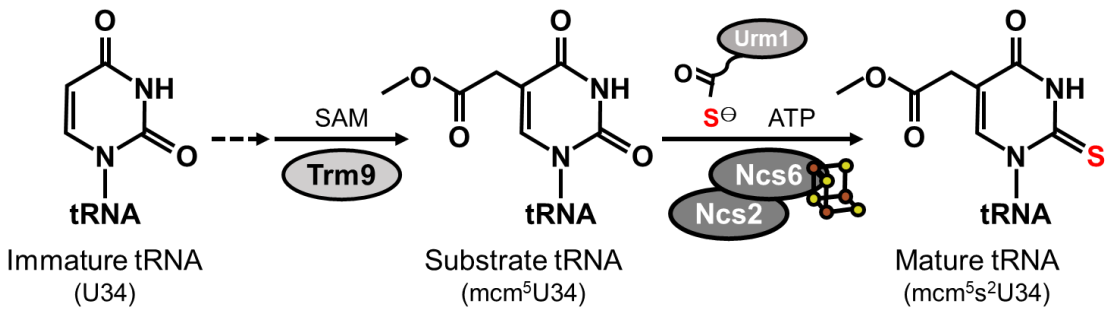

Fig. 1-18 Scheme of 5-methoxycarbonylmethyl-2-thiouridine biosynthesis.
Trm9 catalyzes mcm^5U34 synthesis using a co-factor SAM after multiple modifications of U34. Ncs6 transfers sulfur from the C-terminus of Urm1 to substrate tRNA with ATP and Ncs2. The type of Fe-S cluster is under discussion, but is shown as [3Fe-4S] in this figure. Note that some organisms without *urm1* gene catalyze mcm^5s^2U34 biosynthesis using inorganic sulfur from the environment.

In 2016, electron paramagnetic resonance (EPR) and Mössbauer spectroscopic research showed that Ncs6 from *M. maripaludis* (*Mma*Ncs6) and from *S. cerevisiae* (*Sce*Ncs6) contains [3Fe-4S] cluster, respectively (Fig. 1-19a, b)[69]. On the other hand, more recently, the crystal structure of [4Fe-4S]-*Mma*Ncs6 has been determined under strictly anaerobic conditions. This structure showed that the CXXC…C motif of Ncs6 coordinates the [4Fe-4S] and the presence of the unique Fe similar to TtuA (Fig. 1-19c, d)[67]. The inconsistent identification of the Fe-S cluster in Ncs6 comes from the oxidative sensitivity of [4Fe-4S] similar to [4Fe-4S] in aconitase (Aco2)[88], pyruvate formate-lyase activating enzyme (PFL-AE)[89], and isopentenyl-diphosphate (IspH)[90] (Fig. 1-20).

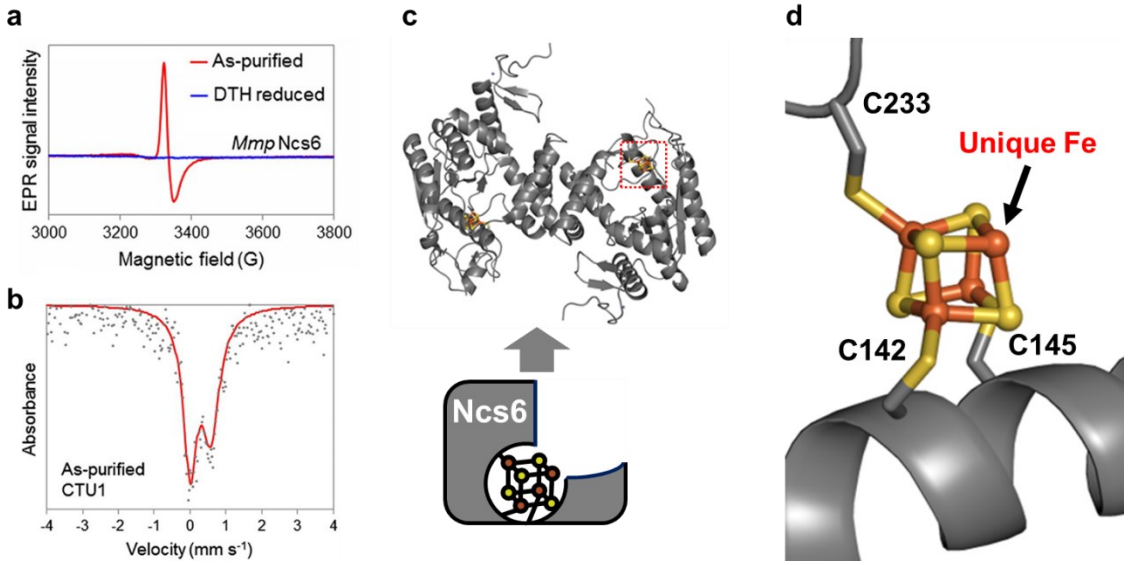

Fig. 1-19 Experimental evidences for the type of Fe-S clusters in Ncs6.

(**a**) X-bad EPR spectra of [3Fe-4S]-*Mma*Ncs6 in the as-purified (red) and sodium dithionite (DTH)-reduced (blue) states[69]. (**b**) The zero-field ^{57}Fe Mössbauer spectrum of the as-purified *Sce*Ncs6[69]. (**c**) Overall structure of the [4Fe-4S]-*Mma*Ncs6 complex dimer (PDB ID: 6SCY)[67]. The catalytic site is marked by the red dotted frame. (**d**) Close-up view of the catalytic center of *Mma*Ncs6. The brown and yellow balls represent Fe and S, respectively. Three of the four Fe atoms in [4Fe-4S] are coordinated by Cys142, Cys145, and Cys233.

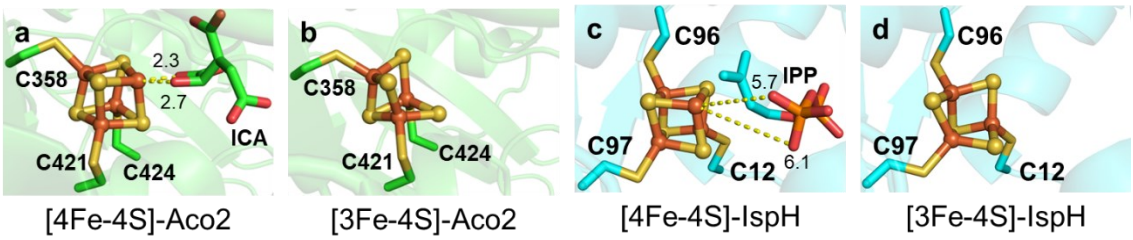

Fig. 1-20 Misidentification of Fe-S clusters.

(**a**) The unique Fe of [4Fe-4S]-Aco2 (PDB ID: 1B0J) coordinates with isocitric acid (ICA). (**b**) Inactive [3Fe-4S]-Aco2 (PDB ID: 5ACN) produced by oxidation of [4Fe-4S]-Aco2. (**c**) The unique Fe of [4Fe-4S]-IspH (PDB ID: 3KE9) coordinates with isopentenyl diphosphate (IPP). (**d**) Inactive [3Fe-4S]-IspH (PDB ID: 3F7T) produced by oxidation of [4Fe-4S]-IspH. The dashed lines indicate distances between unique Fe atoms and each ligand with distance in angstrom units.

1-5-3. 2-thiocytidine synthetase TtcA

TtcA catalyzes s^2C32 biosynthesis in bacterial $tRNA^{Arg1(ICG)}$ with ATP and inorganic sulfur (Fig. 1-21), which was identified in *E. coli* (*Eco*TtcA) and *Salmonella typhimurium* (*Sty*TtcA) in 2004[33]. The sulfur source for s^2C32 is free L-cysteine, which is desulfurized by desulfurase (IscS)[91]. In 2014, spectroscopic and biochemical research showed that [4Fe-4S] is essential for the enzymatic activity of *Eco*TtcA[71]. TtcA contains the PPase domain and two CXXC motifs, and three of the four cysteines (Cys122, Cys125, and Cys213) are essential for the catalytic activity of *Eco*TtcA, whereas the C210A mutant showed 50% of enzymatic activity[71]. These biochemical results indicated that [4Fe-4S]-TtcA contains the unique Fe.

In addition to the biochemical characterization, physiological insight on TtcA has recently been provided, which showed that TtcA from *Pseudomonas aeruginosa* (*Pae*TtcA) protects against oxidative stress via catalase activity[92]. Although the crystal structure of TtcA has not been determined, 3D structural models of *Eco*TtcA have been reported using AlphaFold and RoseTTAFold[93]. The predicted structures also support the presence of the unique Fe, but the possibility that C210 could be a ligand of [4Fe-4S] still remains. Therefore, the structural determination of TtcA by X-ray crystallography is highly desired.

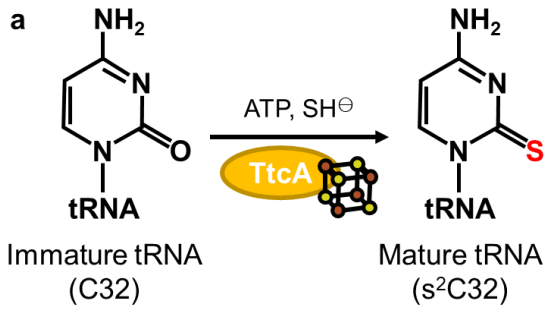

b

	NTD	PPase	CTD
*Eco*TtcA		S_{47}GGXDS$_{52}$ C_{122}XXC_{125} C_{210}XXC_{213}	
*Pae*TtcA		S_{40}DGXDS$_{45}$ C_{115}XXC_{118} C_{203}XXC_{206}	
*Ppu*TtcA		S_{40}GGXDS$_{45}$ C_{115}XXC_{118} C_{203}XXC_{206}	
*Son*TtcA		S_{45}DGXDS$_{50}$ C_{120}XXC_{123} C_{208}XXC_{211}	
*Sty*TtcA		S_{47}DGXDS$_{52}$ C_{122}XXC_{125} C_{210}XXC_{213}	

Fig. 1-21 Scheme of 2-thiocytidine biosynthesis and characterization of TtcA.
(**a**) TtcA catalyzes s^2C32 synthesis using ATP and inorganic sulfur source. TtcA transfers sulfur provided by IscS system. (**b**) Domain construct and the location of critical residues in typical TtcA. TtcA contains the N-terminal domain (NTD), catalytic PPase domain, and C-terminal domain (CTD). The cysteine residues binding to [4Fe-4S] are indicated in red based on the previous study on *Eco*TtcA[71]. The abbreviations of the protein source are the same as in Fig. 1-13.

1-5-4. 2-thiouridine synthetase MnmA

MnmA (formerly AsuE or TrmU) catalyzes s^2U34 biosynthesis in bacterial $tRNA^{Glu}$, $tRNA^{Gln}$, and $tRNA^{Lys}$ with ATP and an inorganic sulfur (Fig. 1-22). MnmA was identified in *E. coli* (*Eco*MnmA) in 2003[94]. In 2006, the structures of the *Eco*MnmA-$tRNA^{Glu}$ complex have been determined (Fig. 1-23), showing that the flexible loop of MnmA prevents the inactivation of the AdetRNA by the influx of solvent[95]. Based on this structure, the two possible catalytic mechanisms were proposed that MnmA catalyzes s^2U34 synthesis via persulfide (R-SSH).

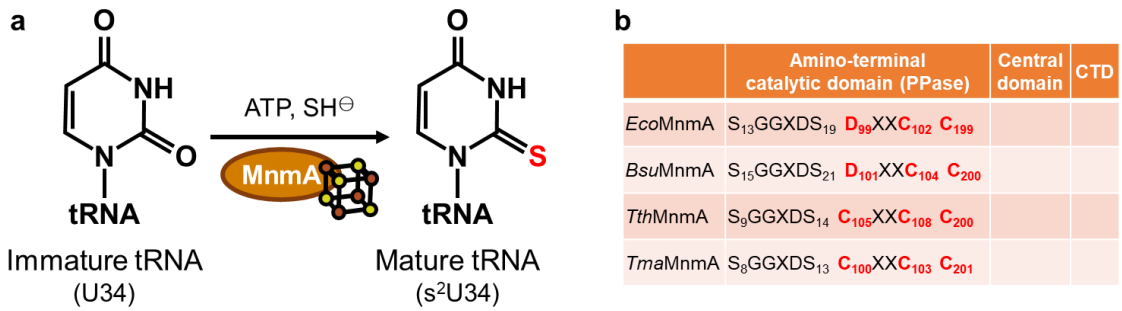

	Amino-terminal catalytic domain (PPase)	Central domain	CTD
*Eco*MnmA	$S_{13}GGXDS_{19}$ $D_{99}XXC_{102}$ C_{199}		
*Bsu*MnmA	$S_{15}GGXDS_{21}$ $D_{101}XXC_{104}$ C_{200}		
*Tth*MnmA	$S_{9}GGXDS_{14}$ $C_{105}XXC_{108}$ C_{200}		
*Tma*MnmA	$S_{8}GGXDS_{13}$ $C_{100}XXC_{103}$ C_{201}		

Fig. 1-22 Scheme of 2-thiouridine biosynthesis and characterization of MnmA.
(**a**) MnmA catalyzes s^2U34 synthesis using ATP and inorganic sulfur source. (**b**) Domain construct and the location of critical residues in typical MnmA. MnmA contains the amino-terminal catalytic domain (PPase), central domain, and carboxy-terminal β-barrel domain (CTD)[95]. The [4Fe-4S]-binding residues are indicated in red.

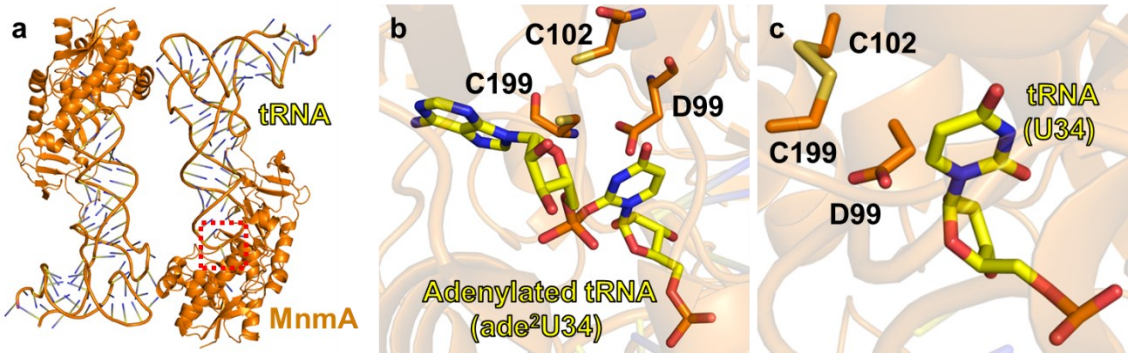

Fig. 1-23 Crystal structure of the *Eco*MnmA-$tRNA^{Glu}$ complexes[95].
(**a**) Overall structure of the MnmA-adenylated tRNA complex (PDB ID: 2DEU). The catalytic site is marked by the red dotted frame. Close-up view of the catalytic center of MnmA (**b**) in the adenylated intermediate state and (**c**) in the initial tRNA binding state (PDB ID: 2DER). Cys102 and Cys199 can form a disulfide bond.

Although the structural understanding of s^2U34 biosynthesis was advanced, the enzymatic activity of apo-MnmA was very weak[94–97]. Recently, spectroscopic and biochemical research showed that MnmA from *T. thermophilus* (*Tth*MnmA) contains [4Fe-4S] cluster coordinated by Cys105, Cys108, and C200[70]. Furthermore, it was reported that the enzymatically active form of *Eco*MnmA contains a [4Fe-4S] coordinated by Asp99, Cys102, and Cys199[77]. Although the experimental structure of the [4Fe-4S]-MnmA complex has not been determined, the [4Fe-4S]-MnmA model has been reported[93]. These recent studies updated the sulfur relay system. Previously, the sulfur source for s^2U34 is considered to be free L-cysteine transferred via the sulfur relay system involving persulfide proteins IscS[98,99] and TusABCDE in typical bacteria (Fig. 1-24a)[96,100] or YrvO in *B. subtilis* (Fig. 1-24b)[97]. On the other hand, owing to the structural insights of [4Fe-5S]-*Pho*TtuA and [4Fe-5S]-TudS[76,101], we can assume a new sulfur relay system involving [4Fe-5S]-MnmA (Fig. 1-24c).

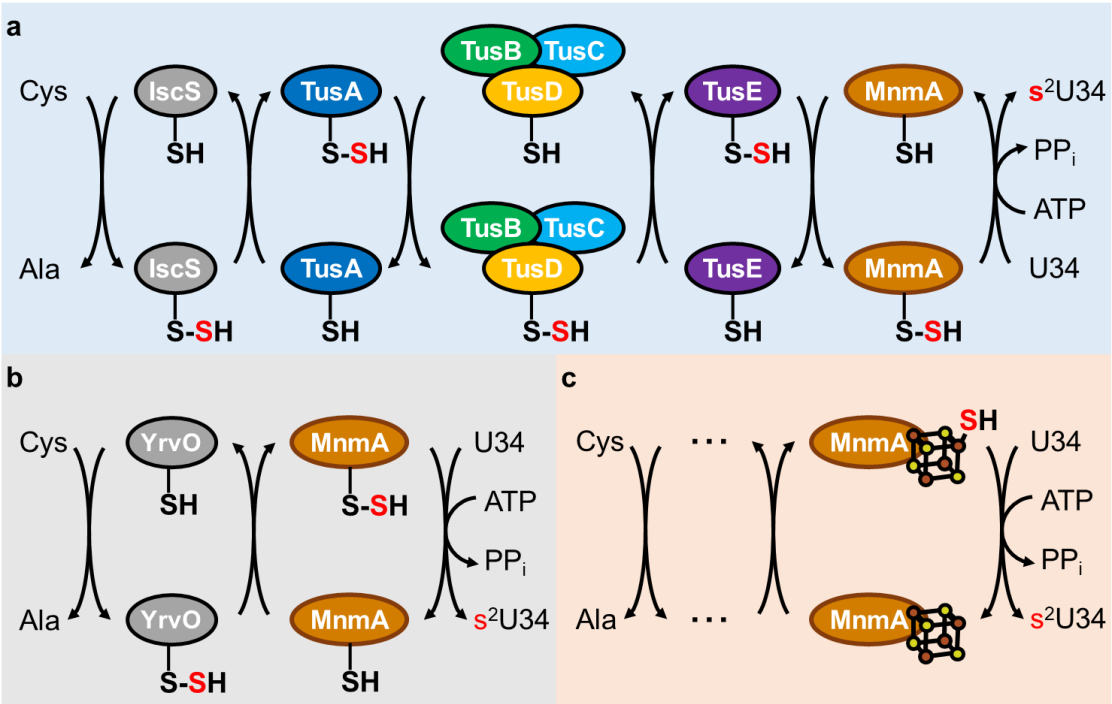

Fig. 1-24 Sulfur relay system for the biosynthesis of s^2U34 catalyzed by MnmA. Previously proposed pathway mediated via (**a**) the IscS-TusABCDE system in typical bacteria and (**b**) YrvO in some bacteria. (**c**) New putative pathway mediated via [4Fe-5S]-MnmA. The upstream of MnmA involves persulfide proteins that differ among species, as previous studies have shown.

1-5-5. 4-thiouridine synthetase ThiI

ThiI catalyzes the s^4U8 biosynthesis in prokaryotic $tRNA^{Trp}$, $tRNA^{Phe}$, $tRNA^{Arg}$, $tRNA^{Val}$, $tRNA^{Asp}$, $tRNA^{Gly}$, $tRNA^{Met}$, and $tRNA^{His}$ with ATP and inorganic sulfur (Fig. 1-25a). ThiI was identified in *E. coli* (*Eco*ThiI) in 1998[13], and it was proposed the catalytic mechanism of s^4U8 biosynthesis involves the disulfide bond between Cys344 at the PP-loop domain and Cys456 at the rhodanese-like domain (RLD) (Fig. 1-26)[98]. However, the structures of ThiI from *B. anthracis* (*Ban*ThiI) with the THUMP domain responsible for tRNA-binding showed that RLD is absent in some organisms (Fig. 1-25b)[102]. These bacteria also have specific cysteine desulfurase NifZ, which enables s^4U8 synthesis without RLD in ThiI[103]. In most archaea in the absence of NifZ, their ThiI contains catalytic cysteines in the PP-loop domain instead of RLD[104].

Furthermore, the crystal structure of the ThiI from *Thermotoga maritima* (*Tma*ThiI) complex with truncated $tRNA^{Phe}$ has been determined (Fig. 1-27), which revealed the interaction manner between tRNA and the THUMP domain of *Tma*ThiI, and demonstrated that dynamic structural change of the substrate tRNA with ACCA 3'-end is required for s^4U8 formation[105]. However, the catalytic mechanism of ThiI is still unclear because the substrate base U8 did not enter the active site.

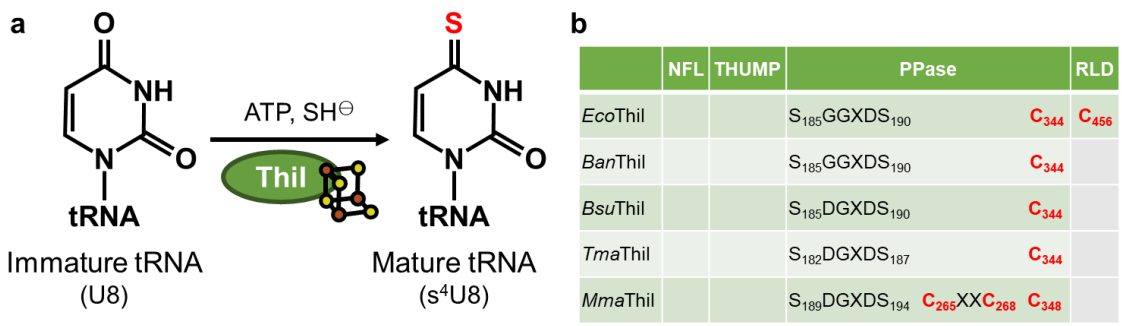

Fig. 1-25 Scheme of 4-thiouridine biosynthesis and characterization of ThiI.
(**a**) ThiI catalyzes s^4U8 synthesis using ATP and inorganic sulfur source. The type of Fe-S cluster is still under discussion, but is shown as [3Fe-4S] in this figure. (**b**) Domain construct and the location of critical residues in typical ThiI. ThiI contains an N-terminal ferredoxin-like (NFL) domain, RNA binding domain (THUMP), catalytic PPase domain, and only *Eco*ThiI contains the rhodanese-like domain (RLD) among the five sources shown in this figure. The catalytic cysteines are indicated in red. The abbreviations of the protein source are the same as in Fig. 1-13.

In 2016, spectroscopic and biochemical research showed that the catalytic form of ThiI from *Methanococcus maripaludis* (*Mma*ThiI) contains a [3Fe-4S] cluster[69]. On the other hand, the preliminary report on the structural determination of [4Fe-4S]-*Mma*ThiI has been published under strictly anaerobic conditions[67]. Therefore, the reaction mechanism of s^4U8 synthesis catalyzed by ThiI involving an Fe-S cluster is still unclear.

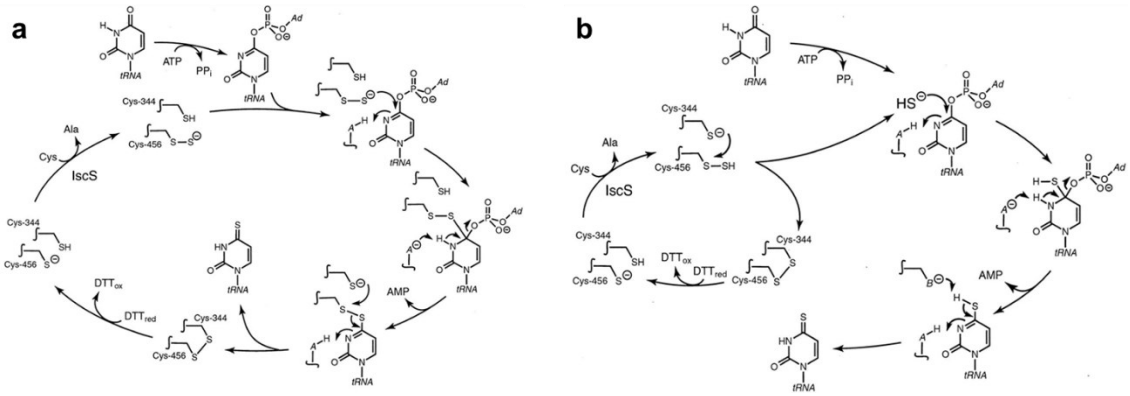

Fig. 1-26 Proposed reaction mechanism of s^4U8 synthesis[98].

(**a**) Direct pathway. Persulfide on Cys456 nucleophilically attacks the adenylated tRNA. (**b**) Indirect pathway. Cys344 and Cys456 generate hydrogen sulfide, which serves as a nucleophile to attack the adenylated tRNA.

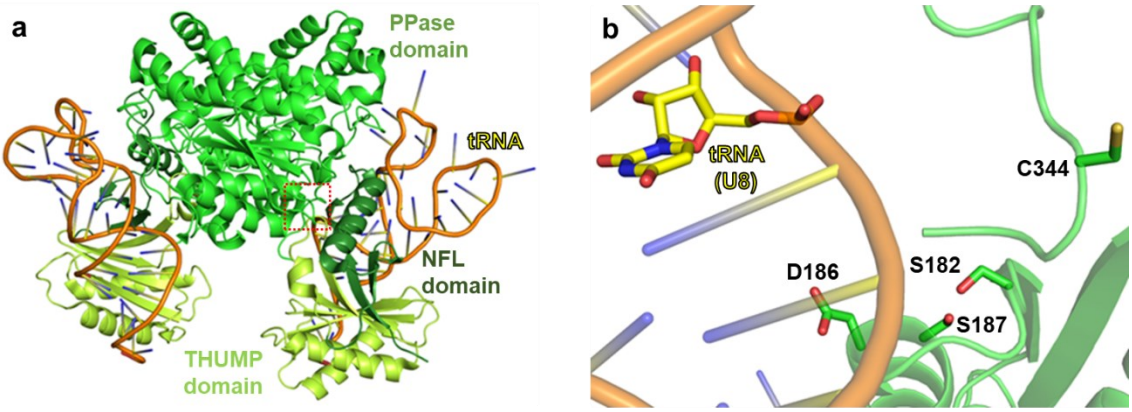

Fig. 1-27 Crystal structure of the *Tma*ThiI-$tRNA^{Phe}$ (39-mer) complex[105].

(**a**) Overall structure of the *Tma*ThiI-truncated $tRNA^{Phe}$ complex (PDB ID: 4KR6). The catalytic site is marked by the red dotted frame. (**b**) Close-up view of the catalytic center of *Tma*ThiI. The side chains of the critical residues in the PPase domain are shown as a stick model.

1-6. The similarity of 2-thiouridine synthesis catalyzed by TtuA and Ncs6

TtuA and Ncs6 belong to the TtuA/Ncs6 family which contains zinc finger domains (CXXC…CXX[C/H] motif) and the PPase domain (SGGXD[S/T] motif) with [4Fe-4S]-binding site (CXXC…C motif) (Fig. 1-28a)[92]. Two zinc fingers are predicted as tRNA binding sites and the PPase domain is identified as an ATP-binding site[72,76]. Not only the amino acid sequence of *Tth*TtuA and *Mma*Ncs6, but their 3D structure is also similar (Cα RMSD = 1.649 Å, Fig. 1-28b). The inside of their catalytic pocket is positively charged, which is suitable for tRNA binding (Fig. 1-28c, d)[92]. TtuA and Ncs6 also have two tunnels for sulfur donor protein and tRNA (Fig. 1-28e)[72]. These structural similarities strongly support the similar catalytic mechanism of tRNA-thiolation.

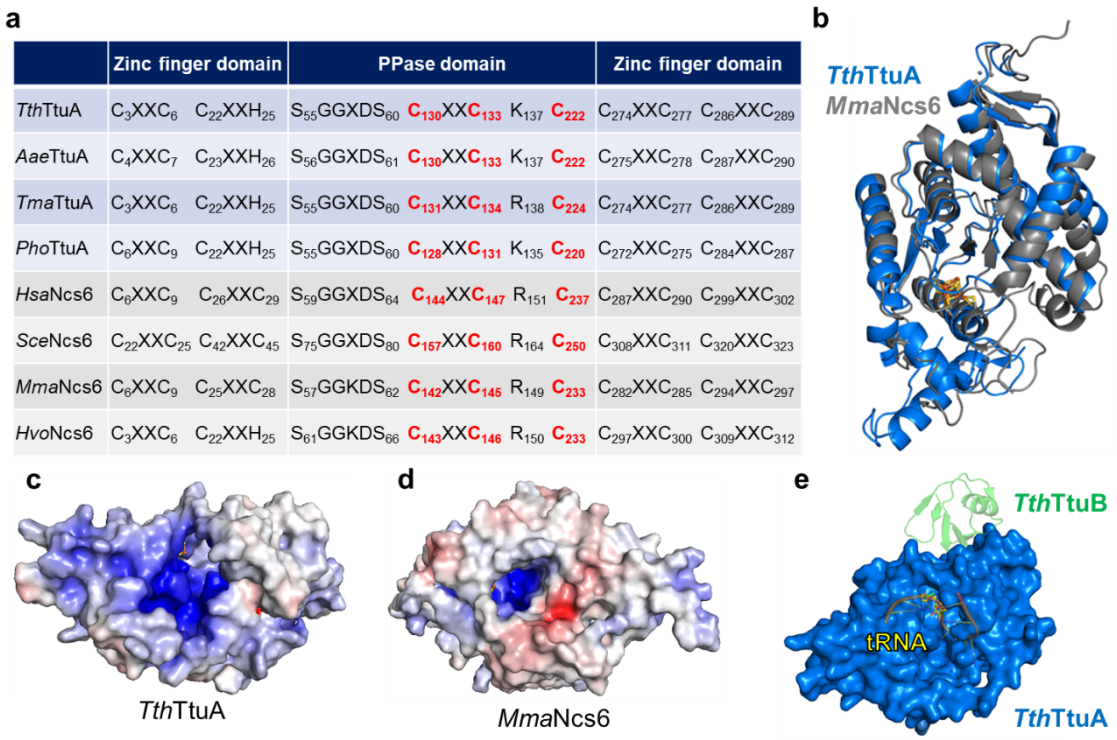

	Zinc finger domain		PPase domain				Zinc finger domain	
*Tth*TtuA	C_3XXC_6	$C_{22}XXH_{25}$	$S_{55}GGXDS_{60}$	$C_{130}XXC_{133}$	K_{137}	C_{222}	$C_{274}XXC_{277}$	$C_{286}XXC_{289}$
*Aae*TtuA	C_4XXC_7	$C_{23}XXH_{26}$	$S_{56}GGXDS_{61}$	$C_{130}XXC_{133}$	K_{137}	C_{222}	$C_{275}XXC_{278}$	$C_{287}XXC_{290}$
*Tma*TtuA	C_3XXC_6	$C_{22}XXH_{25}$	$S_{55}GGXDS_{60}$	$C_{131}XXC_{134}$	R_{138}	C_{224}	$C_{274}XXC_{277}$	$C_{286}XXC_{289}$
*Pho*TtuA	C_6XXC_9	$C_{22}XXH_{25}$	$S_{55}GGXDS_{60}$	$C_{128}XXC_{131}$	K_{135}	C_{220}	$C_{272}XXC_{275}$	$C_{284}XXC_{287}$
*Hsa*Ncs6	C_6XXC_9	$C_{26}XXC_{29}$	$S_{59}GGXDS_{64}$	$C_{144}XXC_{147}$	R_{151}	C_{237}	$C_{287}XXC_{290}$	$C_{299}XXC_{302}$
*Sce*Ncs6	$C_{22}XXC_{25}$	$C_{42}XXC_{45}$	$S_{75}GGXDS_{80}$	$C_{157}XXC_{160}$	R_{164}	C_{250}	$C_{308}XXC_{311}$	$C_{320}XXC_{323}$
*Mma*Ncs6	C_6XXC_9	$C_{25}XXC_{28}$	$S_{57}GGKDS_{62}$	$C_{142}XXC_{145}$	R_{149}	C_{233}	$C_{282}XXC_{285}$	$C_{294}XXC_{297}$
*Hvo*Ncs6	C_3XXC_6	$C_{22}XXH_{25}$	$S_{61}GGKDS_{66}$	$C_{143}XXC_{146}$	R_{150}	C_{233}	$C_{297}XXC_{300}$	$C_{309}XXC_{312}$

Fig. 1-28 Sequential and structural comparisons of TtuA and Ncs6.

(**a**) Domain construct and the location of critical residues in typical TtuA (blue) and Ncs6 (gray). TtuA and Ncs6 contain Zinc finger domains in the N and C-terminus regions. The [4Fe-4S]-binding cysteines are indicated in red. The abbreviations of the protein source are the same as in Fig. 1-13. (**b**) Superposition of the overall structures of [4Fe-4S]-*Tth*TtuA (PDB ID: 5B4F) and [4Fe-4S]-*Mma*Ncs6 (PDB ID: 6SCY). The zinc atoms are shown as gray balls. Electrostatic potential of the (**c**) *Tth*TtuA (PDB ID: 5B4F) and (**d**)

*Mma*Ncs6 (PDB ID: 6SCY). For clearness, [4Fe-4S] is also shown after the calculation of the potential with the APBS plugin installed in PyMOL[106]. The positively and negatively charged surface is colored blue (+10 kT/e) and red (-10 kT/e), respectively. (**e**) The [4Fe-4S]-TtuA-TtuB-tRNA complex model[72]. The two tunnels through the catalytic site of TtuA allow TtuB and tRNA to enter the active site simultaneously.

Furthermore, some organisms employ TtuA or Ncs6 with sulfur donor protein TtuB or Urm1, respectively. Interestingly, the sulfur relay system from free L-cysteine to tRNA is very similar (Fig. 1-29)[107,108]. In the first step, cysteine desulfurases IscS/SufS or Nfs1 transfer sulfur from L-cysteine to the rhodanese-like domain of TtuD or Tum1 (Yor251c), respectively[87,107]. Next, TtuD or Tum1 transfers sulfur to the C-terminus of adenylated sulfur donor proteins (adenylated TtuB or Urm1, respectively) activated by E1-like proteins TtuC or UBA4, respectively[79,85]. Finally, ubiquitin-like sulfur donors (TtuB or Urm1) transfer sulfur to substrate tRNA, which is catalyzed by TtuA or Ncs6, respectively.

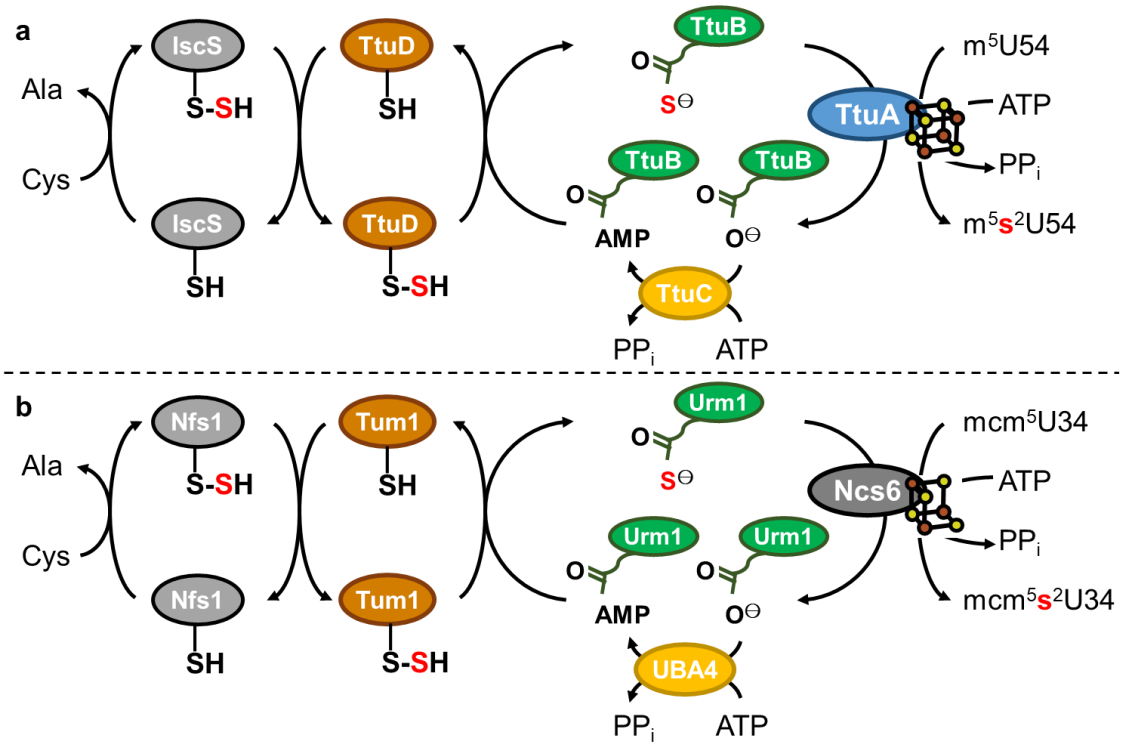

Fig. 1-29 Sulfur relay system in ubiquitin-like systems.

(**a**) m^5s^2U54 synthesis pathway. (**b**) mcm^5s^2U34 synthesis pathway. The type of Fe-S cluster in Ncs6 is still under discussion, but is shown as [3Fe-4S] in this figure.

1-7. Research question and purpose of this study

Considering the sequence identity (Fig. 1-13, Table 1-1), the similarity of 3D-structure (Fig. 1-28), and sulfur relay system (Fig. 1-29) among tRNA-thiolation enzymes, the opposite reports of [3Fe-4S]-Ncs6 and [4Fe-4S]-Ncs6 raised the question of whether TtuA only requires [4Fe-4S] or both [4Fe-4S] and [3Fe-4S] for its function. In previous studies on TtuA, [4Fe-4S] was reconstituted by excess iron and sulfur sources *in vitro* under anaerobic conditions[72,76,83]. In other words, the possibility that TtuA contains [3Fe-4S] has not been examined. Furthermore, whereas the detailed mechanisms of sulfur transition catalyzed by Fe-S cluster-independent enzymes have been understood (Fig. 1-16), that of desulfurization from TtuB involved in Fe-S clusters was unknown.

In this study, I aimed to elucidate the detailed catalytic mechanism of tRNA thiolation based on the exact type of Fe-S clusters (Fig. 1-30). To achieve this purpose, I reconstituted [4Fe-4S]-TtuA and oxidized it to [3Fe-4S]-TtuA under strictly anaerobic conditions. Then, I analyzed the structure of the Fe-S cluster in the two types of TtuA using EPR spectroscopy in time-course and evaluated their activity. Furthermore, I analyzed the enzymatic activity of TtuA mutants and the condition of sulfur transition from TtuB to tRNA by biochemical assays. Then, I examined the structural similarity of tRNA-thiolation enzymes based on the bioinformatics approaches. Finally, I integrated all results and discuss the general catalytic mechanism of tRNA thiolation. Our findings would address the biochemical question of why all organisms employ oxygen-sensitive [4Fe-4S] in essential tRNA-thiolation.

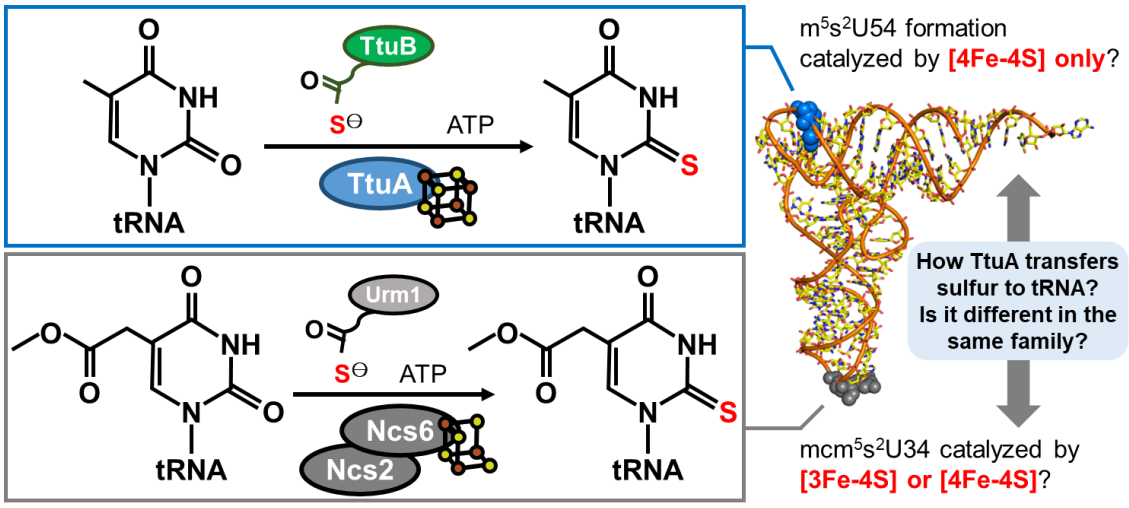

Fig. 1-30 Graphical abstract of this study.

Chapter 2. Materials and Methods

2-1. Expression of TtuA and TtuB

*Tth*TtuA (WT, UniProt ID: Q72LF3) was expressed as a C-terminal His6-tagged protein in *E. coli* (B834 DE3 strain) using the pET26 vector (Novagen)(Fig. 2-1a)[72]. *Tth*TtuA (MT) was expressed as a N-terminal His6-tagged protein in *E. coli* (Rosetta DE3) using the pET15b vector (Fig. 2-1b)[18]. Point mutations were introduced using the QuikChange II site-Directed Mutagenesis Kits (Stratagene) and designed primers (Sigma) (Table 2-1). I cultured recombinant *E. coli* in 3 L of lysogeny broth (LB) medium (Miller) containing 25 μg/mL kanamycin for C-His6-tagged TtuA or 100 μg/mL ampicillin for N-His6-tagged TtuA at 37°C and 150 rpm until the absorption at 600 nm (OD_{600}) reached 0.6. Then, I induced overexpression of TtuA with 1 mM isopropyl β-D-1-thiogalactopyranoside (IPTG) after 7°C cold shocks for 45 min, and cultured the cells at 25°C and 150 rpm for 16 hours. The cells were collected by centrifugation at 5,000 × *g* for 30 min and stored at -30°C.

*Tth*TtuB (UniProt ID: Q72LF4) was expressed as a C-terminal intein-tagged protein in *E. coli* (B834 DE3 strain) with the pTYB1 vector (New England BioLabs)(Fig. 2-1c)[72]. I cultured recombinant *E. coli* in 3 L of LB containing 100 μg/mL ampicillin at 37°C and 150 rpm until OD_{600} = 0.6. Then, I induced overexpression of TtuB and cultured the cells in the same manner as TtuA.

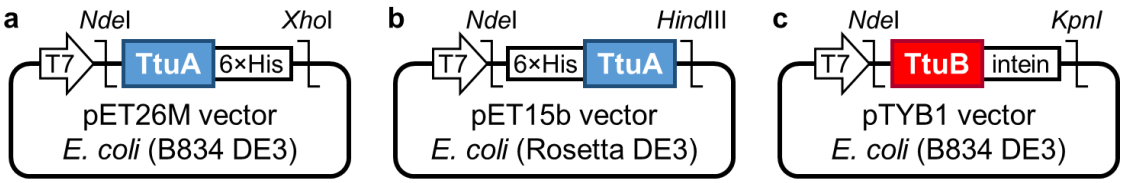

Fig. 2-1 Expression constructs of TtuA and TtuB.

(**a**) C-terminal His6-tagged TtuA for spectroscopic and biochemical analyses. (**b**) N-terminal His6-tagged TtuA for mutation assays. (**c**) C-terminal intein-tagged TtuB. All of these protein genes were inserted between the indicated multi-cloning site.

Sample Name	DNA sequence	Tm [℃]	GC ratio [%]	μg/OD	Mw
S55A_forward	CGGGGGGGAAGGACTCC	62	76	31.9	5301.5
S55A_reverse	CGACCGCCACCAGAACCC	59	72	32.7	5383.6
K58A_forward	GCGGACTCCCTGGCCC	54	81	35.4	4819.2
K58A_reverse	CCCCCCCGAGACCGC	63	87	34.7	4444.0
D59A_forward	GCCTCCCTGGCCCTTTGG	56	72	36.7	5418.6
D59A_reverse	CTTCCCCCCCGAGACCG	61	76	34.8	5052.4
S60A_forward	GCCCTGGCCCTTTGGGAC	61	72	35.3	5467.6
S60A_reverse	GTCCTTCCCCCCCGAGAC	60	72	34.6	5356.5
K137A_forward	GCGCGCTACATCATCAACCAGG	58	59	32.0	6689.4
K137A_reverse	GGAGAGGCCGCAGGCG	64	81	31.5	4997.3
K137R_forward	CGGCGCTACATCATCAACCAGG	58	59	32.0	6689.4
K137R_reverse	GGAGAGGCCGCAGGCG	64	81	31.5	4997.3
D161A_forward	GCCGAGGCCGCCGTC	57	87	34.4	4555.0
D161A_reverse	GTCCAGGTTGTGCCCCGTG	62	67	34.0	5811.8
E203A_forward	GAGGGAGGTCCTCTCCTACAC	58	62	32.5	6407.2
E203A_reverse	GCGCTAAAGCGGTAGAAGGGC	61	62	30.9	6545.3
E221A_forward	GCGTGCCCGAACGCCAAG	58	72	32.5	5494.6
E221A_reverse	CTCGTGGAGGTAGCGGATCC	60	65	32.3	6174.1
K234A_forward	GCGGAGGCCCTGAACCTG	55	72	33.1	5525.6
K234A_reverse	GTAGAGGAGGCTTTTCGCCCC	62	62	33.0	6438.2

Table 2-1　Designed primers for mutagenesis in the N-terminal His6-tagged TtuA. Each primer is shown with its DNA sequence, melting temperature (Tm), GC ratio, conversion factor (μg/OD), and molecular weight (Mw). Tm values were calculated by a nearest neighbor thermodynamic algorithm with SnapGene Viewer version ver6.2 (https://www.snapgene.com/)[109]. Nucleotides colored in red indicate mutation sites for the QuikChange method.

2-2. Anaerobic purification of TtuA

Lysis of recombinant *E. coli* and purification of TtuA were performed under strictly anaerobic conditions with 5% H_2 and 95% N_2 (Fig. 2-2a)[72]. The collected cells cultured in 1 L of LB were lysed by sonication on ice for 45 min in the deoxidized purification buffer (50 mM HEPES-KOH (pH 7.6), 200 mM ammonium sulfate, 50 mM ammonium acetate, 5 mM magnesium chloride, 10% (v/v) glycerol, and 7 mM 2-mercaptoethanol) containing 0.1% Triton X-100. Then the cells were heat treated at 70°C for 20 min, and

the precipitates were removed by centrifugation at 7,000 × *g* for 60 min and a 0.22-µm filter (Millipore). The supernatant was loaded onto a Ni-affinity chromatography (NiAC) column (1 mL His-Trap HP; GE Healthcare) equilibrated with the purification buffer. Non-specifically bound proteins were removed using the wash buffer (purification buffer containing 50 mM imidazole). TtuA was eluted with a gradient of 50-500 mM imidazole in the purification buffer (Fig. 2-2b). Further, I purified the eluted samples with a size exclusion chromatography (SEC) column (HiLoad 16/60 Superdex 200, GE Healthcare) equilibrated with the purification buffer (Fig. 2-2c). I checked the sample purity using 12.5% (v/v) SDS-PAGE at 40 mA for 60 min, then protein bands were visualized by CBB-G250 stain and detected using the Amersham Imager 680 (GE Healthcare) (Fig. 2-2d).

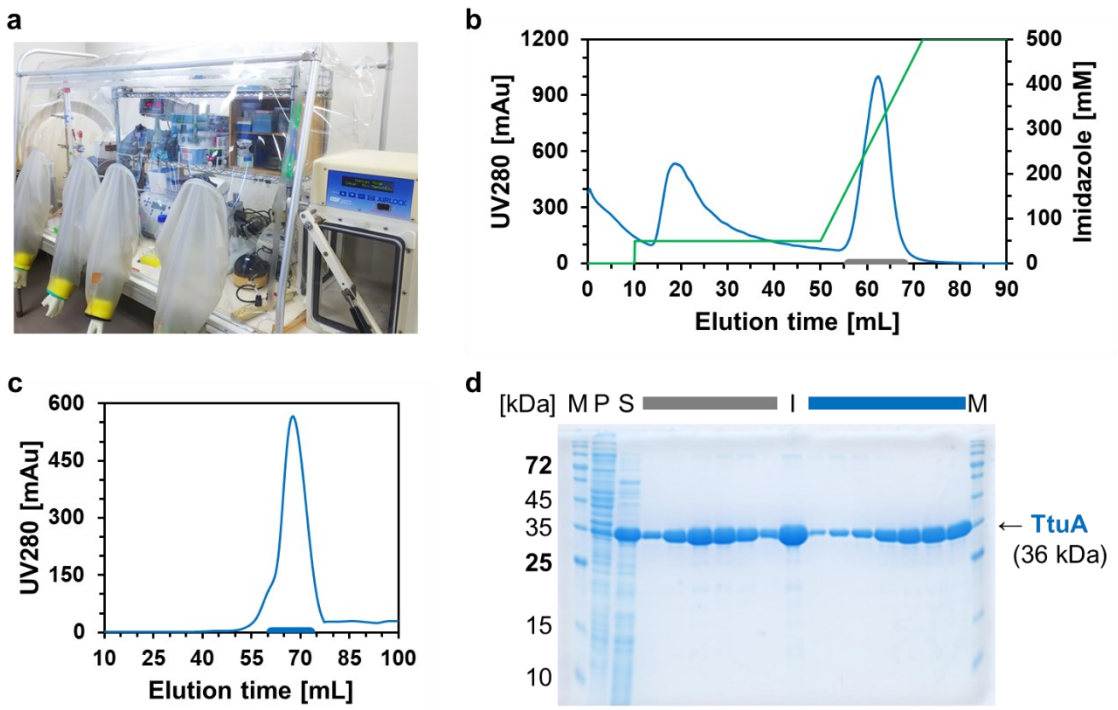

Fig. 2-2 Purification of TtuA (WT) in the anaerobic conditions.

(**a**) Vinyl Anaerobic Chamber (COY). (**b**) NiAC spectrum measured at wavelength of 280 nm (UV280). The collected sample was indicated in the gray band. (**c**) SEC spectrum measured at UV280. The collected sample was indicated in the blue band. (**d**) 12.5% (v/v) SDS-PAGE stained with CBB-G250. The two bold numbers indicate the molecular mass of reference bands of the PM1500 marker (SMOBIO). Sample M, P, S, and I are marker, precipitant of *E. coli* cells, supernatant, and injection to the SEC column, respectively.

2-3. Purification of thiocarboxylated TtuB (TtuB-COSH)

I sonicated the collected cells for 30 min in the purification buffer (20 mM Tris-HCl (pH 8.5 at 25°C) and 500 mM NaCl) with 0.1% Triton X-100, 0.5 mg/mL lysozyme (Sigma), and 0.1 mg/mL DNase I (Sigma). The precipitates were removed by centrifugation at 40,000 × *g* for 30 min and a 0.22-µm filter (Fig. 2-3a, lane P). The supernatant was loaded onto a chitin resin (New England BioLabs) equilibrated with the purification buffer (Fig. 2-3a, lanes S and F). Non-specifically bound proteins were removed using 20 column volumes (CV) of the purification buffer (Fig. 2-3a, lane W). To cleave the intein tag from the TtuB-intein fusion protein, 1 CV of the purification buffer containing 50 mM ammonium sulfide ($(NH_4)_2S$) was added to the chitin resin and incubated at room temperature (RT) for 20 hours.

TtuB was eluted in a 7°C cold room with the purification buffer and then concentrated using an Amicon Ultra Centrifugal Filter (3-kDa cutoff). Excess $(NH_4)_2S$ was removed with the Sephadex PD-10 desalting column (GE Healthcare) equilibrated with the storage buffer (14 mM Tris-HCl (pH 8.5) at 25°C, 350 mM NaCl, and 30% (v/v) glycerol). The fractions containing TtuB were collected, concentrated using an Amicon Ultra Centrifugal Filter (3-kDa cutoff), and stored at -80°C. I confirmed the purity of TtuB by 15% (v/v) SDS-PAGE similar to TtuA (Fig. 2-3a, lane E). Note that the intein tag was removed from the C-terminus of TtuB without protease treatment[110].

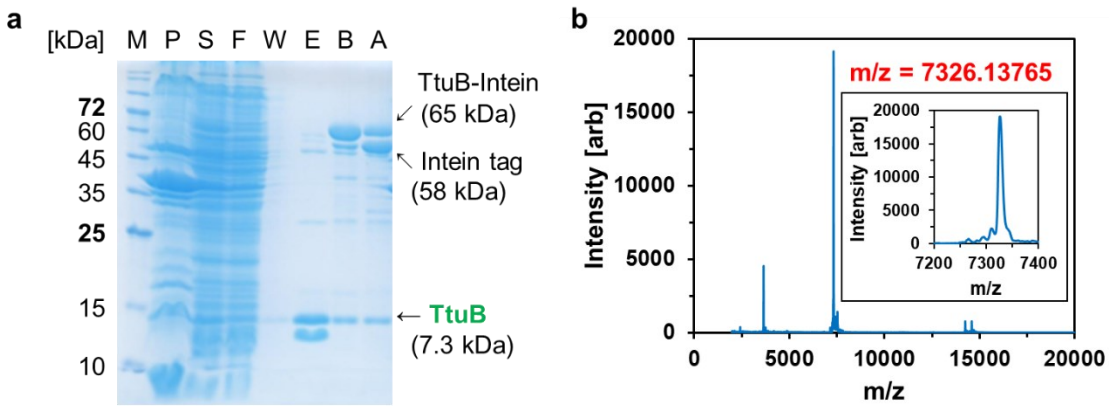

Fig. 2-3 Purification of TtuB-COSH.

(**a**) 15% (v/v) SDS-PAGE stained with CBB-G250. The two bold numbers indicate the molecular mass of reference bands of the PM1500 marker. Sample M, P, S, W, E, B, and A are a marker, a precipitant of *E. coli* cells, supernatant, flow-through, wash, elution,

before the cleavage reaction, and after the cleave reaction, respectively. (**b**) Overall and enlarged MALDI-TOF MS spectra showed that the C-terminus of TtuB is not carboxylate group (m/z = 7310.32), but thiocarboxylate group (m/z = 7326.43).

To confirm the presence of sulfur at the C-terminus of TtuB, I removed salts from TtuB solution on ice with the C4 ZipTip (Millipore) and performed matrix-assisted laser desorption/ionization-time-of-flight mass spectrometry (MALDI-TOF MS) using UltraflexIII (Bruker) with sinapinic acid as the matrix[72]. The concentration of TtuB was determined by the Bradford method[111] using Protein Assay Dye Reagent Concentrate (Bio-Rad) because *Tth*TtuB does not contain tyrosine and tryptophan.

2-4. Reconstitution of [4Fe-4S]-TtuA and [3Fe-4S]-TtuA

All steps to reconstitute [4Fe-4S]-TtuA and [3Fe-4S]-TtuA were performed under strictly anaerobic conditions (Fig. 2-2a). Firstly, I measured the concentration of eluted TtuA after SEC with the Nanodrop DU 1000 U (Thermo Fisher). To incorporate [4Fe-4S] into TtuA, I incubated TtuA with 5 mM dithiothreitol (DTT) for 10 min at RT. Then, I added 9-fold molar excess of ferric chloride ($FeCl_3$) to the solution and incubated the mixture for a further 10 min at RT. Subsequently, 9-fold molar excess sodium sulfide (Na_2S) was added and the mixture was incubated for 3 hours at RT. The precipitate of iron sulfide was removed by centrifugation at 7,000 × *g* for 10 min and a 0.22-µm filter. [4Fe-4S]-TtuA was concentrated using an Amicon Ultra Centrifugal Filter (30-kDa cutoff). Excess $FeCl_3$ and Na_2S were removed using the Sephadex PD-10 desalting column equilibrated with the purification buffer (Fig. 2-4a).

To remove the unique Fe and produce [3Fe-4S]-TtuA, I added 6-fold molar excess $K_3[Fe(CN)_6]$ to [4Fe-4S]-TtuA and incubated the mixture at RT for 10 min. The precipitates were removed using centrifugation at 7,000 × *g* for 30 sec and a 0.22-µm filter. $K_3[Fe(CN)_6]$ and free Fe were removed with a Sephadex PD-10 desalting column equilibrated with the purification buffer (Fig. 2-4b). Notably, I used oxidized TtuA immediately for EPR spectroscopy or activity assay due to the instability of [3Fe-4S]-TtuA.

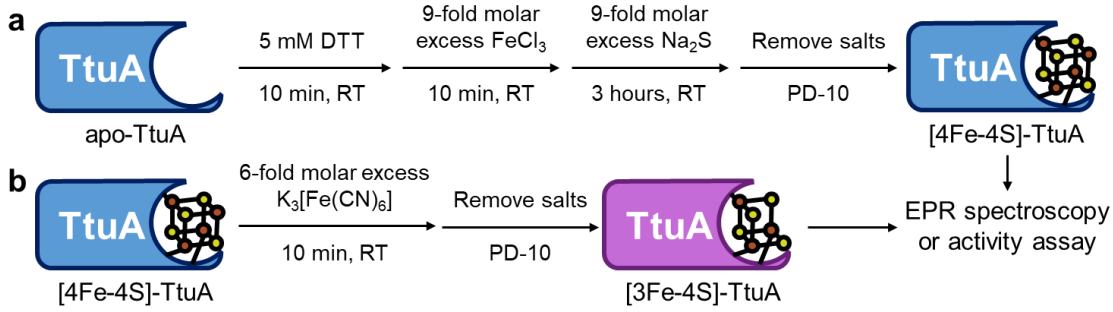

Fig. 2-4 Reconstitution of TtuA with an Fe-S cluster in the anaerobic chamber. Reconstitution of (**a**) [4Fe-4S]-TtuA using an excess amount of iron and sulfur sources under reduced conditions and (**b**) [3Fe-4S]-TtuA using an excess amount of oxidant, $K_3[Fe(CN)_6]$.

2-5. Structural determination of Fe-S clusters by time-course EPR spectroscopy

To analyze the structure of the Fe-S cluster bound to TtuA in time-course, I prepared EPR samples under strictly anaerobic conditions. Because $[4Fe\text{-}4S]^{2+}$ and Fe^{2+} are EPR-silent, I evaluated $[4Fe\text{-}4S]^{1+}$, $[3Fe\text{-}4S]^{1+}$, and free Fe^{3+} using EPR spectroscopy to determine the structure of the Fe-S cluster in TtuA. I transformed reconstituted $[4Fe\text{-}4S]^{2+}$-TtuA into $[4Fe\text{-}4S]^{1+}$-TtuA with a reductant, dithionite (DT) to obtain the spectra of [4Fe-4S]-TtuA[72] and evaluated $[3Fe\text{-}4S]^{1+}$ and free Fe^{3+} for oxidized [4Fe-4S]-TtuA (Fig. 2-5).

Immediately after [3Fe-4S]-TtuA was prepared, I divided fresh 0.5 mM [3Fe-4S]-TtuA into 14 samples (200 μL/sample). For analyzing [3Fe-4S]-TtuA, DT was not added to the sample 5 min after preparation of [3Fe-4S]-TtuA (sample 1). To analyze [4Fe-4S]-TtuA, I added 5-fold molar excess DT to the sample 5 min after preparation of [3Fe-4S]-TtuA (sample 2) and incubated the sample at 25°C for 10 min. To prevent degradation of the Fe-S clusters, samples 1 and 2 were aliquoted into quartz EPR tubes (Agri) and frozen simultaneously with liquid N_2 in the anaerobic chamber. Similarly, I froze samples 10 min (samples 3 and 4), 20 min (samples 5 and 6), 30 min (samples 7 and 8), 1 hour (samples 9 and 10), 2 hours (samples 11 and 12), and 24 hours (samples 13 and 14) after preparation of [3Fe-4S]-TtuA (Fig. 2-6). Moreover, 200 μL of 0.5 mM [4Fe-4S]-TtuA was frozen as control to analyze the amount of [4Fe-4S]-TtuA before oxidation (sample 0).

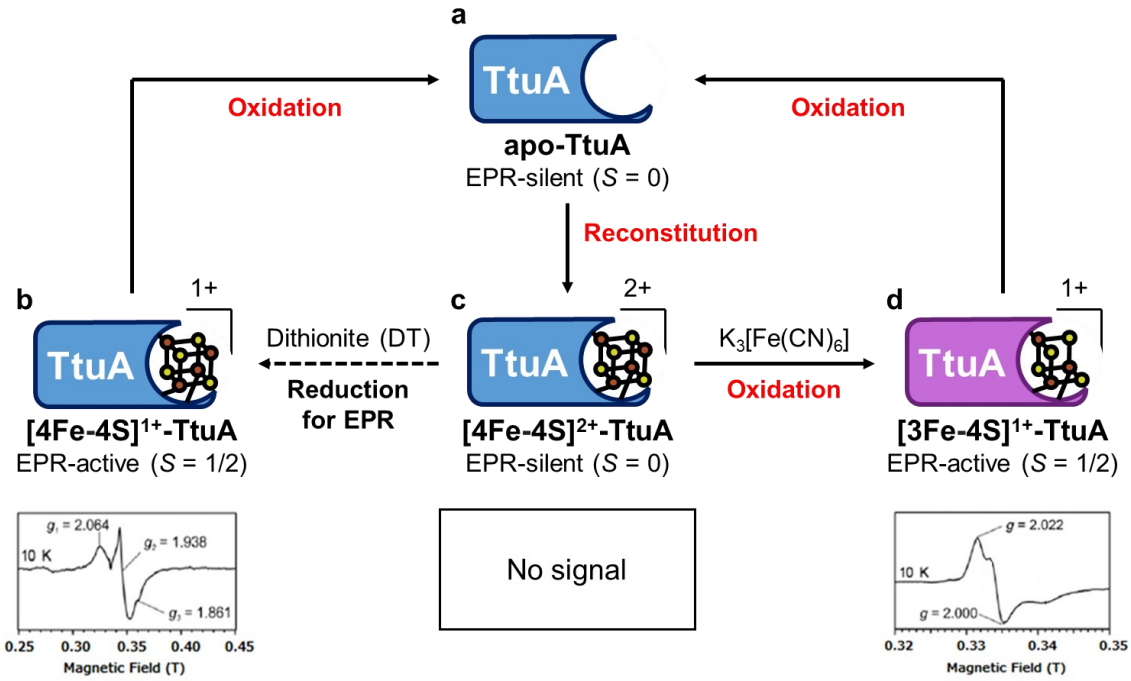

Fig. 2-5 Redox states of TtuA and their detectability by EPR spectroscopy.

(**a**) Reconstructed TtuA is +2 charged with spin quantum number $S = 0$ and EPR-silent. (**b**) Reduction using DT enables EPR detection of [4Fe-4S]-TtuA as +1 charged state. (**c**) The normal state of TtuA with $[4Fe\text{-}4S]^{2+}$. (**d**) Oxidation with $K_3[Fe(CN)_6]$ enables EPR detection of [3Fe-4S]-TtuA. These EPR spectra were cited from our previous research[72].

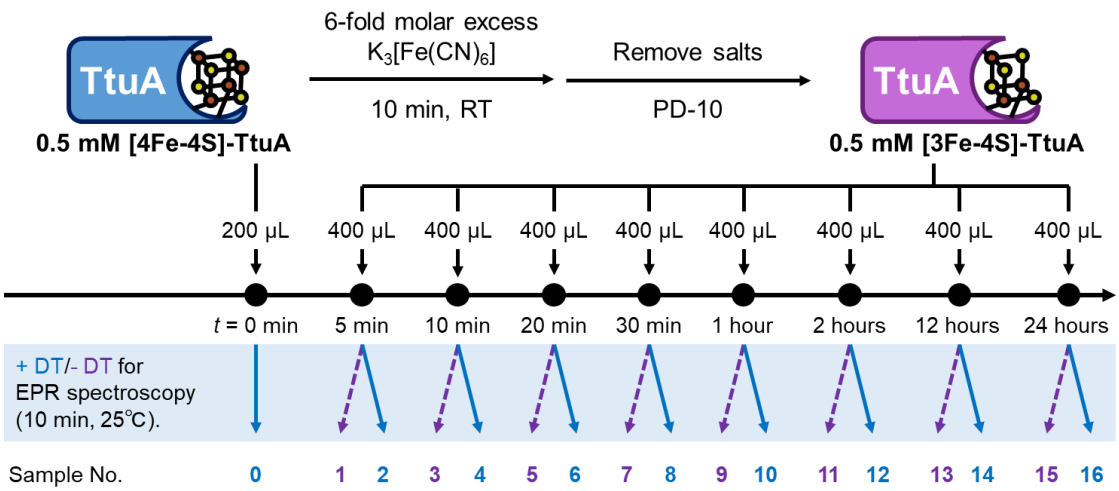

Fig. 2-6 Anaerobic preparation of EPR samples in time-course[112].

Even-numbered EPR samples contain DT to evaluate [4Fe-4S] (blue solid arrows). Odd-numbered EPR samples do not contain DT to evaluate [3Fe-4S] (purple dashed arrows).

2-6. Interaction analysis between TtuA and TtuB by EPR spectroscopy

To analyze the interaction between [3Fe-4S]-TtuA and TtuB-COSH, I prepared EPR samples using a slightly modified version of our protocol[83]. Fresh [3Fe-4S]-TtuA was mixed with TtuB to a final concentration of 0.5 mM and incubated at RT for 5 min under strictly anaerobic conditions. The sample mixture was incubated with a 5-fold molar excess DT at RT for 10 min, aliquoted into quartz EPR tubes, and frozen with liquid N_2 in the anaerobic chamber. The EPR samples were stored in liquid N_2 and transported to the Center for Experimental Science and Analysis at Saga University or Institute for Molecular Science in Okazaki. Continuous wave (CW) X-band EPR spectra were measured with parameters described in the original paper[112].

To quantify [4Fe-4S] and [3Fe-4S] in each sample, I double-integrated the EPR spectra with the peak areas of [4Fe-4S] and [3Fe-4S]. For estimating the maximum amount of [3Fe-4S] regardless of the quick structural change of [3Fe-4S] to [4Fe-4S], I plotted the signal intensity of [3Fe-4S] versus time after oxidation, and then performed linear approximation by using samples up to 120 min after oxidation. I calculated the R^2 value with Microsoft Excel 2019 and found that the result (0.9276) was reliable.

2-7. Activity assay for [3Fe-4S]-TtuA and [4Fe-4S]-TtuA by HPLC

The formation of m^5s^2U54 on substrate tRNA was conducted under strictly anaerobic conditions[83]. The standard assay was performed in 30 μL of reaction buffer (50 mM HEPES-KOH (pH 7.6), 100 mM KCl, 10 mM $MgCl_2$, and 0.1 mM DTT) containing 2.5 μM TtuA, 15 μM brewer's yeast total tRNA (Sigma), 15 μM TtuB, and 5 mM ATP at 60°C for 10 min or 30 min. Because [3Fe-4S] in TtuA quickly transforms into [4Fe-4S], it was necessary to initiate tRNA-thiolation immediately after removing $K_3[Fe(CN)_6]$ from the TtuA solution and limit reaction time. In our previous study, I incubated 4-fold molar excess of TtuB (20 μM) with 5 μM of TtuA at 60°C for 30 min[83]. In this study, I obtained a final concentration of 2.5 μM for TtuA and analyzed the time-course of enzymatic activity (Fig. 2-7). To detect enzymatic activity even at low concentrations of TtuA and short reaction times, I added 6-fold molar excess of TtuB (15 μM).

tRNA-thiolation was stopped with 120 μL stop buffer (75 μL Isogen (Nippon Gene) and 45 μL deionized water) and then frozen at -30°C until tRNA extraction. tRNA was

extracted with phenol:chloroform (5:1 (pH 4.5); Thermo Fisher), precipitated with ethanol, and digested at 37°C for 4 hours with digestion buffer (100 mM HEPES-NaOH (pH 7.5)) containing 6.2 mU/μL nuclease P1 (Yamasa) and 5.0 mU/μL bacterial alkaline phosphatase (Takara Bio). The digested samples were loaded onto the Inertsil ODS-3 column (2.1 mm × 150 mm × 3 μm; GL Science) equilibrated with high-performance liquid chromatography (HPLC) buffer (0.1% formic acid and 2% acetonitrile). m^5s^2U was eluted with a gradient of 2%-36% acetonitrile. The amount of m^5s^2U was detected with UV280 using the Extrema HPLC system (Jasco) (Fig. 2-8).

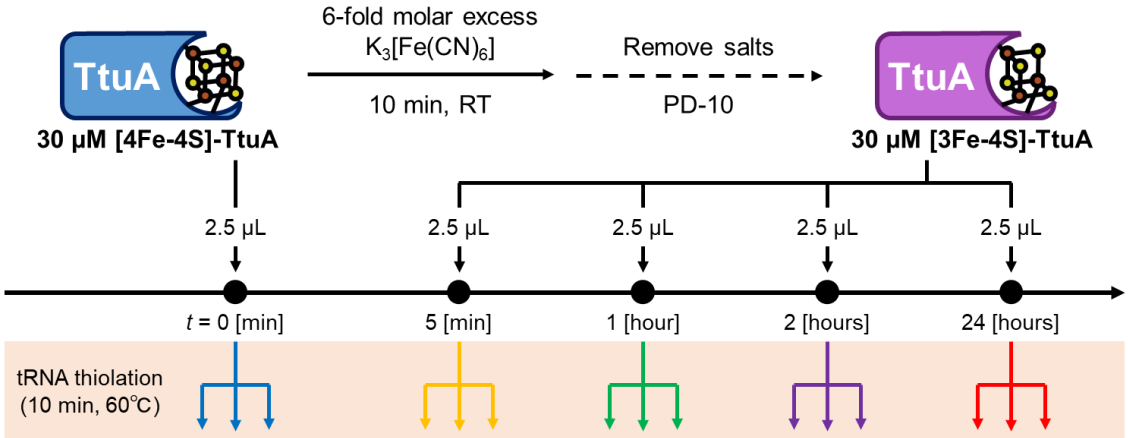

Fig. 2-7 Anaerobic preparation of samples for time-course activity assay.
The enzymatic reaction was started at 60°C for 10 min immediately after the preparation of [3F4-S]-TtuA. Desalination is an optional step. All assays were performed three times.

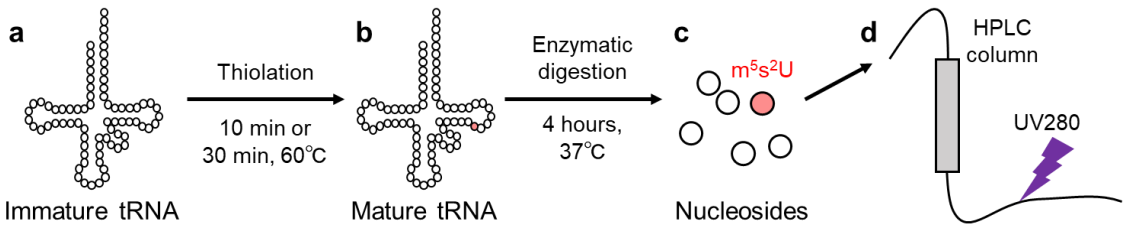

Fig. 2-8 Scheme of activity assay of TtuA by HPLC.
(**a**) tRNA without m^5s^2U54 modification. (**b**) TtuA with an active form of Fe-S cluster catalyzes m^5s^2U54 synthesis. The reaction time is 10 min for time-course assay using [3Fe-4S]-TtuA and 30 min for mutation assays, respectively. (**c**) Enzymatic digestion of tRNA at 37°C for 4 hours. (**d**) Sample injection to the HPLC column and detect compounds by UV280.

2-8. Desulfurization assay by mercury-gel electrophoresis (APM-PAGE)

To reveal the condition when TtuB releases sulfur from its C-terminus, I performed desulfurization assays by 15% (v/v) SDS-PAGE with 12 μg/mL of [(*N*-Acryloylamino) phenyl]mercuric chloride (APM; Toronto Research Chemicals) in the lower gel (Fig. 2-9a)[104,113]. Since APM is toxic, I performed APM-PAGE using protective masks as well as gloves and lab coats, and experimental tools and waste liquid contaminated by APM were collected properly (Fig. 2-9b). Mercury in APM strongly interacts with sulfur atoms of TtuB, which enables to distinguish between carboxylated TtuB (TtuB-COOH) and thiocarboxylated TtuB (TtuB-COSH) (Fig. 2-9c).

APM-gel was prepared at 25°C (lower gel: 15% acrylamide/bis mixed solution, 360 mM Tris-HCl (pH 8.5), 0.1% SDS, 12 μg/mL APM, upper gel: 4.5% acrylamide/bis mixed solution, 120 mM Tris-HCl (pH 6.0) at 25°C, 0.1% SDS) at RT. Then, I performed APM-PAGE at 20 mA for 80 min in 7°C cold room to stabilize TtuB-COSH. Protein bands were visualized by CBB-G250 stain and detected using the LAS-3000 imaging system (Fujifilm) (Fig. 2-9d).

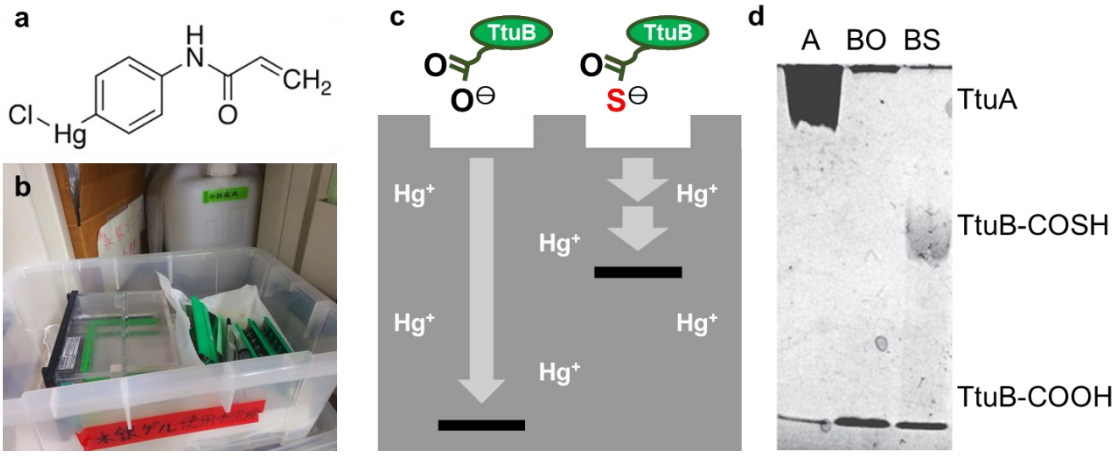

Fig. 2-9 Desulfurization assay by APM-PAGE.

(**a**) Structural formula of AMP. (**b**) Experimental tools. (**c**) Concept of APM-PAGE. (**d**) Visualization of proteins in APM-gel. Sample A, BO, and BS are 600 pmol of [4Fe-4S]-TtuA, TtuB-COOH, and TtuB-COSH, respectively. The image was cited from our original paper[83]. I prepared TtuB-COOH using DTT in the cleavage reaction instead of $(NH_4)_2S$. Note that TtuB-COSH contains a small amount of TtuB-COOH as a byproduct in the cleavage reaction.

2-9. Structural prediction and comparison of tRNA-thiolation enzymes

I downloaded 3D structures models of *Hsa*Ncs6, *Eco*TtcA, and *Mma*ThiI predicted from the AlphaFold Protein Structure Database on 17th November 2022[114]. Since these models do not contain Fe-S clusters, I superimposed the predicted models with [4Fe-4S]-*Tth*TtuA (PDB ID: 5B4F) using the "align" command for Ncs6 and TtcA, whereas I used the "super" command for MnmA (PDB ID: 2DEU) and the PPase domain of *Mma*ThiI (G182-H354) in PyMOL ver1.7. (Fig. 2-10).

Furthermore, I predicted the structure of *Hsa*Ncs6-*Hsa*Urm1 complex using local version of AlphaFold version 2.0 (AF2)[115] with default parameters. I chose one model with the highest reliability based on the predicted local-distance difference test (pLDDT) score among the five predicted structures. To build enzyme-tRNA complex models, I superimposed tRNA-thiolation enzymes with a tRNA-modification enzyme TilS complexed with tRNA (PDB ID: 3A2K) in the same method as our previous study[72]. TilS catalyzes lysidine synthesis at position C34 of $tRNA^{Ile(CAU)}$[116,117].

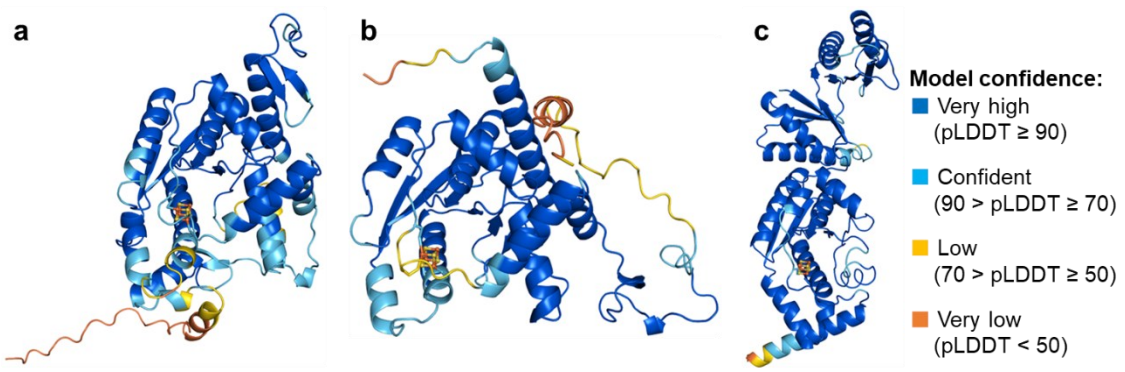

Fig. 2-10 Overall structure of tRNA-thiolation enzymes predicted by AlphaFold2. (**a**) [4Fe-4S]-*Hsa*Ncs6 model. (**b**) [4Fe-4S]-*Eco*TtcA model. (**c**) [4Fe-4S]-*Mma*ThiI model. To visualize the reliability of predicted structures, regions other than [4Fe-4S] were colored based on the pLDDT score (pLDDT ≥ 90 in blue, 90 > pLDDT ≥ 70 in cyan, 70 > pLDDT ≥ 50 in yellow, pLDDT < 50 in orange, respectively). The Cα RMSD between each AF2 model and *Tth*TtuA is 1.314 Å (for *Hsa*Ncs6), 2.173 Å (for *Eco*TtcA), and 2.766 Å (for *Mma*ThiI), respectively.

Chapter 3. Results

3-1. [3Fe-4S]-TtuA spontaneously and quickly transforms into [4Fe-4S]-TtuA

The EPR spectra of fresh oxidized TtuA showed a peak of $[3Fe\text{-}4S]^{1+}$ (g = [2.02, 2.01, 1.97]) (Fig. 3-1a)[72] and that of free Fe^{3+} (g = 4.3) (Fig. 3-1b)[118]. Considering that free Fe and excess $K_3[Fe(CN)_6]$ were removed by desalination, free Fe should come from [3Fe-4S]-TtuA. Notably, signal intensity of $[3Fe\text{-}4S]^{1+}$ and free Fe decreased with time after desalination under strictly anaerobic conditions (Fig. 3-1a, 3-1b). This observation indicated that [3Fe-4S] cluster in TtuA is unstable and quickly transforms into [4Fe-4S]. Even I skipped the desalination in the preparation of [3Fe-4S]-TtuA (which means that the solution contains free Fe and excess $K_3[Fe(CN)_6]$), the signal intensity of $[3Fe\text{-}4S]^{1+}$ decreased similar to that after removing excess free Fe and $K_3[Fe(CN)_6]$ (Fig. 3-2).

Furthermore, to evaluate the amount of [4Fe-4S] in all the test samples, I reduced the samples with DT and analyzed their EPR spectra. The signal intensity of $[4Fe\text{-}4S]^{1+}$ increased with time (Fig. 3-1c). The DT addition to the solution did not affect the conformational change of Fe-S clusters in TtuA (Fig. 3-2c).

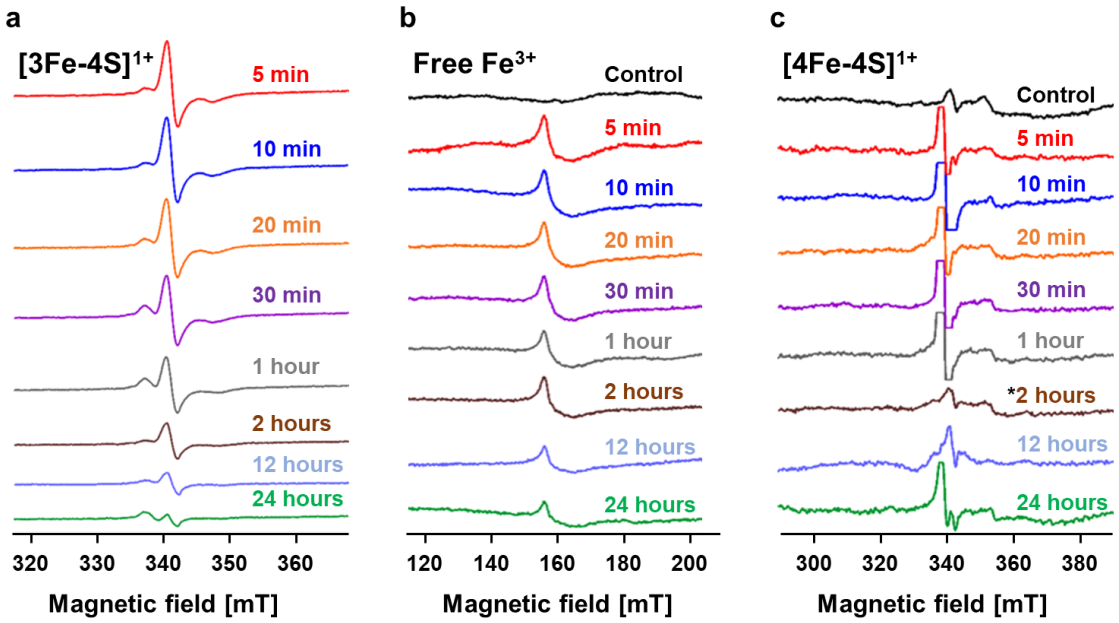

Fig. 3-1 EPR spectra of TtuA oxidized with $K_3[Fe(CN)_6]$[112].

Signal peak of (**a**) $[3Fe\text{-}4S]^{1+}$ measured at 40 K, (**b**) free Fe^{3+} measured at 40 K, and (**c**) $[4Fe\text{-}4S]^{1+}$ measured at 12 K. An asterisk (*) in Fig. 3-1c indicates a weak signal with a relatively lager experiment error.

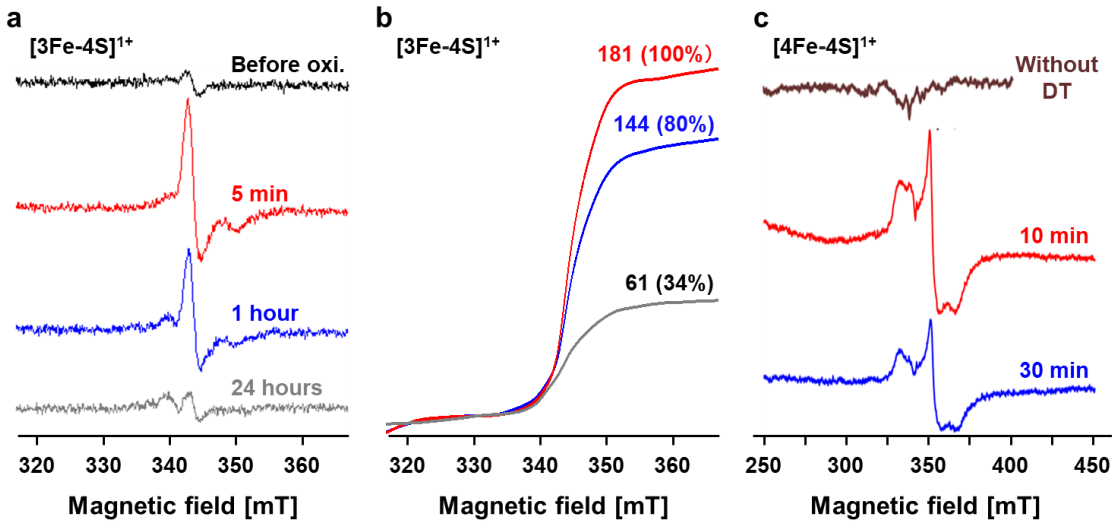

Fig. 3-2 Effect of excess $K_3[Fe(CN)_6]$ and DT in EPR samples of TtuA[112].

(**a**) [4Fe-4S]-TtuA was oxidized to [3Fe-4S]-TtuA with excess $K_3[Fe(CN)_6]$ (without desalination) and incubated for 5 min (red), 1 hour (blue), and 24 hours (gray). The sample before oxidation ([4Fe-4S]-TtuA) was used as a reference (black). $[3Fe\text{-}4S]^{1+}$ was detected in the absence of DT at 40 K. (**b**) Double integration of Fig. 3-2a. The ratio of signal intensity is shown in parentheses, where the intensity at 5 min after oxidation is normalized to 100%. (**c**) Spectroscopic characterization of TtuA with excess DT. EPR spectra of [4Fe-4S]-TtuA before DT reduction (brown) and reduced with DT and incubated for 10 min (red) and 30 min (blue). $[4Fe\text{-}4S]^{1+}$ were detected with DT at 12 K.

Next, I analyzed the amount of [4Fe-4S] and [3Fe-4S] in the time-course EPR spectroscopy (Fig. 3-3a). Since quantifying the amount of [3Fe-4S] immediately (0 min) after oxidation is challenging due to experimental limitations, I estimated an approximate line correlation coefficient of 3.877 for the signal intensity of [3Fe-4S] as a standard value to calculate the amount of [3Fe-4S] (Fig. 3-3b). When the amount of [4Fe-4S] is normalized to 100% in TtuA before oxidation, [3Fe-4S]-TtuA was estimated to contain ~10% [4Fe-4S] after 5 min of oxidation. Nearly one-third of [3Fe-4S]-TtuA transformed into [4Fe-4S]-TtuA after 1 hour of oxidation (Table 3-1). The collapse of [3Fe-4S] and a corresponding increase in [4Fe-4S] indicated that the unstable [3Fe-4S] cluster of [3Fe-4S]-TtuA spontaneously transformed into stable [4Fe-4S] ([4Fe-4S]-TtuA) within one hour.

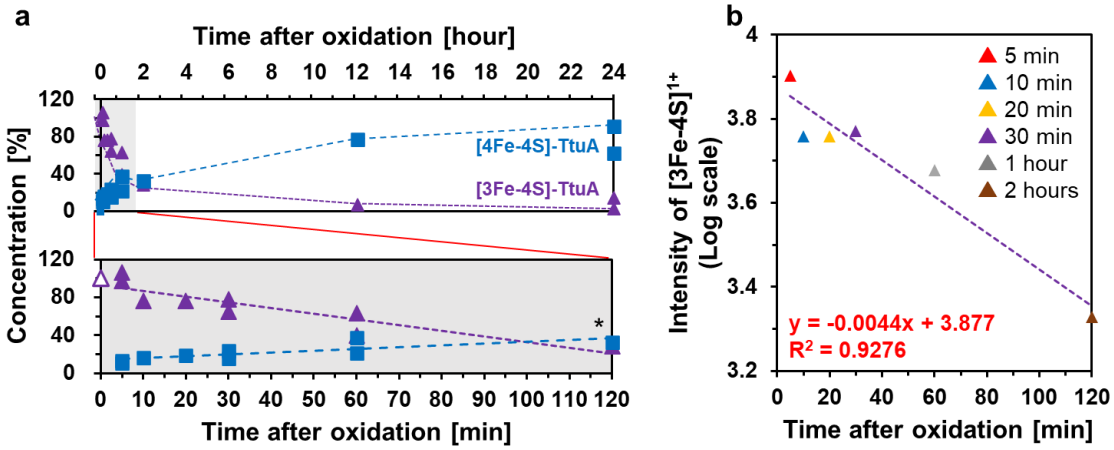

Fig. 3-3 Quantification of the structural changes in the Fe-S cluster in TtuA[112].
(**a**) The plot of structural changes of Fe-S clusters in time-course, which was calculated from Fig. 3-1a and c. An asterisk (*) in Fig. 3-3a indicates a weak signal with a relatively lager experiment error. (**b**) Calibration curve of the signal intensity of $[3Fe\text{-}4S]^{1+}$ versus time after oxidation. Each point is colored in the same as Fig. 3-1.

Table 3-1. Spectroscopic quantification of the Fe-S cluster in TttuA[112].

Time after oxidation	[3Fe-4S]	[4Fe-4S]
Before oxidation	—	100%
Immediately after oxidation (0 min)	(100%)	—
5 min†	99%±7%	12%±1%
10 min	76%	16%
20 min	76%	19%
30 min†	70%±8%	20%±4%
1 hour†	50%±13%	30%±8%
2 hours*	28%	33%
12 hours	7%	77%
24 hours†	9%±6%	77%±14%

EPR measurements were performed twice under condition marked with daggers (†) and one time without the dagger. The standard deviation was calculated by $N = 2$. The parentheses indicate the estimated amount from the calibration curve (Fig. 3-3b). The asterisk (*) indicates a weak signal with a relatively lager experiment error.

3-2. [3Fe-4S]-TtuA is an inactive form in tRNA thiolation

To analyze the enzymatic activity of [3Fe-4S]-TtuA, I performed activity assays of TtuA in time-course under strictly anaerobic conditions. Since [3Fe-4S] transforms into [4Fe-4S] within one hour (Fig. 3-3a), limiting reaction time is essential. I optimized the reaction conditions, including TtuA and TtuB concentrations and temperature, to monitor enzymatic activity in a relatively short reaction time.

I measured the yield of m^5s^2U54 using oxidized [4Fe-4S]-TtuA in the presence and absence of $K_3[Fe(CN)_6]$. Whereas m^5s^2U was detectable using [4Fe-4S]-TtuA, nearly no m^5s^2U was synthesized 5 min after oxidation, indicating that [3Fe-4S]-TtuA has no enzymatic activity. By contrast, the amount of m^5s^2U synthesized by TtuA increased with time (1, 2, and 24 hours after oxidation) regardless of whether excess $K_3[Fe(CN)_6]$ was removed from the solution or not (Fig. 3-4). When the enzymatic activity of TtuA before oxidation was normalized to 100%, it recovered 30%-50% in 1 hour, >50% in 2 hours, and 60%-80% in 24 hours (Table 3-2). Combining these results with EPR results, according to which [3Fe-4S] transformed into [4Fe-4S] with time (Fig. 3-3a, Table 1), it is clear that TtuA showed higher activity as the amount of [4Fe-4S] in TtuA increased.

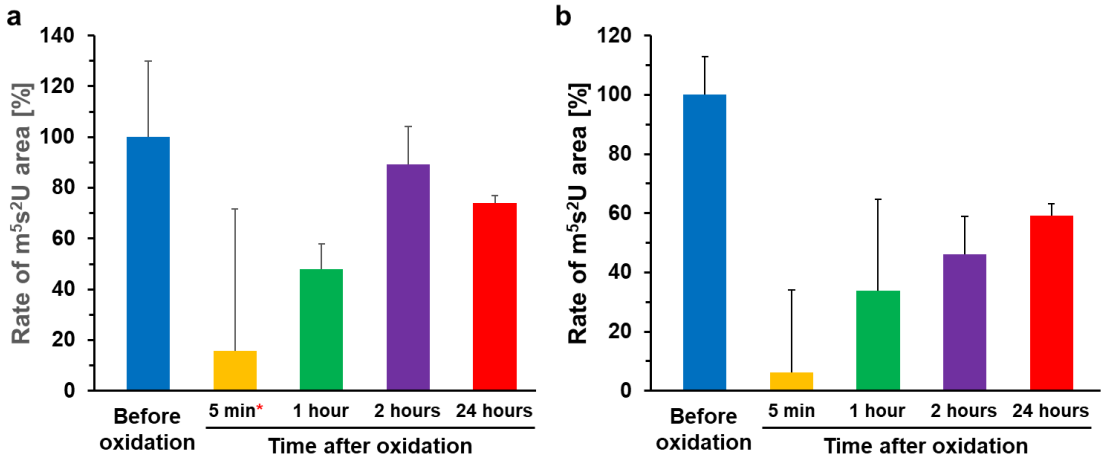

Fig. 3-4 Activity assay of [3Fe-4S]-TtuA and [4Fe-4S]-TtuA[112].

Enzymatic activity of TtuA in the absence (**a**) and presence (**b**) of $K_3[Fe(CN)_6]$. The tRNA-thiolation activity of TtuA before oxidation was normalized to 100%. All data are presented with standard deviation (SD) values (N = 3, red asterisk (*): one time was measured from a different lot and scaling by the activity of [Before oxidation]). The quantification result of this assay is shown in Table 3-2.

Table 3-2. Quantification of the activity of [3Fe-4S]-TtuA and [4Fe-4S]-TtuA[112].

Time after oxidation	Enzymatic activity without $K_3[Fe(CN)_6]$	Enzymatic activity with $K_3[Fe(CN)_6]$
Before oxidation	100% ± 30%	100% ± 13%
5 min	16 ± 56%*	6% ± 28%
1 hour	48% ±10%	34% ± 31%
2 hours	89% ± 15%	46% ± 13%
24 hours	74% ± 3%	59% ± 4%

All data were measured three times and shown with standard deviation. Asterisk (*): one time was measured from a different lot and scaling by the activity of [Before oxidation].

3-3. The unique Fe in [4Fe-4S]-TtuA is required to bind the C-terminus of TtuB

To reveal the detailed function of the unique Fe in [4Fe-4S]-TtuA and evaluate why [3Fe-4S]-TtuA is inactive, I performed EPR spectroscopy of TtuA with TtuB-COSH and each type of Fe-S cluster. The EPR spectra of [3Fe-4S]-TtuA (freshly oxidized [4Fe-4S]-TtuA) showed a peak of $[3Fe\text{-}4S]^{1+}$ ($g \sim 2.01$), which supported that the unique Fe is absent (Fig. 3-5a). Then, I measured the EPR spectra of [3Fe-4S]-TtuA with TtuB-COSH and found that there is no significant difference in the spectra between [3Fe-4S]-TtuA alone and [3Fe-4S]-TtuA with TtuB-COSH (Fig. 3-5a). On the other hand, the addition of TtuB-COSH to [4Fe-4S]-TtuA changed the shape and intensity of the EPR spectra, showing the change in the redox potential when the thiocarboxylate group at the C-terminus of TtuB-COSH binds to [4Fe-4S]-TtuA (Fig. 3-5b)[83].

Now, the structure of [4Fe-4S]-TtuA-TtuB complex shows that the C-terminus of TtuB directly coordinates with the unique Fe of [4Fe-4S]-TtuA (Fig. 1-17b)[83]. Furthermore, the superposition of the structures of [4Fe-4S]-TtuA-TtuB and apo-TtuA-TtuB showed that the [4Fe-4S] cluster does not affect the interaction of TtuA and TtuB except for the C-terminus of TtuB-COSH (Fig. 3-6, Fig. 3-7). Therefore, the EPR spectra showed that [3Fe-4S]-TtuA cannot bind to the C-terminus of TtuB-COSH, indicating that the unique Fe of [4Fe-4S]-TtuA is necessary to coordinate with TtuB-COSH for transferring the sulfur atom to the substrate tRNA.

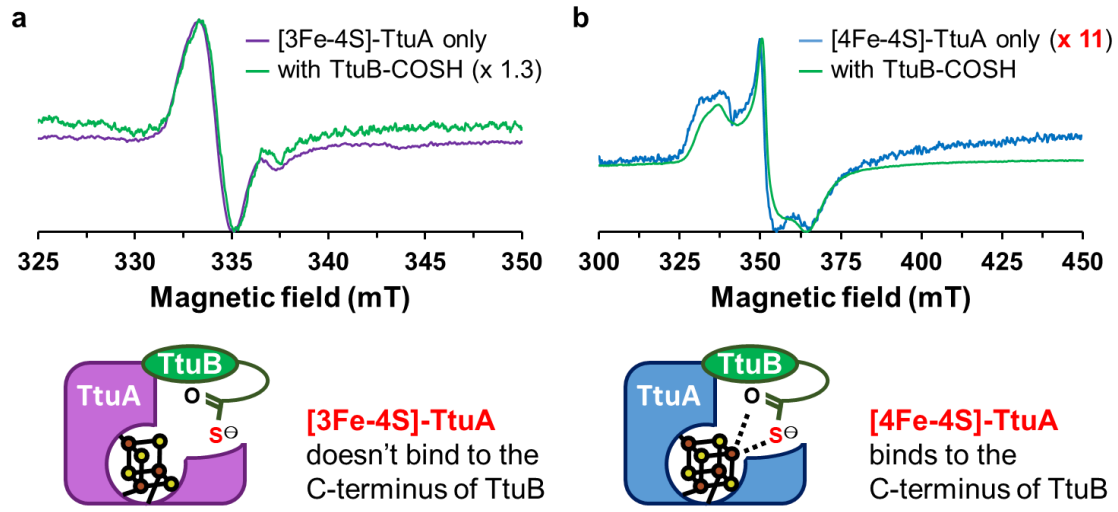

Fig. 3-5 Spectroscopic characterization of [3Fe-4S]-TtuA and [4Fe-4S]-TtuA with or without TtuB-COSH[112].

(**a**) EPR spectra of [3Fe-4S]-TtuA in the absence (purple) and presence (green) of TtuB-COSH. (**b**) EPR spectra of [4Fe-4S]-TtuA in the absence (blue) and presence (green) of TtuB-COSH[83]. The EPR spectra are normalized for comparison by indicated ratio.

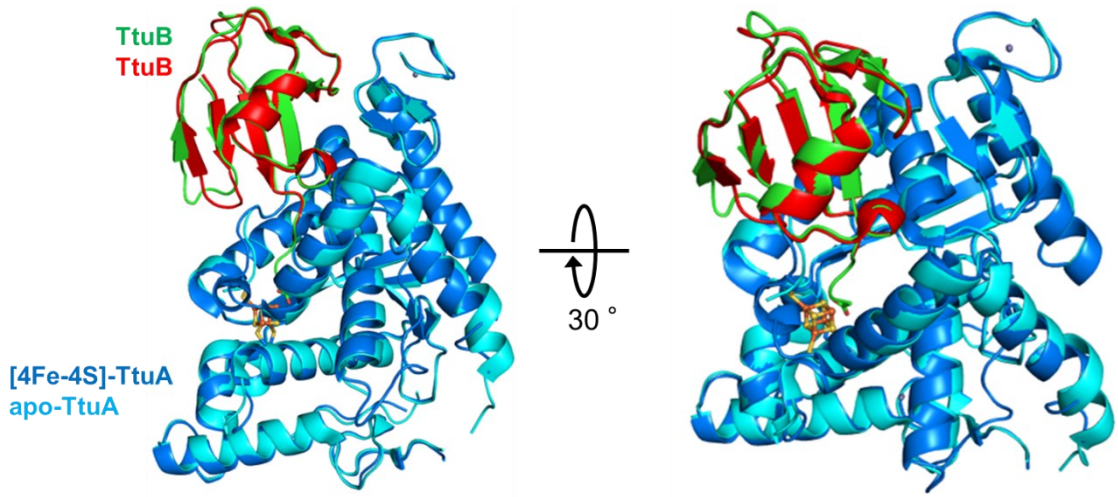

Fig. 3-6 Comparison of the overall structures of the [4Fe-4S]-TtuA-TtuB complex and the apo-TtuA-TtuB complex [112].

TtuA and TtuB-COOH (WT) of the [4Fe-4S]-TtuA-TtuB complex (PDB ID: 5ZTB) are colored in blue and green, respectively[83]. TtuA and TtuB-COOH (G65C) of the apo-TtuA-TtuB complex (PDB ID: 5GHA) are colored in cyan and red, respectively[72]. Cα RMSD value is 0.483 Å, which was calculated by the "align" command of PyMOL ver1.7. The GG motif at the C-terminus of TtuB is disordered when [4Fe-4S] is absent.

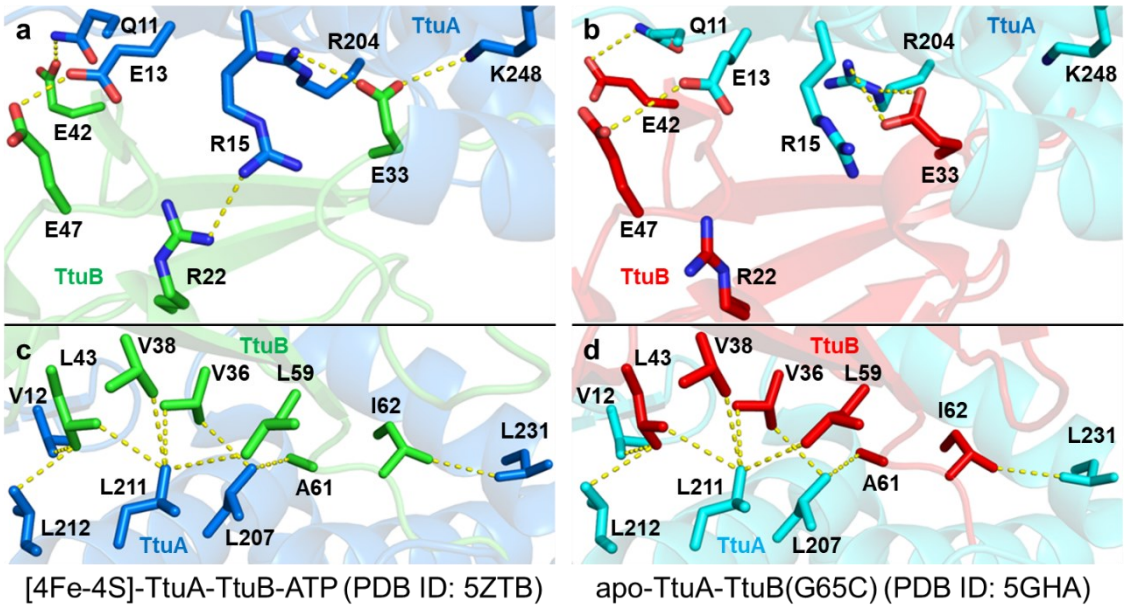

Fig. 3-7 Comparison of the binding site of the [4Fe-4S]-TtuA-TtuB complex and the apo-TtuA-TtuB complex[112].

(**a**) The binding site I and (**c**) site II of the [4Fe-4S]-TtuA-TtuB complex (PDB ID: 5ZTB). TtuA and TtuB-COOH (WT) are colored in blue and green, respectively. (**b**) The binding site I and (**d**) site II of the apo-TtuA-TtuB complex (PDB ID: 5GHA). TtuA and TtuB-COOH (G65C) are colored in cyan and red, respectively. The yellow dashed lines indicate electrostatic or hydrophobic interactions.

3-4. TtuB does not release sulfur before tRNA activation

To understand the catalytic mechanism of [4Fe-4S]-TtuA, I analyzed the conditions under which TtuB releases sulfur from its C-terminus by APM-PAGE. I confirmed that the C-terminus of TtuB was thiocarboxylated (Fig. 3-8a, lane1). Whereas TtuB did not release sulfur in the presence of [4Fe-4S]-TtuA and either tRNA or ATP (Fig. 3-8a lanes 1 and 2), TtuB was desulfurized when [4Fe-4S]-TtuA, tRNA, and ATP were added together and incubated for 10 min or longer (Fig. 3-8a, lanes 5 and 6). I also detected m^5s^2U in conditions that TtuB released sulfur by HPLC (Fig. 3-9b, c). These observations demonstrated that the binding of TtuB-COSH to TtuA is not sufficient for desulfurization, but TtuA, TtuB-COSH, substrate tRNA, and ATP are necessary.

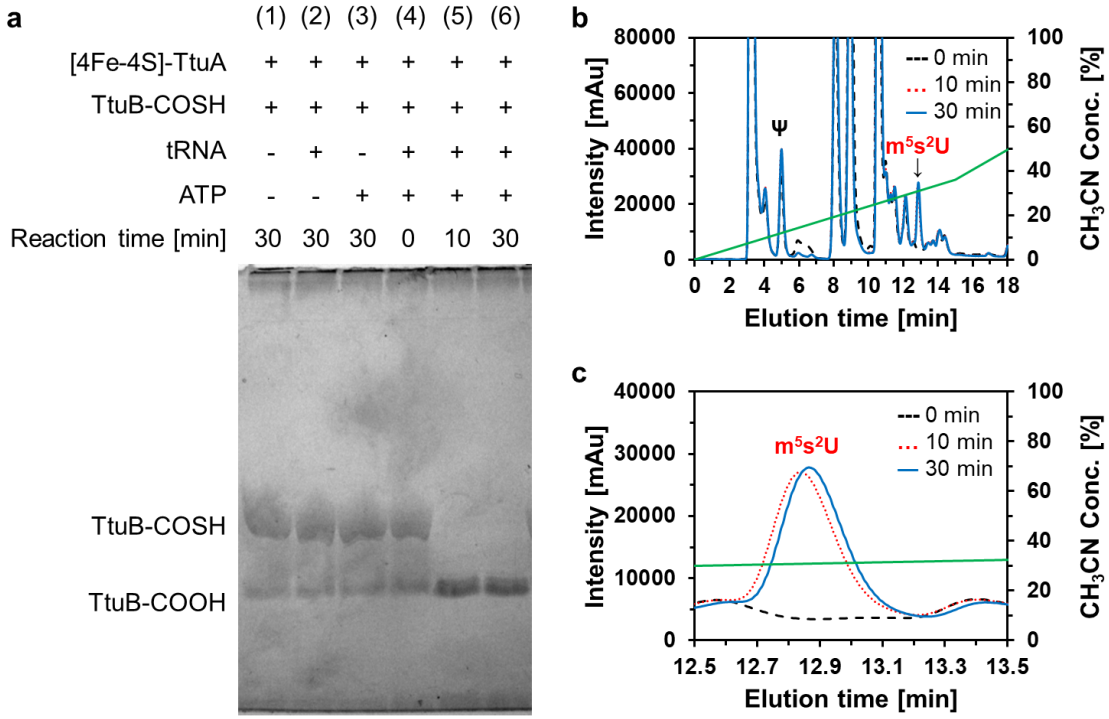

Fig. 3-8 Tracing sulfur atom from C-terminus of TtuB[83].

(**a**) APM-gel for desulfurization assay. (**b**) Overall and (**c**) close-up view of HPLC spectra of desulfurization assay. The HPLC samples 0 min, 10 min, and 30 min were prepared in the same conditions in Fig. 3-8a lanes 4, 5, and 6, respectively. The reference peak of pseudouridine (Ψ) and the product peak of 5-methyl-2-thiouridine (m^5s^2U) are indicated. The green lines indicate the concentration of acetonitrile (CH_3CN).

3-5. Identification of critical residues of TtuA in tRNA thiolation

To identify the critical residues of TtuA for tRNA thiolation, I prepared 10 mutants of TtuA based on the structure of the [4Fe-4S]-TtuA-TtuB-ATP complex (Fig. 3-9a). These residues are conserved and located around the ATP-binding site ($S_{55}GGXDS_{60}$ motif) or the unique Fe of [4Fe-4S]-TtuA. The HPLC spectra showed that the enzymatic activities of S55A, D59A, K137A, and D161A were dramatically decreased (Fig. 3-9b). Furthermore, I evaluated the enzymatic activities of these four mutants in the presence of 10 mM Na_2S instead of TtuB-COSH to identify the catalytic residue of TtuA for desulfurization. Interestingly, only the K137A mutant recovered the activity, showing that Lys137 is essential for the sulfur transition from TtuB to tRNA (Fig. 3-9c). Notably, the

activity of Lys137 was not completely recovered even when Na_2S was supplied, suggesting that Lys137 might be involved in activation of tRNA. This conclusion is also supported by the result of APM-PAGE (Fig. 3-10a).

Interestingly, some organisms have TtuA or Ncs6 with Arg137 instead of Lys137 (the residue number is from *Tth*TtuA) (Fig. 1-28a) and our results of HPLC and AMP-PAGE also showed an enzymatic activity in K137R (Fig. 3-9b, Fig. 3-10). On the other hand, the enzymatic activity of S55A, D59A, and D161A did not recover in the presence of Na_2S. These residues are known to be responsible for ATP binding and hydrolysis[119,120]. Therefore, I concluded that the positively charged residue at position 137 are critical for sulfur transition, and the other three residues activates tRNA (Fig. 3-11).

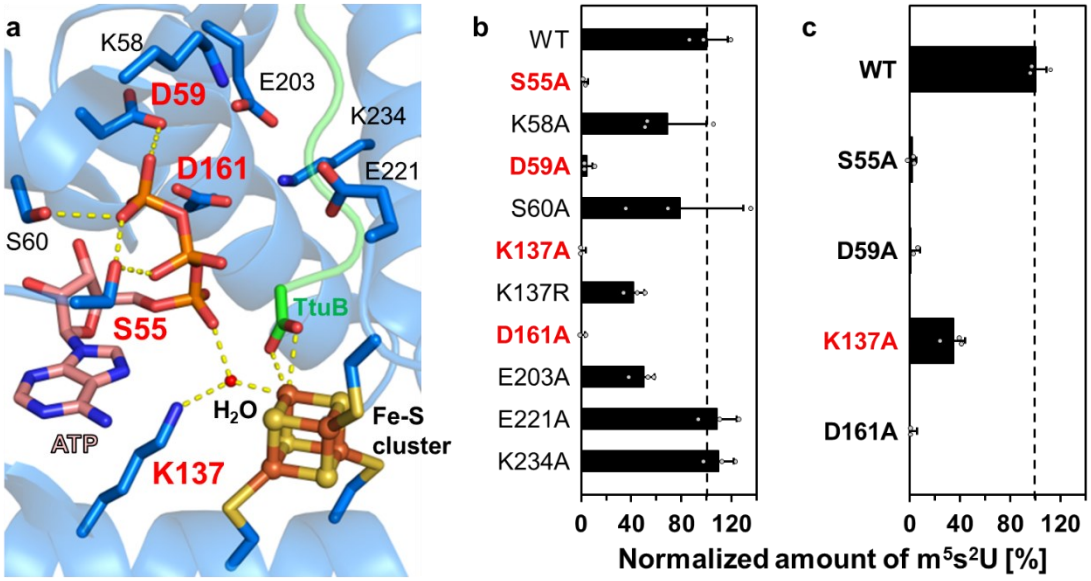

Fig. 3-9 Identification of critical residues of TtuA by HPLC[83].

(**a**) Close-up view of the catalytic site of the [4Fe-4S]-TtuA-TtuB-ATP complex (PDB ID: 5ZTB). The dashed yellow lines indicate hydrogen bonds or coordination bonds. Mutational analysis of TtuA in the presence of (**b**) 20 μM TtuB-COSH and (**c**) 10 mM Na_2S. All activity assays were examined three times and these results were presented with data plots and SD values.

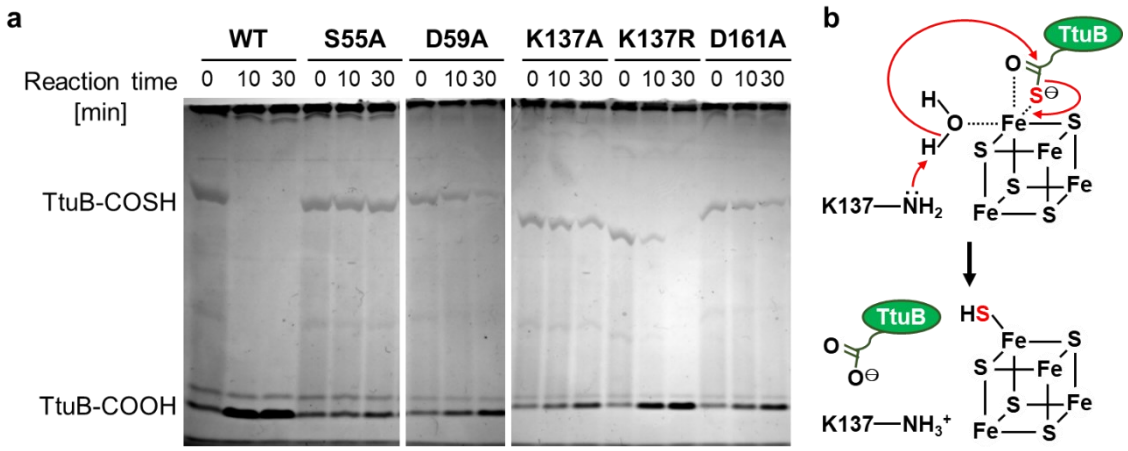

Fig. 3-10 Identification of critical residues of TtuA by APM-PAGE[83].

(**a**) Desulfurization assay of TtuB catalyzed by TuA mutants. (**b**) Proposed mechanism of desulfurization of TtuB catalyzed by Lys137 of TtuA.

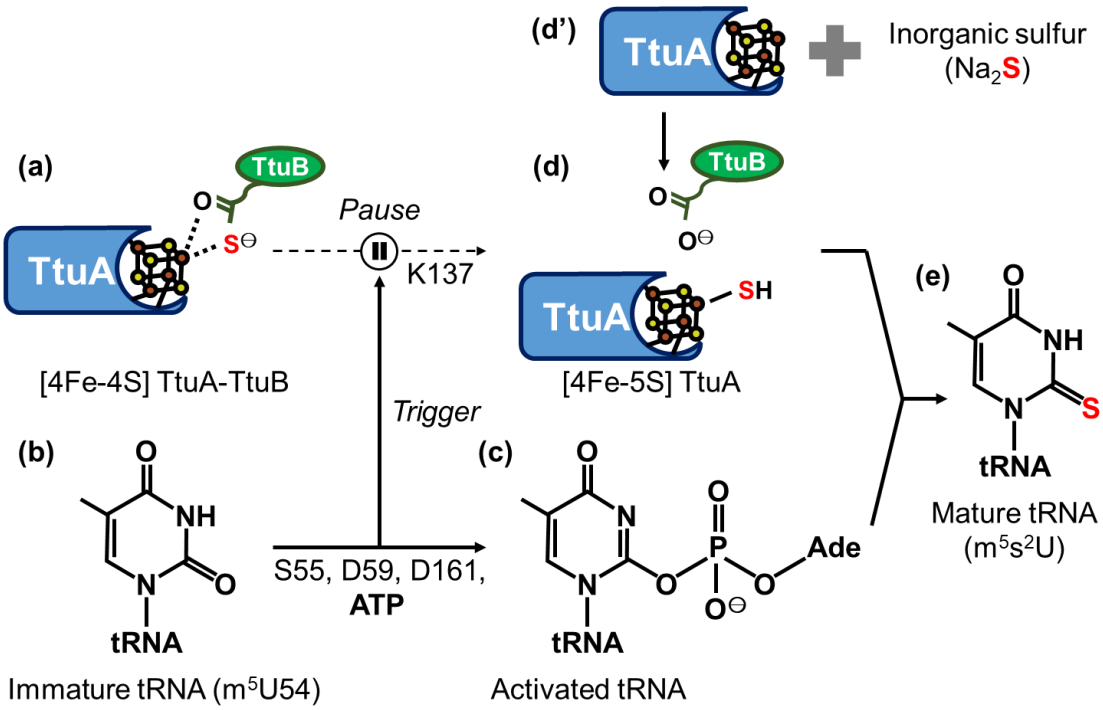

Fig. 3-11 Proposed scheme of 5-methyl-2-thiouridine (m^5s^2U54) biosynthesis[83].

(**a**) Formation of the [4Fe-4S]-TtuA-TtuB complex. TtuB cannot release sulfur from its C-terminus until the activation of tRNA. (**b**) 5-methyl-uridine (m^5U54) is adenylated using ATP involving Ser55, Asp59, and Asp161. (**c**) Adenylated tRNA triggers sulfur transition from TtuB to TtuA. (**d**) [4Fe-5S]-TtuA intermediate is formed by Lys137 or (**d'**) addition of inorganic sulfur source. (**e**) tRNA thiolation is completed.

Chapter 4. Discussion

4-1. [3Fe-4S]-TtuA stores Fe sources for the reconstitution of [4Fe-4S]-TtuA

Fe-S clusters are widely used cofactors and are responsible for various biological roles. Thus, it is necessary to identify the type of Fe-S cluster in the enzyme to understand the catalytic mechanism. To clarify whether TtuA uses [4Fe-4S] only or both [4Fe-4S] and [3Fe-4S], I performed time-resolved EPR spectroscopy under strictly anaerobic conditions. The results showed that [3Fe-4S]-TtuA was unstable and spontaneously transformed into [4Fe-4S]-TtuA within one hour (Fig. 3-3). Furthermore, interaction analysis by EPR spectroscopy demonstrated that [3Fe-4S]-TtuA cannot bind to the C-terminus of TtuB-COSH (Fig. 3-5). The enzymatic activity of [3Fe-4S]-TtuA (oxidized [4Fe-4S]-TtuA) recovered with an increase in [4Fe-4S]-TtuA, but did not completely recover (Fig. 3-4). These observations indicated that the reaction solution contained apo-TtuA, which was generated by the degradation of [3Fe-4S] (Fig. 4-1). Taking our results together, I concluded that only [4Fe-4S]-TtuA has enzymatic activity, and the unique Fe is essential as a binding site for TtuB-COSH for the sulfur transition to tRNA.

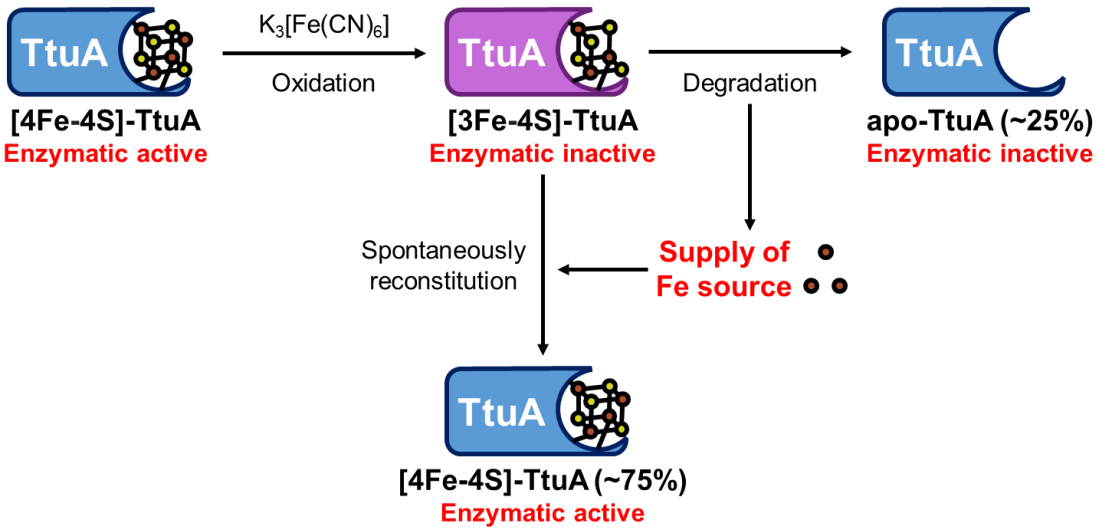

Fig. 4-1 Schematic diagram of the proposed changes of the Fe-S cluster in TtuA[112]. One [3Fe-4S]-TtuA molecule provides three free Fe^{3+} ions with inactive apo-TtuA molecules to form active [4Fe-4S]-TtuA. The parentheses indicate the maximum ratio of apo-TtuA and [4Fe-4S]-TtuA.

Considering that TtuA catalyzes m^5s^2U biosynthesis which is essential for thermophiles to survive under high-temperature environments[18], thermophiles eliminate inactive [3Fe-4S]-TtuA and reconstitute active [4Fe-4S]-TtuA. One of the biological roles of [3Fe-4S] is iron and sulfur source in iron regulatory protein 1 (IRP1)[121]. Thus, the transformation of [3Fe-4S]-TtuA into [4Fe-4S]-TtuA maybe occur *in vivo*, but we need further study to demonstrate the possibility.

4-2. Time-course analyses are essential to identify the exact type of Fe-S clusters

Fe-S clusters are sensitive to oxidation and readily decayed. Their instability sometimes caused incorrect structural determination of Fe-S clusters even with the smallest amount of oxygen contaminant during the experiments (Fig. 1-20). Our findings demonstrated that the Fe-S cluster in TtuA is highly sensitive to redox levels and [3Fe-4S] clusters quickly and spontaneously transform into [4Fe-4S] clusters within one hour, even under strictly anaerobic conditions. Unexpectedly, [3Fe-4S]-TtuA is more unstable than [4Fe-4S]-TtuA even though all of the Fe atoms of [3Fe-4S] are coordinated with cysteines. Hence, misidentification of [3Fe-4S] and [4Fe-4S] easily lead to an improper proposal of the catalytic mechanism of the Fe-S enzyme without the correlation analysis between the structure of Fe-S clusters and the enzymatic activity in time-course under strictly anaerobic conditions.

Many proteins that employ the Fe-S cluster are overlooked as apo-type proteins because Fe-S clusters are degraded easily due to their oxygen-sensitivity. Today, 779 of [4Fe-4S]-binding proteins and 42 of [3Fe-4S]-binding proteins are deposited in the protein database (UniProt) from 21 organisms including *E. coli*, *S. cerevisiae*, and *H. sapiens*[122]. However, some of them are annotated based on only sequence similarity, which means that we need experimental evidence to demonstrate the type of Fe-S clusters. Considering the recent advances in our understanding of expanding role of Fe-S clusters, we can expect the exponential discovery of new Fe-S proteins in the future. Therefore, we have to perform spectroscopic, structural, and biochemical experiments on Fe-S proteins under strictly anaerobic conditions to minimize the risk of proposing an incorrect catalytic mechanism.

4-3. Sequence similarity of critical residues of tRNA-thiolation enzymes

I found that only [4Fe-4S]-TtuA is the enzymatically active form. Interestingly, some groups have reported that the TtuA/Ncs6 family members (TtuA, Ncs6, and TtcA6) bind to [4Fe-4S][67,71,72,76,83], whereas others have indicated that the active form of Ncs6 and Thil is [3Fe-4S][69]. Notably, the mechanism of sulfur transition catalyzed by TtuA and Ncs6 is believed to be similar[107], because their sulfur relay systems involving ubiquitin-like sulfur donor proteins are similar (Fig. 1-29), despite the different positions of tRNA thiolation. To evaluate whether [4Fe-4S] is the unique ligand of TtuA or common among tRNA-thiolation enzymes, I compared amino acids around the active site of the TtuA/Ncs6 family members, MnmA, and ThiI. Although MnmA and ThiI do not belong to the TtuA/Ncs6 family (Fig. 1-13, Table 1-1), recent studies reported that *Eco*MnmA contains [4Fe-4S] and *Mma*ThiI has [3Fe-4S], respectively[69,77].

A previous study has shown that Asp59, Cys130, Cys133, Asp161, and Cys222 in apo-*Tth*TtuA are critical in tRNA thiolation[82], but the mutational analysis was performed in aerobic conditions because the presence of [4Fe-4S] in TtuA has not reported at that time. Our group previously reported that Cys130, Cys133, and Cys222 are [4Fe-4S]-binding residues[72], and I identified that Ser55, Asp59, Lys137, and Asp161 are essential residues in strictly anaerobic conditions (Fig. 3-9)[83]. Ser55 and Asp59 are located at the PP-loop motif ($S_{55}GGXDS_{60}$) which are responsible for ATP binding and hydrolysis[119,120]. Lys137 catalyzes sulfur transition from TtuB to tRNA, stabilizing [4Fe-5S]-TtuA intermediate[76], and potentially involved in tRNA adenylation[83]. Asp161 is also predicted as a critical residue for ATP binding and hydrolysis from the structural insight of the PPase family although Asp161 is 5-Å away from ATP[83,120].

Interestingly, these residues are highly conserved in not only the TtuA/Ncs6 family, but also in MnmA and ThiI with a few exceptions, such as D190 in the PP-loop of *Mma*ThiI and D99/D101 coordinated to [4Fe-4S] in *Eco*MnmA/*Bsu*MnmA (Fig. 4-2, Fig. 4-3). Notably, one of the [4Fe-4S]-binding residues is aspartic acid instead of cysteine in some MnmA similar to ferredoxin, Fnr, IscA, and BchB[77,123,124].

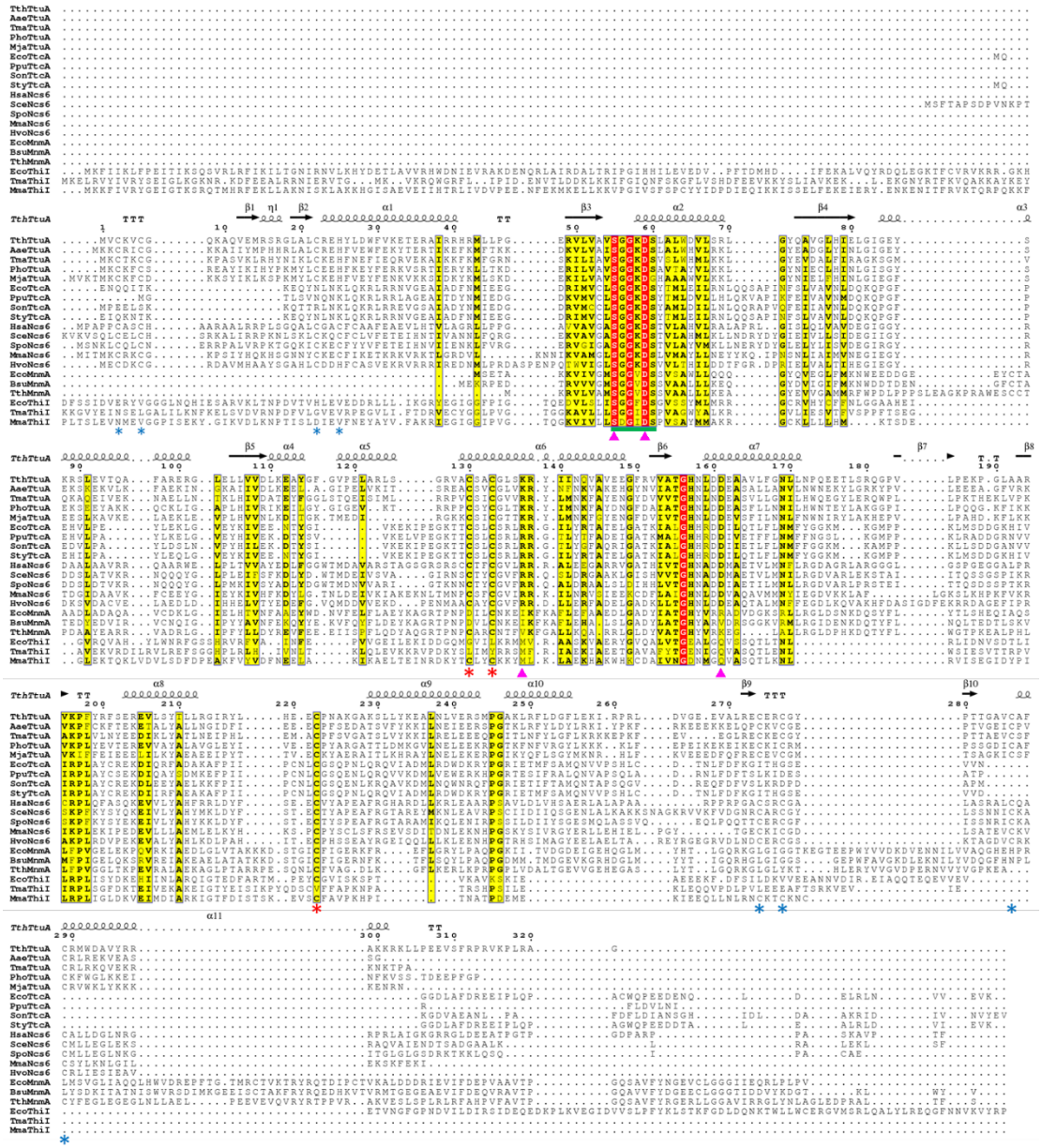

Fig. 4-2 Sequence alignment of tRNA-thiolation enzymes.

The secondary structures of *Tth*TtuA (PDB ID: 5B4F) are shown at the top. Completely conserved residues are highlighted in red and highly conserved residues are highlighted in yellow, respectively. Key residues in the ATP-binding motif (PP-loop, a green line); the three cysteine residues bound to the Fe-S cluster (red asterisks); the cysteine or histidine residues involved in the tRNA-binding motif (Zn finger, blue asterisks); and key residues of *Tth*TtuA (magenta triangles)[82,83]. The alignment was performed using Clustal Omega[125] and ESPrint 3.0[126] was used for illustration. Note that V345 of *Tma*ThiI aligns with C222 of *Tth*TtuA because their sequence identity is only 13.9%; however, C344 is the catalytic residue of *Tma*ThiI[105]. The abbreviations of protein names are the same as that in Fig. 1-13.

Enzymes	Organisms	Identified critical residues																
TtuA	*T. thermophilus*	**S55**	G56	G57	K58	**D59**	S60	…	**C130***	…	**C133***	…	**K137**	…	**D161**	…	**C222***
TtuA	*A. aeolicus*	**S56**	G57	G58	K59	**D60**	S61	…	**C130***	…	**C133***	…	**K137**	…	**D161**	…	**C222***
TtuA	*T. maritima*	**S55**	G56	G57	K58	**D59**	S60	…	**C131***	…	**C134***	…	**R138**	…	**D162**	…	**C224***
TtuA	*P. horikoshii*	**S55**	G56	G57	K58	**D59**	S60	…	**C128***	…	**C131***	…	**K135**	…	**D159**	…	**C220***
TtuA	*M. jannaschii*	**S59**	G60	G61	K62	**D63**	G64	…	**C130***	…	**C133***	…	**K137**	…	**D161**	…	**C222***
TtcA	*E. coli*	**S47**	G48	G49	K50	**D51**	S62	…	**C122***	…	**C125***	…	**R129**	…	**D153**	…	**C213***
TtcA	*P. putida*	**S40**	G41	G42	K43	**D44**	S45	…	**C115***	…	**C118***	…	**R122**	…	**D146**	…	**C206***
TtcA	*S. oneidensis*	**S45**	S46	G47	K48	**D49**	S50	…	**C120***	…	**C123***	…	**R127**	…	**D151**	…	**C211***
TtcA	*S. typhimurium*	**S47**	G48	G49	K50	**D51**	S52	…	**C122***	…	**C125***	…	**R129**	…	**D153**	…	**C213***
Ncs6	*H. sapiens*	**S59**	G60	G61	K62	**D63**	S64	…	**C144***	…	**C147***	…	**R151**	…	**D175**	…	**C237***
Ncs6	*S. cerevisiae*	**S75**	G76	G77	K78	**D79**	S80	…	**C157***	…	**C160***	…	**R164**	…	**D188**	…	**C250***
Ncs6	*S. pombe*	**S59**	G60	G61	K62	**D63**	S64	…	**C142***	…	**C145***	…	**R149**	…	**D173**	…	**C235***
Ncs6	*M. maripaludis*	**S57**	G58	G59	K60	**D61**	S62	…	**C142***	…	**C145***	…	**R149**	…	**D173**	…	**C233***
Ncs6	*H. volcanii*	**S61**	G62	G63	K64	**D65**	S66	…	**C143***	…	**C146***	…	**R150**	…	**D174**	…	**C242***
MnmA	*E. coli*	**S13**	G14	G15	V16	**D17**	S18	…	D99*	…	**C102***	…	I106	…	R132	…	**C199***
MnmA	*B. subtilis*	**S15**	G16	G17	V18	**D19**	S20	…	D101*	…	**C104***	…	I108	…	V133	…	**C200***
MnmA	*T. thermophilus*	**S9**	G10	G11	V12	**D13**	S14	…	**C105***	…	**C108***	…	V112	…	K137	…	**C200***
ThiI	*E. coli*	**S185**	G186	G187	F188	**D189**	S190	…	G261	…	L264	…	M268	…	Q292	…	C344
ThiI	*M. maripaludis*	**S189**	D190	G191	I192	**D193**	S194	…	**C265***	…	**C268***	…	M272	…	Q296	…	**C348***
ThiI	*T. maritima*	**S182**	G183	G184	I185	**D186**	S187	…	L260	…	Y263	…	M267	…	Q291	…	C344

Fig. 4-3 Sequence alignment of critical residues of TtuA for tRNA-thiolation[112]. The abbreviations of source organisms are the same as that in Fig. 1-13. Residues with asterisks are coordinated to Fe-S clusters. The conserved residues are indicated in red.

4-4. [4Fe-4S] is an active form in tRNA-thiolation enzymes

Until now, only three 3D structures of *Tth*TtuA, *Pho*TtuA, and *Mma*Ncs6 has been deposited in the Protein Data Bank (PDB) among tRNA-thiolation enzymes complexed with Fe-S clusters (all of them are [4Fe-4S]). Furthermore, [4Fe-4S]-*Tth*TtuA is the only reported complex structure with sulfur donor protein, and no complex structures with tRNA has been reported among the TtuA/Ncs6 family. These limited structural information makes it difficult to discuss whether [4Fe-4S] is generally active form in tRNA thiolation. Recently, AlphaFold version 2 (AF2) enabled us to predict 3D structure of *Eco*TtcA and *Mma*ThiI, and compare the positions of critical residues Ser55, Asp59,

Cys130, Cys133, Lys137, Asp161, and Cys222 in tRNA-thiolation enzymes[115]. The superimpositions showed that all key residues are located at similar positions with exceptions of Asp161 and Cys222 of TtuA (Fig. 4-4). Considering conservation of critical residues (Fig. 4-3) and structural similarity of the active site, [4Fe-4S] binding is likely shared by tRNA thiolation enzymes. Notably, ThiI from some organisms do not have [4Fe-4S]-binding cysteines at position 130 and 133 (Fig. 4-5), indicating that these conventual ThiI may catalyzes tRNA thiolation using persulfide as previously proposed (Fig. 1-26)[98].

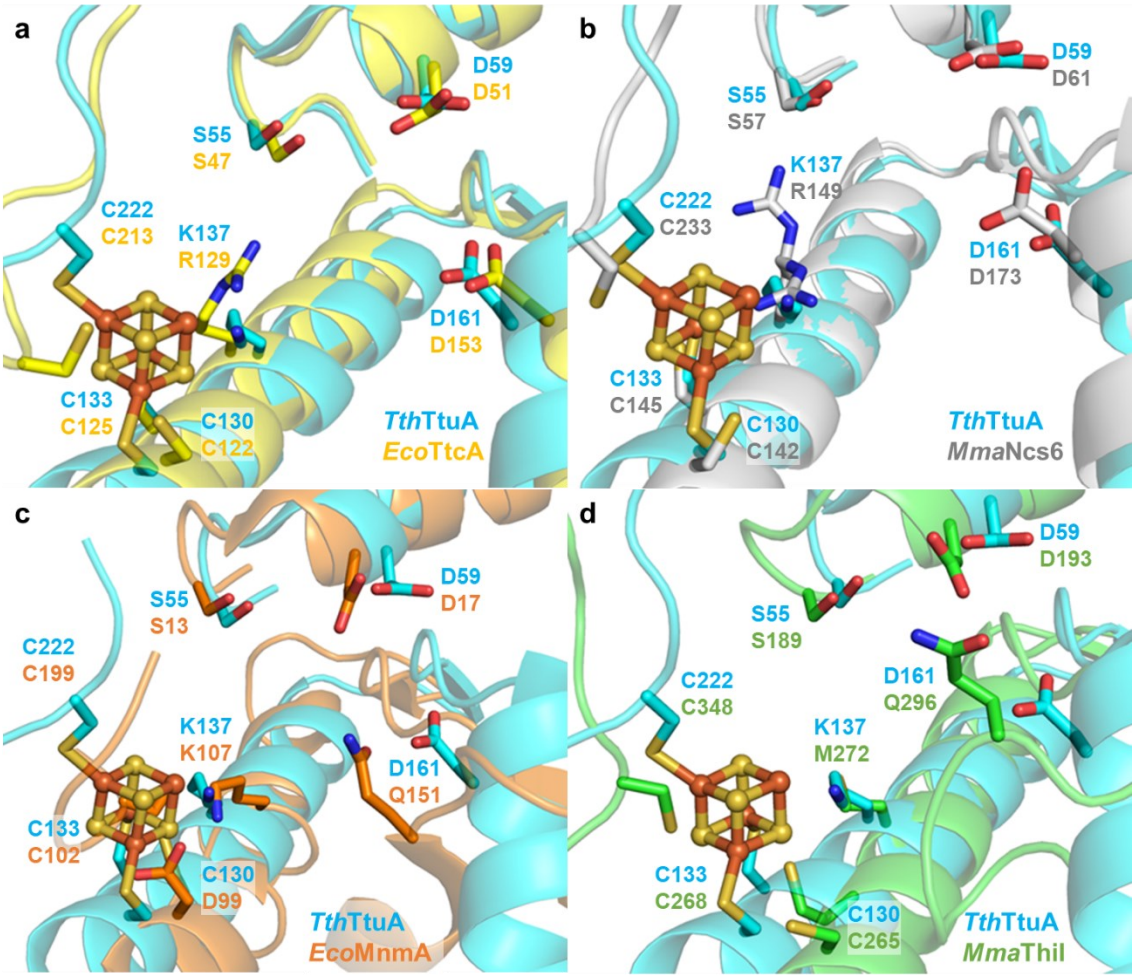

Fig. 4-4 Structural alignment of tRNA-thiolation enzymes[112].

Superposition of *Tth*TtuA (PDB ID: 5B4F) with the (**a**) *Eco*TtcA AF2 model, (**b**) *Mma*Ncs6 (PDB ID: 6SCY), (**c**) *Eco*MnmA (PDB ID: 2DEU), and (**d**) *Mma*ThiI AF2 model. The AF2 models were superposed in the manner described in the Materials and Methods section.

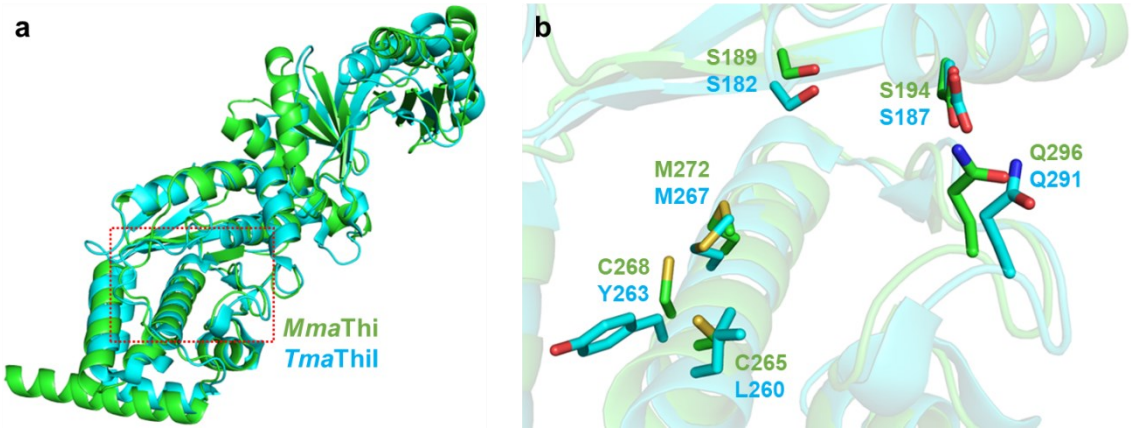

Fig. 4-5 Structural comparison of *Mma*ThiI and *Tma*ThiI.

(**a**) Superposition of overall structures of the *Mma*ThiI AF2 model with *Tma*ThiI (PDB ID: 4KR6). Their Cα RMSD is 2.054 Å. The catalytic site is marked by the red dotted frame. (**b**) Close-up view of their catalytic center. The coordination of the critical residues matches well, but *Tma*ThiI cannot bind to Fe-S clusters because Cys265 and Cys268 of *Mma*ThiI are replaced by Y263 and M267, respectively.

4-5. [4Fe-4S] cluster is a potential scaffold of tRNA adenylation

In this study, our result of APM-PAGE showed that the binding of TtuB to TtuA is not sufficient for desulfurization, but TtuA, TtuB, tRNA, and ATP are necessary (Fig. 3-8). This observation indicated that sulfur transition from TtuA to tRNA occurs after activation of tRNA using ATP. Furthermore, I elucidated the sulfur transition mechanism from TtuB to tRNA catalyzed by Lys137 of [4Fe-4S]-TtuA. However, the catalytic mechanism of tRNA adenylation is unknown.

Previously, the structure of apo-*Eco*MnmA complexed with adenylated tRNA (AdetRNA) has been determined (Fig. 1-23)[95], but the [4Fe-4S] cluster was absent in *Eco*MnmA. Furthermore, our group reported the [4Fe-4S]-TtuA-TtuB-AMPPNP-tRNA complex model based on the structure of the TilS-tRNA complex (Fig. 4-6)[72]. Although the Cα RMSD between *Tth*TtuA and TilS is 1.747 Å, we could not show the accurate model because the target base is position 54 of tRNA in TtuA whereas position 34 of tRNA in TilS. Therefore, the detailed catalytic mechanism of tRNA adenylation involving [4Fe-4S] clusters is still unknown.

Recently, the structure of [4Fe-4S]-*Mma*Ncs6 has been determined and the Cα RMSD between *Mma*Ncs6 and TilS is 1.774 Å. The structural similarity allowed to build [4Fe-4S]-*Mma*Ncs6-tRNA complex model (Fig. 4-7a). In many archaea including *M. maripaludis*, *urm1* gene is missing and assumed that SAMP2 (archaeal Urm1 homolog) is sulfur donor[127]. On the other hand, typical eukaryotes have Urm1 as sulfur donor such as human and yeast, which enabled to predict the structure of the *Hsa*Ncs6-Urm1 complex using AF2 and build the [4Fe-4S]-*Hsa*Ncs6-Urm1-tRNA complex model (Fig. 4-7b).

These enzyme-tRNA complex models show that the unique Fe interacts with position 2 of the substrate uridine, which indicate that [4Fe-4S] cluster is not only a scaffold of sulfur transition, but also that of tRNA adenylation in tRNA-thiolation enzymes. Furthermore, it is suggested that Asp161 is a critical residue for tRNA adenylation similar to that of Asp131 in TilS[116,117].

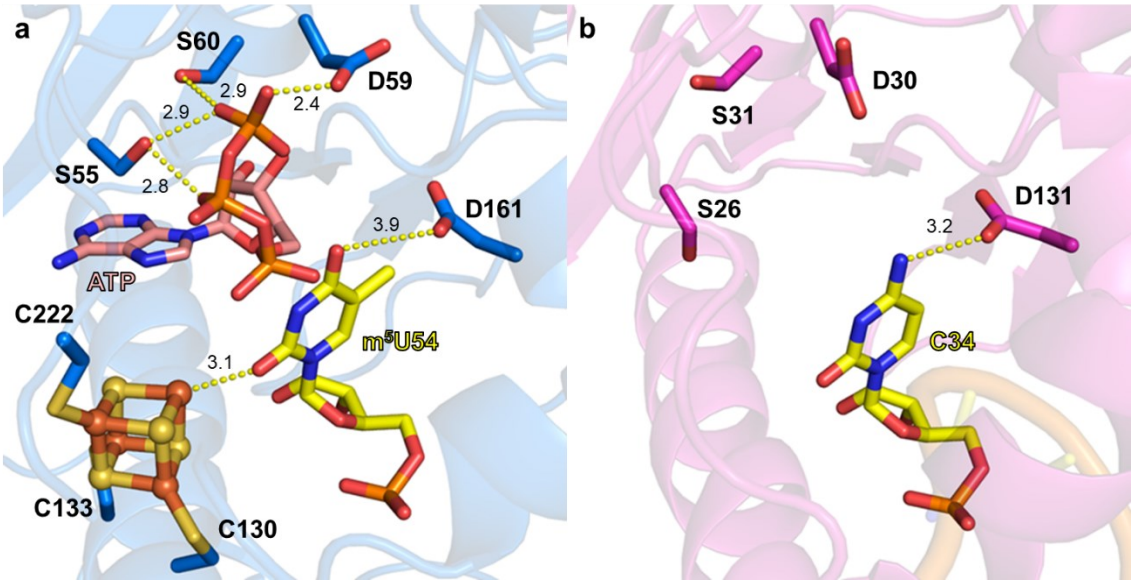

Fig. 4-6 Close-up view of the catalytic center of the TtuA model and TilS complexed with substrate tRNA.

(**a**) The [4Fe-4S]-TtuA-m^{5}U54 complex model. This model was built by superposition of the [4Fe-4S]-TtuA-TtuB-ATP complex (PDB ID: 5ZTB), the TilS-tRNA complex (PDB ID: 3A2K), and *Sce*tRNA^{Phe} (PDB ID: 1EHZ). TtuB and overall tRNA are not show. The substrate uridine is methylated similar to $T_{54}\Psi C_{56}$ loop of *Sce*tRNA^{Phe}. (**b**) The TilS-tRNA complex. Note that TilS is ATP-dependent, but [4Fe-4S]-independent. The yellow dotted lines indicate hydrogen bonds or coordination bonds with distance in angstrom units.

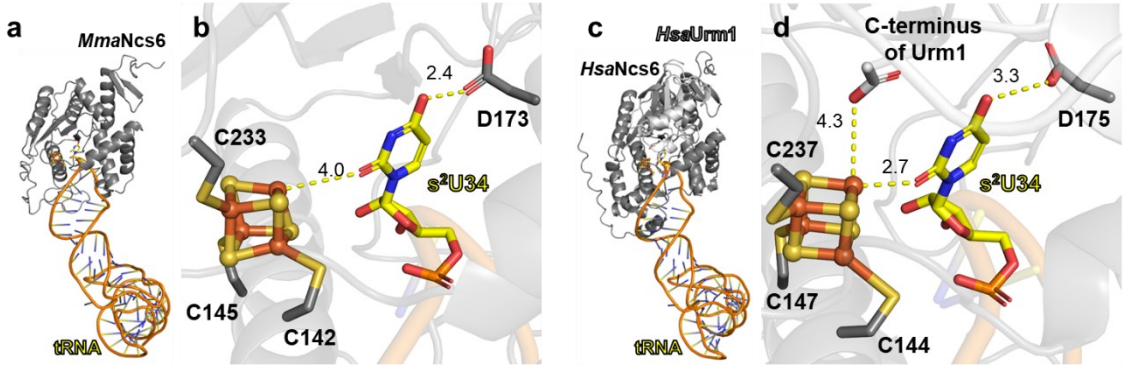

Fig. 4-7 The structure of [4Fe-4S]-Ncs6-tRNA complex model.

(**a**) Overall and (**b**) close-up view of the [4Fe-4S]-*Mma*Ncs6-tRNA complex model, which was built by the TilS-tRNA complex (PDB ID: 3A2K) using the "Super" command in PyMOL ver.1.7. (**c**) Overall and (**d**) close-up view of the [4Fe-4S]-*Hsa*Ncs6-*Hsa*Urm1-tRNA complex model, which was built by superposition of the [4Fe-4S]-TtuA-tRNA complex model using the "Super" command in PyMOL ver.1.7. The yellow dotted lines indicate hydrogen bonds or coordination bonds with distance in angstrom units. Note that the substrate nucleotide of TilS is cytidine and the substrate of Ncs6 is mcm^5U, but I represented that of Ncs6 as uridine for clearness.

4-6. Proposed catalytic mechanism of tRNA-thiolation in the TtuA/Ncs6 family

Taking all results together, I proposed the detailed mechanism of tRNA thiolation catalyzed by [4Fe-4S]-binding enzymes. Firstly, tRNA is activated by using Ser55, Asp59, and Asp161 in the presence of tRNA and ATP (Fig. 4-8a). Secondly, TtuA transfers sulfur from the C-terminus of TtuB to the unique Fe using catalytic residue Lys137, which forms the [4Fe-5S]-TtuA intermediate (Fig. 4-8b). Thirdly, [4Fe-5S]-TtuA transfers sulfur to the substrate tRNA (Fig. 4-8c). Finally, tRNA thiolation is completed and AMP is released from AdetRNA (Fig. 4-8d). Owing to the [4Fe-4S]-TtuA-tRNA complex model, I can describe this schematic diagram in the level of organic chemistry (Fig. 4-9). I would like to emphasize that this study implied that not only TtuA but also tRNA-thiolation enzymes is likely to catalyze tRNA thiolation with [4Fe-4S].

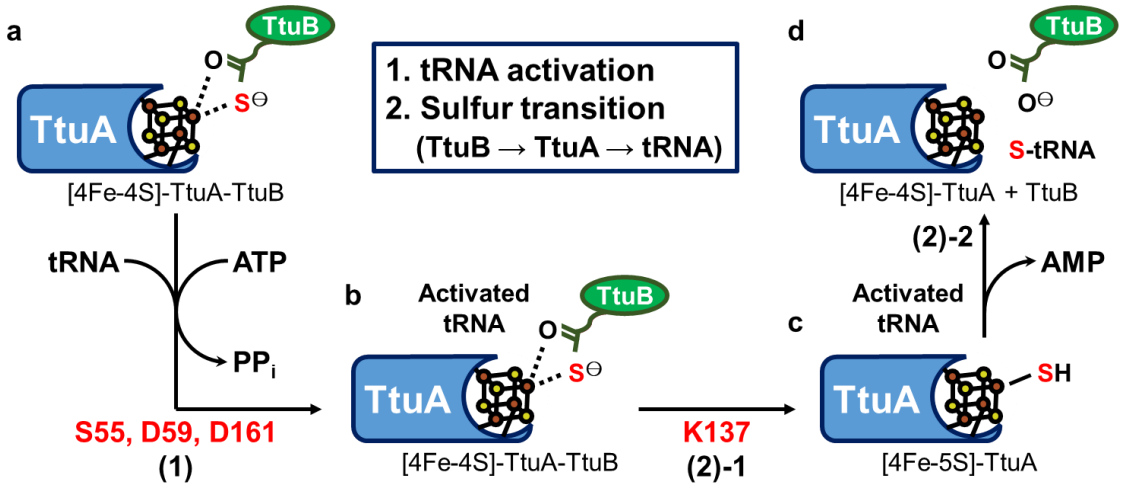

Fig. 4-8 Schematic diagram of the molecular mechanism of tRNA thiolation.

(**a**) The [4Fe-4S]-TtuA-TtuB complex catalyzes tRNA adenylation using ATP with critical residues Ser55, Asp59, and Asp161. (**b**) Lys137 of [4Fe-4S]-TtuA catalyzes sulfur transition from the C-terminus of TtuB to the unique Fe. (**c**) The [4Fe-5S]-TtuA intermediate transfers sulfur to AdetRNA. (**d**) tRNA thiolation is completed.

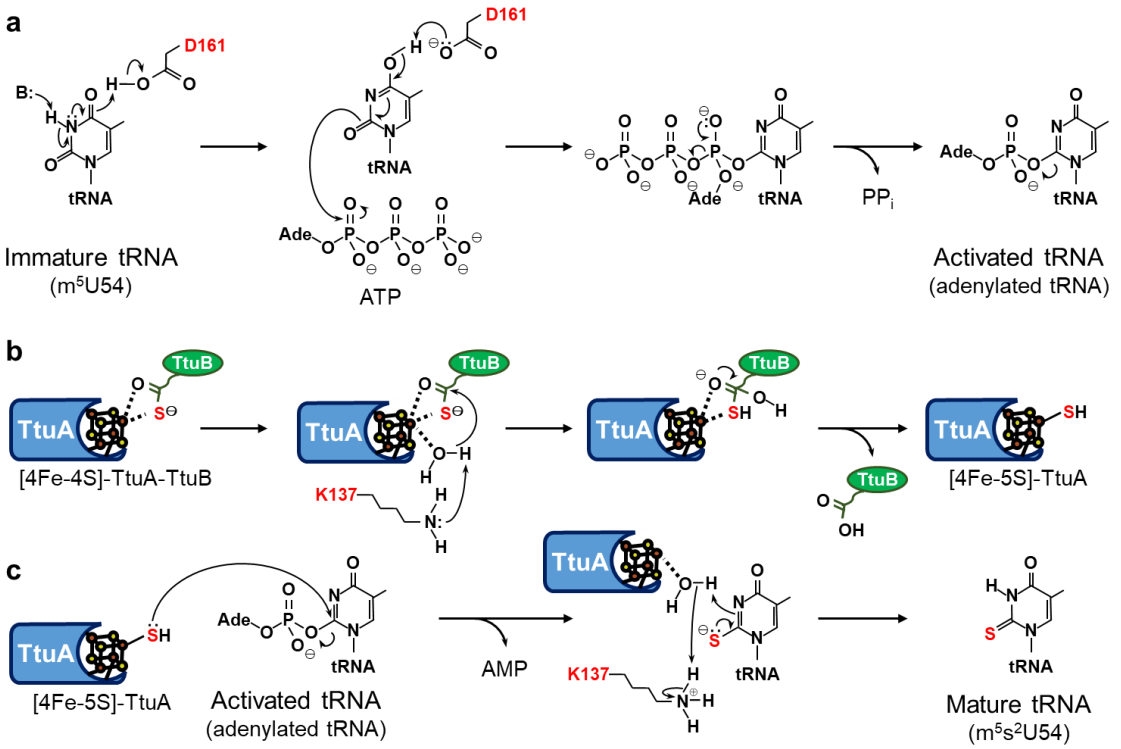

Fig. 4-9 Proposed mechanism of tRNA thiolation catalyzed by [4Fe-4S]-TtuA.

(**a**) tRNA adenylation catalyzed by Asp161. (**b**) Sulfur transition from TtuB to adenylated tRNA catalyzed by Lys137. (**c**) Sulfur transition from [4Fe-5S]-TtuA to adenylated tRNA.

Chapter 5. Perspective

In this study, I built the [4Fe-4S]-TtuA-m^5U54 complex and the [4Fe-4S]-Ncs6-tRNA complex models, showing that the [4Fe-4S] cluster could potentially function as a scaffold of tRNA adenylation. However, the detailed catalytic mechanism of tRNA activation is still unclear. To address this problem, we need to determine the structure of the tRNA-thiolation enzymes with [4Fe-4S] and tRNA using X-ray crystallography, and perform mutation assays involving tRNA activation. This structural determination would be challenging because our preliminary experiments suggested that the binding strength of TtuA to tRNA is too weak to form the TtuA-tRNA complex even under anaerobic conditions (Data not shown).

In tRNA thiolation, it has been believed that the PP-loop motif is responsible for ATP binding/hydrolysis and releases AMP and Pyrophosphate (PP_i) via the AdetRNA intermediate[72,76]. This tRNA activation mechanism is based on the crystal structure of the MnmA-AdetRNA complex (Fig. 1-23) and bioinformatics analysis that ThiI and TilS have conserved PP-loop motifs[128,129]. In ThiI, furthermore, direct evidence for the formation of an AdetRNA intermediate and the release of AMP was reported using α-^{32}P-labeled ATP to quantify adenylated tRNAs[130], and a preliminary observation showed that AMP is produced during s^4U formation[98]. However, I could not find any previous studies that analyze the release of ADP, PPi, and inorganic phosphate (P_i). Therefore, we cannot exclude the possibility that ATP releases AMP and two P_i molecules via the ADP and AdetRNA intermediates.

Recently, we have determined the crystal structures of the [4Fe-4S]-TtuA-ATP complex and the [4Fe-4S]-TtuA-ADP complex (unpublished). We also found about 30% of the m^5s^2U54 synthesis activity of TtuA even when ADP was used instead of ATP (unpublished). Considering these observations and the finding that TtuB does not release sulfur until tRNA activation (Fig. 3-11), two major possibilities still remain in the molecular mechanism of tRNA activation: TtuA catalyzes ATP hydrolysis and releases AMP and PPi (Fig. 5-1, hypothesis 1); ATP is trimmed to ADP and then releases AMP and two P_i molecules (Fig. 5-1, hypotheses 2 and 3).

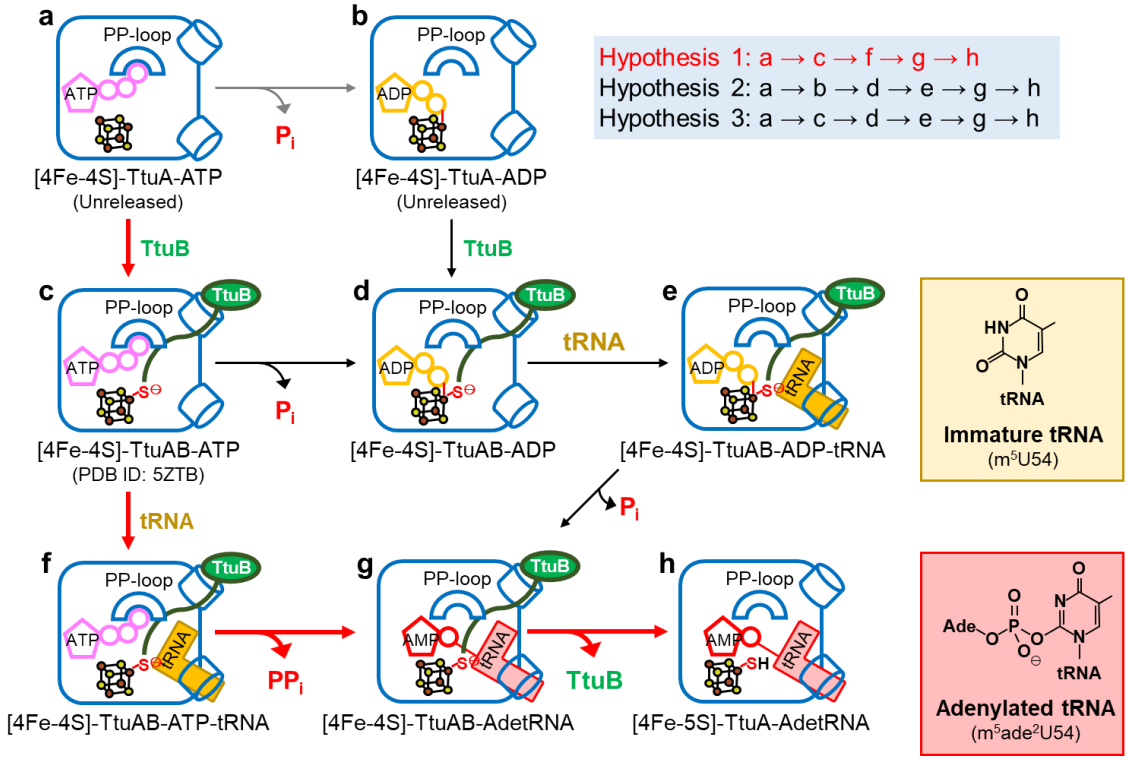

Fig. 5-1 Predicted mechanism of tRNA adenylation catalyzed by [4Fe-4S]-TtuA. Hypothesis 1: (**a**) The PP-loop of [4Fe-4S]-TtuA interacts with ATP. (**c**) TtuB enters the catalytic site of TtuA and forms the [4Fe-4S]-TtuA-TtuB-ATP complex (PDB ID: 5ZTB). (**f**) Substrate tRNA enters the catalytic site of TtuA and forms the [4Fe-4S]-TtuA-TtuB-ATP-tRNA complex. (**g**) TtuA catalyzes tRNA adenylation and forms the [4Fe-4S]-TtuA-TtuB-AdetRNA complex with the release of PP_i. (**h**) TtuA catalyzes sulfur transition from the C-terminus of TtuB to the unique Fe, which forms the [4Fe-5S]-TtuA intermediate. Hypothesis 2: (**a**) TtuA catalyzes ATP trimming and forms (**b**) the [4Fe-4S]-TtuA-ADP complex with release P_i. (**d**) TtuB enters the catalytic site of TtuA and forms the [4Fe-4S]-TtuA-TtuB-ADP complex. (**e**) Substrate tRNA enters the catalytic site of TtuA and forms the [4Fe-4S]-TtuA-TtuB-ADP-tRNA complex. (**g**) TtuA catalyzes tRNA adenylation and forms the [4Fe-4S]-TtuA-TtuB-AdetRNA complex with additional release of P_i. Hypothesis 3: After the formation of the [4Fe-4S]-TtuA-TtuB-ATP complex, (**d**) TtuA catalyzes ATP trimming and form the [4Fe-4S]-TtuA-TtuB-ADP complex with release P_i. Then, (**e**) Substrate tRNA enters the catalytic site of TtuA, and (**g**) TtuA catalyzes tRNA adenylation with further release of P_i.

To elucidate the catalytic mechanism of tRNA thiolation, we also have to understand the regulatory mechanism of two different reactions: tRNA activation and sulfur transition. However, the experimental approaches are limited due to the oxygen sensitivity of [4Fe-4S]. Thus, I also expect that computational approaches such as RoseTTAFoldNA[131] and molecular dynamics (MD) simulations. RoseTTAFoldNA is the newly developed tool that predicts the structure of the protein-nucleic acid complexes using deep learning approaches, which has the potential to provide the structure of the TtuA-tRNA complex.

Furthermore, MD simulations enable to reveal the structural dynamics of TtuA and the free-energy perturbation (FEP) method can calculate the binding energy of ligands[132,133]. Although these approaches are powerful, we have to overcome the problem of force field parameters because [4Fe-4S]-TtuA contains two types of Zn fingers (Fig. 1-28a) and four Fe atoms including the unique Fe (Fig. 5-2). The missing residues of TtuA also make it difficult to perform MD simulations, but these residues maybe regulate the tRNA adenylation and sulfur transition.

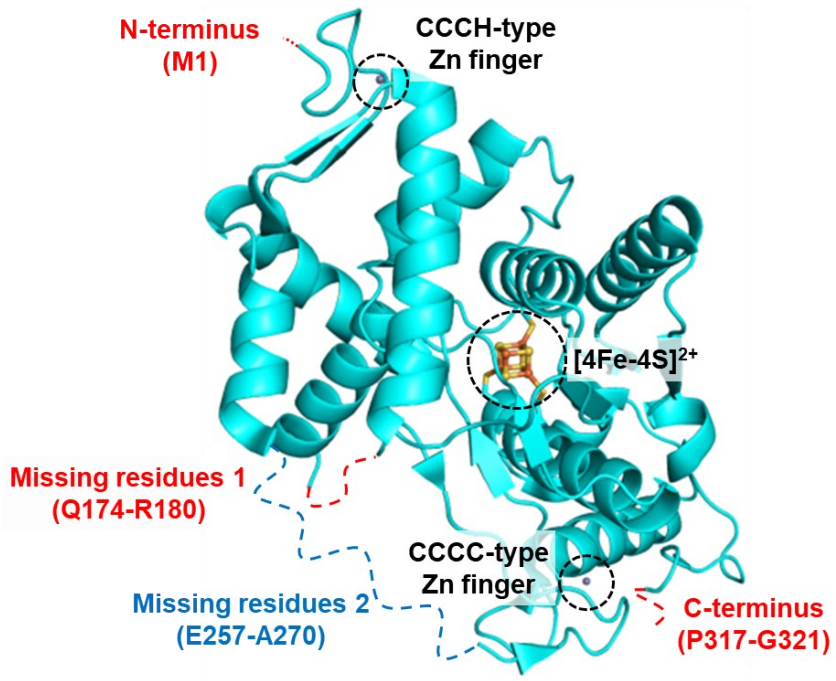

Fig. 5-2 Difficulties of MD simulations in [4Fe-4S]-TtuA.

TtuA (PDB ID: 5B4F) contains the CCCH-type zinc finger at the N-terminus, the CCCC-type zinc finger at the C-terminus, and four missing regions (Met1, Gln174-Arg180, Glu257-Ala270, and Pro317-Gly321).

Chapter 6. Summary

Thiolation at position 54 of tRNA (m^5s^2U54) is catalyzed by 2-thiouridine synthetase TtuA and sulfur donor TtuB, which allows thermophiles to survive in high-temperature environments. Our recent structural analysis of the [4Fe-4S]-TtuA-TtuB-ATP complex showed that an oxygen-sensitive [4Fe-4S] cluster with a non-cysteine coordinated Fe (the unique Fe) is required for the enzymatic activity of TtuA. On the other hand, it was reported that Ncs6, a homolog protein of TtuA, contains [3Fe-4S] or [4Fe-4S]. Therefore, the detailed mechanism of sulfur transition from TtuB to tRNA is unknown (Fig. 1-30).

In this study, I analyzed the structure of Fe-S clusters in TtuA in time-course and their enzymatic activities under strictly anaerobic conditions. As a result, I found that [3Fe-4S]-TtuA spontaneously transformed into [4Fe-4S] within one hour. I also revealed that [3Fe-4S]-TtuA could not bind to the C-terminus of TtuB. These observations supported that only [4Fe-4S] is the active form of TtuA (Fig. 4-1).

Furthermore, the result of APM-PAGE showed that [4Fe-4S]-TtuA does not transfer sulfur from TtuB to substrate tRNA until the tRNA is adenylated. In addition, the mutational analysis in this study revealed that Ser55, Asp59, and Asp161 of TtuA are responsible for tRNA adenylation and Lys137 is the catalytic residue of sulfur transition. These critical residues and the structure of catalytic pocket are conserved in not only the TtuA/Ncs6 family, but also MnmA and ThiI. Taking all result together, I proposed the reaction mechanism of tRNA-thiolation containing tRNA adenylation and sulfur transition via the unique Fe of [4Fe-4S] cluster (Fig. 4-8, Fig. 6-1). Notably, during the preparation of this dissertation, it was reported that some archaeal ThiI such as *Mma*ThiI contains [4Fe-4S] for sulfur transition[134]. Our conclusion is consistent with this recent report that the unique Fe in [4Fe-4S]-*Mma*ThiI is essential to receive sulfur via the [4Fe-5S]-intermediate.

Finally, I showed that the time-course correlation analysis under strictly anaerobic conditions is required to reveal the correct reaction mechanism: the structures of an Fe-S cluster in the enzyme; the catalytic activity of the enzyme. I believe that this study contributes to the accurate understanding of Fe-S proteins which would exponentially be discovered in the future.

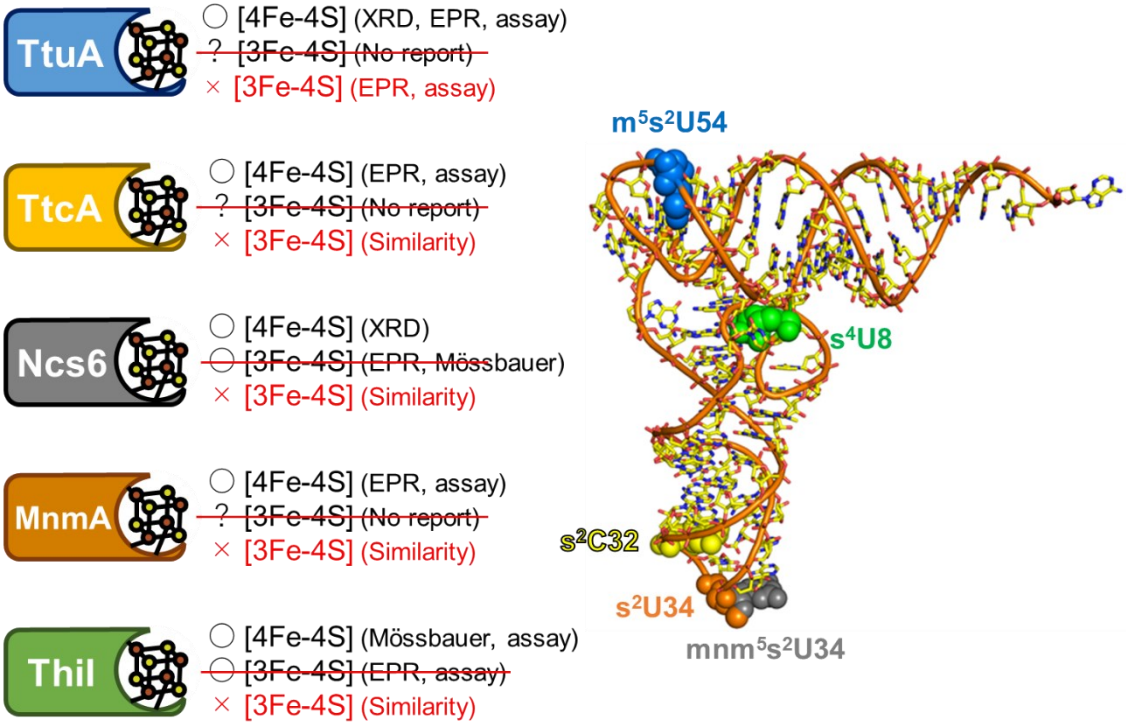

Fig. 6-1 Graphical summary of this study.

Previously, some research groups proposed that the [4Fe-4S] cluster is an active form in tRNA-thiolation enzymes whereas others reported that [3Fe-4S] cluster is a catalytic form in Ncs6 and ThiI. The possibility of the [3Fe-4S] was not considered in TtuA, TtcA, and MnmA (colored in black). This study demonstrated that the [4Fe-4S] cluster is the only active form of TtuA and proposed that all of the tRNA thiolation enzymes contain [4Fe-4S] cluster as the scaffold of tRNA adenylation and sulfur transition (colored in red).

References

1. Boccaletto, P. *et al.* MODOMICS: A database of RNA modification pathways. 2021 update. *Nucleic Acids Res.* **50**, D231–D235 (2022).
2. Suzuki, T. The expanding world of tRNA modifications and their disease relevance. *Nat. Rev. Mol. Cell Biol.* **22**, 375–392 (2021).
3. Torres, A. G., Batlle, E. & Ribas de Pouplana, L. Role of tRNA modifications in human diseases. *Trends Mol. Med.* **20**, 306–314 (2014).
4. Yacoubi, B. E., Bailly, M. & De Crécy-Lagard, V. Biosynthesis and function of posttranscriptional modifications of transfer RNAs. *Annu. Rev. Genet.* **46**, 69–95 (2012).
5. Nedialkova, D. D. & Leidel, S. A. Optimization of codon translation rates via tRNA modifications maintains proteome integrity. *Cell* **161**, 1606–1618 (2015).
6. Shigi, N. Recent advances in our understanding of the biosynthesis of sulfur modifications in tRNAs. *Front. Microbiol.* **9**, 1–9 (2018).
7. Watanabe, K., Shinma, M., Oshima, T. & Nishimura, S. Heat-induced stability of tRNA from an extreme thermophile, Thermus thermophilus. *Biochem. Biophys. Res. Commun.* **72**, 1137–1144 (1976).
8. Shigi, N. *et al.* Temperature-dependent biosynthesis of 2-thioribothymidine of Thermus thermophilus tRNA. *J. Biol. Chem.* **281**, 2104–2113 (2006).
9. Ikeuchi, Y. *et al.* Molecular mechanism of lysidine synthesis that determines tRNA identity and codon recognition. *Mol. Cell* **19**, 235–246 (2005).
10. Krüger, M. K., Pedersen, S., Hagervall, T. G. & Sørensen, M. A. The modification of the wobble base of tRNAGlu modulates the translation rate of glutamic acid codons in vivo. *J. Mol. Biol.* **284**, 621–631 (1998).
11. Yarian, C. *et al.* Accurate translation of the genetic code depends on tRNA modified nucleosides. *J. Biol. Chem.* **277**, 16391–16395 (2002).
12. Caldeira de Araujo, A. & Favre, A. Induction of size reduction in Escherichia coli by near-ultraviolet light. *Eur. J. Biochem.* **146**, 605–610 (1985).
13. Mueller, E. Identification of a gene involved in the generation of 4-thiouridine in tRNA. *Nucleic Acids Res.* **26**, 2606–2610 (1998).
14. Watanabe, K., Oshima, T., Iijima, K., Yamaizumi, Z. & Nishimura, S. Purification and thermal stability of several amino acid-specific tRNAs from an extreme thermophile, Thermus thermophilus HB8. *J. Biochem.* **87**, 1–13 (1980).
15. Bondi, A. Van der waals volumes and radii. *J. Phys. Chem.* **68**, 441–451 (1964).
16. Yokoyama, S., Watanabe, K. & Miyazawa, T. Dynamic structures and functions of transfer ribonucleic acids from extreme thermophiles. *Adv. Biophys.* **23**, 115–

147 (1987).
17. Watanabe, K., Yokoyama, S., Hansske, F., Kasai, H. & Miyazawa, T. CD and NMR studies on the conformational thermostability of 2-thioribothymidine found in the TψC loop of thermophile tRNA. *Biol. Biophys. Res. Commun.* **91**, 671–677 (1979).
18. Shigi, N., Sakaguchi, Y., Suzuki, T. & Watanabe, K. Identification of two tRNA thiolation genes required for cell growth at extremely high temperatures. *J. Biol. Chem.* **281**, 14296–14306 (2006).
19. Shigi, N. Biosynthesis and functions of sulfur modifications in tRNA. *Frontiers in Genetics* vol. 5 67 (2014).
20. Suzuki, T. *et al.* Complete chemical structures of human mitochondrial tRNAs. *Nat. Commun.* **11**, 1–15 (2020).
21. Murphy, F. V, Ramakrishnan, V., Malkiewicz, A. & Agris, P. F. The role of modifications in codon discrimination by tRNALysUUU. *Nat. Struct. Mol. Biol.* **11**, 1186–1191 (2004).
22. Allred, A. L. Electronegativity values from thermochemical data. *J. Inorg. Nucl. Chem.* **17**, 215–221 (1961).
23. Sabin, J. R. Hydrogen bonds involving sulfur. I. Hydrogen sulfide dimer. *J. Am. Chem. Soc.* **93**, 3613–3620 (1971).
24. Yasukawa, T., Suzuki, T., Ishii, N., Ohta, S. & Watanabe, K. Wobble modification defect in tRNA disturbs codon-anticodon interaction in a mitochondrial disease. *EMBO J.* **20**, 4794–4802 (2001).
25. Kirino, Y. & Suzuki, T. Human mitochondrial diseases associated with tRNA wobble modification deficiency. *RNA Biol.* **2**, 41–44 (2005).
26. Rapino, F. *et al.* Codon-specific translation reprogramming promotes resistance to targeted therapy. *Nature* **558**, 605–609 (2018).
27. Barbieri, I. & Kouzarides, T. Role of RNA modifications in cancer. *Nat. Rev. Cancer* **20**, 303–322 (2020).
28. Delaunay, S. *et al.* Elp3 links tRNA modification to IRES-dependent translation of LEF1 to sustain metastasis in breast cancer. *J. Exp. Med.* **213**, 2503–2523 (2016).
29. Vangaveti, S. *et al.* A structural basis for restricted codon recognition mediated by 2-thiocytidine in tRNA containing a wobble position inosine. *J. Mol. Biol.* **432**, 913–929 (2020).
30. Licht, K. *et al.* Inosine induces context-dependent recoding and translational stalling. *Nucleic Acids Res.* **47**, 3–14 (2019).
31. Nakamura, Y., Gojobori, T. & Ikemura, T. Codon usage tabulated from

international DNA sequence databases: Status for the year 2000. *Nucleic Acids Research* vol. 28 292 (2000).

32. Curran, J. F. Decoding with the A:I wobble pair is inefficient. *Nucleic Acids Res.* **23**, 683–688 (1995).
33. Jäger, G., Leipuviene, R., Pollard, M. G., Qian, Q. & Björk, G. R. The conserved Cys-X1-X2-Cys motif present in the TtcA protein is required for the thiolation of cytidine in position 32 of tRNA from Salmonella enterica serovar Typhimurium. *J. Bacteriol.* **186**, 750–757 (2004).
34. Jenner, L. B., Demeshkina, N., Yusupova, G. & Yusupov, M. Structural aspects of messenger RNA reading frame maintenance by the ribosome. *Nat. Struct. Mol. Biol.* **17**, 555–560 (2010).
35. Urbonavičius, J., Qian, Q., Durand, J. M. B., Hagervall, T. G. & Björk, G. R. Improvement of reading frame maintenance is a common function for several tRNA modifications. *EMBO J.* **20**, 4863–4873 (2001).
36. Esberg, B., Leung, H.-C. E., Tsui, H.-C. T., Björk, G. R. & Winkler, M. E. Identification of the miaB gene, involved in methylthiolation of isopentenylated A37 derivatives in the tRNA of Salmonella typhimurium and Escherichia coli. *J. Bacteriol.* **181**, 7256–7265 (1999).
37. Arragain, S. *et al.* Identification of eukaryotic and prokaryotic methylthiotransferase for biosynthesis of 2-methylthio-N6-threonylcarbamoyladenosine in tRNA. *J. Biol. Chem.* **285**, 28425–28433 (2010).
38. Kang, B. Il *et al.* Identification of 2-methylthio cyclic N6-threonylcarbamoyladenosine (ms2ct6A) as a novel RNA modification at position 37 of tRNAs. *Nucleic Acids Res.* **45**, 2124–2136 (2017).
39. Wei, F. Y. *et al.* Deficit of tRNALys modification by Cdkal1 causes the development of type 2 diabetes in mice. *J. Clin. Invest.* **121**, 3598–3608 (2011).
40. Wei, F. Y. *et al.* Cdk5rap1-mediated 2-methylthio modification of mitochondrial tRNAs governs protein translation and contributes to myopathy in mice and humans. *Cell Metab.* **21**, 428–442 (2015).
41. Ching, Y. P., Pang, A. S. H., Lam, W. H., Qi, R. Z. & Wang, J. H. Identification of a neuronal Cdk5 activator-binding protein as Cdk5 inhibitor. *J. Biol. Chem.* **277**, 15237–15240 (2002).
42. Steinthorsdottir, V. *et al.* A variant in CDKAL1 influences insulin response and risk of type 2 diabetes. *Nat. Genet.* **39**, 770–775 (2007).
43. Zhang, B. *et al.* First step in catalysis of the radical S-adenosylmethionine methylthiotransferase MiaB yields an intermediate with a [3Fe-4S]0-like auxiliary

cluster. *J. Am. Chem. Soc.* **142**, 1911–1924 (2020).
44. Griffey, R. H., Davis, D. R. & Yamaizumi, Z. 15N-labeled tRNA. Identification of 4-thiouridine in Escherichia coli tRNA1(Ser) and tRNA2(Tyr) by 1H-15N two-dimensional NMR spectroscopy. *J. Biol. Chem.* **261**, 12074–12078 (1986).
45. Carre, D. S., Thomas, G. & Favre, A. Conformation and functioning of tRNAs: cross-linked tRNAs as substrate for tRNA nucleotidyl-transferase and aminoacyl synthetases. *Biochimie* **56**, 1089–1101 (1974).
46. Favre, A., Michelson, A. M. & Yaniv, M. Photochemistry of 4-thiouridine in Escherichia coli transfer RNA1Val. *J. Mol. Biol.* **58**, 367–379 (1971).
47. Ramabhadran, T. V. & Jagger, J. Mechanism of growth delay induced in Escherichia coli by near ultraviolet radiation. *Proc. Natl. Acad. Sci. U. S. A.* **73**, 59–63 (1976).
48. Kramer, G. F., Baker, J. C. & Ames, B. N. Near-UV stress in Salmonella typhimurium: 4-Thiouridine in tRNA, ppGpp, and ApppGpp as components of an adaptive response. *J. Bacteriol.* **170**, 2344–2351 (1988).
49. Kimura, S. & Waldor, M. K. The RNA degradosome promotes tRNA quality control through clearance of hypomodified tRNA. *Proc. Natl. Acad. Sci. U. S. A.* **116**, 1394–1403 (2019).
50. Palenchar, P. M., Buck, C. J., Cheng, H., Larson, T. J. & Mueller, E. G. Evidence that ThiI, an enzyme shared between thiamin and 4-thiouridine biosynthesis, may be a sulfurtransferase that proceeds through a persulfide intermediate. *J. Biol. Chem.* **275**, 8283–8286 (2000).
51. Ledoux, S., Olejniczak, M. & Uhlenbeck, O. C. A sequence element that tunes Escherichia coli tRNAGGCAla to ensure accurate decoding. *Nat. Struct. Mol. Biol.* **16**, 359–364 (2009).
52. Ikeuchi, Y., Kitahara, K. & Suzuki, T. The RNA acetyltransferase driven by ATP hydrolysis synthesizes N 4-acetylcytidine of tRNA anticodon. *EMBO J.* **27**, 2194–2203 (2008).
53. Tanaka, Y. *et al.* Deduced RNA binding mechanism of ThiI based on structural and binding analyses of a minimal RNA ligand. *Rna* **15**, 1498–1506 (2009).
54. Shigi, N. Biosynthesis and degradation of sulfur modifications in tRNAs. *Int. J. Mol. Sci.* **22**, 11937 (2021).
55. Nicolet, Y., Rohac, R., Martin, L. & Fontecilla-Camps, J. C. X-ray snapshots of possible intermediates in the time course of synthesis and degradation of protein-bound Fe4S4 clusters. *Proc. Natl. Acad. Sci.* **110**, 7188–7192 (2013).
56. Beinert, H., Holm, R. H. & Münck, E. Iron-sulfur clusters: Nature's modular,

multipurpose structures. *Science (80-.).* **277**, 653–659 (1997).
57. Goldford, J. E., Hartman, H., Smith, T. F. & Segrè, D. Remnants of an ancient metabolism without phosphate. *Cell* **168**, 1126-1134.e9 (2017).
58. Boncella, A. E. *et al.* The expanding utility of iron-sulfur clusters: Their functional roles in biology, synthetic small molecules, maquettes and artificial proteins, biomimetic materials, and therapeutic strategies. *Coord. Chem. Rev.* **453**, 214229 (2022).
59. Netz, D. J. A. *et al.* Eukaryotic DNA polymerases require an iron-sulfur cluster for the formation of active complexes. *Nat. Chem. Biol.* **8**, 125–132 (2012).
60. Rudolf, J., Makrantoni, V., Ingledew, W. J., Stark, M. J. R. & White, M. F. The DNA repair helicases XPD and FancJ have essential iron-sulfur domains. *Mol. Cell* **23**, 801–808 (2006).
61. Maio, N. *et al.* Fe-S cofactors in the SARS-CoV-2 RNA-dependent RNA polymerase are potential antiviral targets. *Science (80-.).* **373**, 236–241 (2021).
62. White, M. F. & Dillingham, M. S. Iron-sulphur clusters in nucleic acid processing enzymes. *Current Opinion in Structural Biology* vol. 22 94–100 (2012).
63. Rouault, T. A. & Tong, W. H. Iron-sulfur cluster biogenesis and human disease. *Trends in Genetics* vol. 24 398–407 (2008).
64. Sheftel, A., Stehling, O. & Lill, R. Iron-sulfur proteins in health and disease. *Trends Endocrinol. Metab.* **21**, 302–314 (2010).
65. Wenxin, Z., Li, X., Hongting, Z. & Kuanyu, L. Mammalian mitochondrial iron–sulfur cluster biogenesis and transfer and related human diseases. *Biophys. Reports* **7**, 127–141 (2021).
66. Wagner, T., Koch, J., Ermler, U. & Shima, S. Methanogenic heterodisulfide reductase (HdrABC-MvhAGD) uses two noncubane [4Fe-4S] clusters for reduction. *Science (80-.).* **357**, 699–703 (2017).
67. Bimai, O., Arragain, S. & Golinelli-Pimpaneau, B. Structure-based mechanistic insights into catalysis by tRNA thiolation enzymes. *Curr. Opin. Struct. Biol.* **65**, 69–78 (2020).
68. Madeira, F. *et al.* Search and sequence analysis tools services from EMBL-EBI in 2022. *Nucleic Acids Res.* **50**, W276–W279 (2022).
69. Liu, Y. *et al.* A [3Fe-4S] cluster is required for tRNA thiolation in archaea and eukaryotes. *Proc. Natl. Acad. Sci. U. S. A.* **113**, 12703–12708 (2016).
70. Shigi, N., Horitani, M., Miyauchi, K., Suzuki, T. & Kuroki, M. An ancient type of MnmA protein is an iron-sulfur cluster-dependent sulfurtransferase for tRNA anticodons. *RNA* **26**, 240–250 (2020).

71. Bouvier, D. *et al.* TtcA a new tRNA-thioltransferase with an Fe-S cluster. *Nucleic Acids Res.* **42**, 7960–7970 (2014).
72. Chen, M. *et al.* Biochemical and structural characterization of oxygen-sensitive 2-thiouridine synthesis catalyzed by an iron-sulfur protein TtuA. *Proc. Natl. Acad. Sci. U. S. A.* **114**, 4954–4959 (2017).
73. Dewez, M. *et al.* The conserved wobble uridine tRNA thiolase Ctu1-Ctu2 is required to maintain genome integrity. *Proc. Natl. Acad. Sci. U. S. A.* **105**, 5459–5464 (2008).
74. Lauhon, C. T., Skovran, E., Urbina, H. D., Downs, D. M. & Vickery, L. E. Substitutions in an active site loop of Escherichia coli IscS result in specific defects in Fe-S cluster and thionucleoside biosynthesis in vivo. *J. Biol. Chem.* **279**, 19551–19558 (2004).
75. Leipuviene, R., Qian, Q. & Björk, G. R. Formation of thiolated nucleosides present in tRNA from Salmonella enterica serovar Typhimurium occurs in two principally distinct pathways. *J. Bacteriol.* **186**, 758–766 (2004).
76. Arragain, S. *et al.* Nonredox thiolation in tRNA occurring via sulfur activation by a [4Fe-4S] cluster. *Proc. Natl. Acad. Sci. U. S. A.* **114**, 7355–7360 (2017).
77. Zhou, J. *et al.* Iron–sulfur biology invades tRNA modification: the case of U34 sulfuration. *Nucleic Acids Res.* **49**, 3997–4007 (2021).
78. Combet, C., Blanchet, C., Geourjon, C. & Deléage, G. NPS@: Network protein sequence analysis. *Trends Biochem. Sci.* **25**, 147–150 (2000).
79. Shigi, N., Sakaguchi, Y., Asai, S. I., Suzuki, T. & Watanabe, K. Common thiolation mechanism in the biosynthesis of tRNA thiouridine and sulphur-containing cofactors. *EMBO J.* **27**, 3267–3278 (2008).
80. Nishimasu, H. *et al.* Atomic structure of a folate/FAD-dependent tRNA T54 methyltransferase. *Proc. Natl. Acad. Sci. U. S. A.* **106**, 8180–8185 (2009).
81. Yamagami, R. *et al.* The tRNA recognition mechanism of folate/FAD-dependent tRNA methyltransferase (TrmFO). *J. Biol. Chem.* **287**, 42480–42494 (2012).
82. Nakagawa, H. *et al.* Crystallographic and mutational studies on the tRNA thiouridine synthetase TtuA. *Proteins Struct. Funct. Bioinforma.* **81**, 1232–1244 (2013).
83. Chen, M. *et al.* The [4Fe-4S] cluster of sulfurtransferase TtuA desulfurizes TtuB during tRNA modification in Thermus thermophilus. *Commun. Biol.* **3**, 168 (2020).
84. Goehring, A., Rivers, D. & Sprague, G. Urmylation: a ubiquitin-like pathway that functions during invasive growth and budding in yeast. *Mol. Biol. Cell* **14**, 4329–4341 (2003).

85. Furukawa, K., Mizushima, N., Noda, T. & Ohsumi, Y. A protein conjugation system in yeast with homology to biosynthetic enzyme reaction of prokaryotes. *J. Biol. Chem.* **275**, 7462–7465 (2000).
86. Leidel, S. *et al.* Ubiquitin-related modifier Urm1 acts as a sulphur carrier in thiolation of eukaryotic transfer RNA. *Nature* **458**, 228–232 (2009).
87. Huang, B., Lu, J. & Bystro, A. S. A genome-wide screen identifies genes required for formation of the wobble nucleoside in Saccharomyces cerevisiae. *RNA* **14**, 2183–2194 (2008).
88. Lloyd, S. J., Lauble, H., Prasad, G. S. & Stout, C. D. The mechanism of aconitase: 1.8 Å resolution crystal structure of the S642A:citrate complex. *Protein Sci.* **8**, 2655–2662 (1999).
89. Vey, J. L. *et al.* Structural basis for glycyl radical formation by pyruvate formate-lyase activating enzyme. *Proc. Natl. Acad. Sci. U. S. A.* **105**, 16137–16141 (2008).
90. Gräwert, T. *et al.* Probing the reaction mechanism of IspH protein by x-ray structure analysis. *Proc. Natl. Acad. Sci. U. S. A.* **107**, 1077–1081 (2010).
91. Ajitkumar, P. & Cherayil, J. D. Thionucleosides in transfer ribonucleic acid: diversity, structure, biosynthesis, and function. *Microbiol. Rev.* **52**, 103–113 (1988).
92. Romsang, A. *et al.* Pseudomonas aeruginosa ttcA encoding tRNA-thiolating protein requires an iron-sulfur cluster to participate in hydrogen peroxide-mediated stress protection and pathogenicity. *Sci. Rep.* **8**, 1–15 (2018).
93. Golinelli-Pimpaneau, B. Prediction of the iron–sulfur binding sites in proteins using the highly accurate three-dimensional models calculated by AlphaFold and RoseTTAFold. *Inorganics* **10**, (2022).
94. Kambampati, R. & Lauhon, C. T. MnmA and IscS are required for in vitro 2-thiouridine biosynthesis in Escherichia coli. *Biochemistry* **42**, 1109–1117 (2003).
95. Numata, T., Ikeuchi, Y., Fukai, S., Suzuki, T. & Nureki, O. Snapshots of tRNA sulphuration via an adenylated intermediate. *Nature* **442**, 419–424 (2006).
96. Ikeuchi, Y., Shigi, N., Kato, J. I., Nishimura, A. & Suzuki, T. Mechanistic insights into sulfur relay by multiple sulfur mediators involved in thiouridine biosynthesis at tRNA wobble positions. *Mol. Cell* **21**, 97–108 (2006).
97. Black, K. A. & dos Santos, P. C. Abbreviated pathway for biosynthesis of 2-thiouridine in Bacillus subtilis. *J. Bacteriol.* **197**, 1952–1962 (2015).
98. Mueller, E. G., Palenchar, P. M. & Buck, C. J. The role of the cysteine residues of ThiI in the generation of 4-thiouridine in tRNA. *J. Biol. Chem.* **276**, 33588–33595 (2001).

99. Xi, J., Ge, Y., Kinsland, C., McLafferty, F. W. & Begley, T. P. Biosynthesis of the thiazole moiety of thiamin in Escherichia coli: Identification of an acyldisulfide-linked protein - Protein conjugate that is functionally analogous to the ubiquitin/E1 complex. *Proc. Natl. Acad. Sci. U. S. A.* **98**, 8513–8518 (2001).
100. Numata, T., Fukai, S., Ikeuchi, Y., Suzuki, T. & Nureki, O. Structural basis for sulfur relay to RNA mediated by heterohexameric TusBCD complex. *Structure* **14**, 357–366 (2006).
101. Zhou, J. *et al.* Structural evidence for a [4Fe-5S] intermediate in the non-redox desulfuration of thiouracil. *Angew. Chemie Int. Ed.* **60**, 424–431 (2020).
102. Waterman, D. G., Ortiz-Lombardía, M., Fogg, M. J., Koonin, E. V. & Antson, A. A. Crystal structure of Bacillus anthracis ThiI, a tRNA-modifying enzyme containing the predicted RNA-binding THUMP domain. *J. Mol. Biol.* **356**, 97–110 (2006).
103. Rajakovich, L. J., Tomlinson, J. & Dos Santos, P. C. Functional analysis of Bacillus subtilis genes involved in the biosynthesis of 4-thiouridine in tRNA. *J. Bacteriol.* **194**, 4933–4940 (2012).
104. Liu, Y. *et al.* Biosynthesis of 4-thiouridine in tRNA in the methanogenic archaeon Methanococcus maripaludis. *J. Biol. Chem.* **287**, 36683–36692 (2012).
105. Neumann, P. *et al.* Crystal structure of a 4-thiouridine synthetase–RNA complex reveals specificity of tRNA U8 modification. *Nucleic Acids Res.* **42**, 6673–6685 (2014).
106. Jurrus, E. *et al.* Improvements to the APBS biomolecular solvation software suite. *Protein Sci.* **27**, 112–128 (2018).
107. Shigi, N., Asai, S. & Watanabe, K. Identification of a rhodanese-like protein involved in thiouridine biosynthesis in Thermus thermophilus tRNA. *FEBS Lett.* **590**, 4628–4637 (2016).
108. Noma, A., Sakaguchi, Y. & Suzuki, T. Mechanistic characterization of the sulfur-relay system for eukaryotic 2-thiouridine biogenesis at tRNA wobble positions. *Nucleic Acids Res.* **37**, 1335–1352 (2009).
109. SantaLucia, J. & Hicks, D. The thermodynamics of DNA structural motifs. *Annu. Rev. Biophys.* **33,** 415–440 (2004).
110. Kinsland, C., Taylor, S. V., Kelleher, N. L., McLafferty, F. W. & Begley, T. P. Overexpression of recombinant proteins with a C-terminal thiocarboxylate: Implications for protein semisynthesis and thiamin biosynthesis. *Protein Sci.* **7**, 1839–1842 (1998).
111. Bradford, M. M. A rapid and sensitive method for the quantitation of microgram

quantities of protein utilizing the principle of protein-dye binding. *Anal. Biochem.* **72**, 248–254 (1976).

112. Ishizaka, M. *et al.* Quick and spontaneous transformation between [3Fe–4S] and [4Fe–4S] iron–sulfur clusters in the tRNA-thiolation enzyme TtuA. *Int. J. Mol. Sci.* **24**, 833 (2023).
113. Miranda, H. V. *et al.* E1- and ubiquitin-like proteins provide a direct link between protein conjugation and sulfur transfer in archaea. *Proc. Natl. Acad. Sci. U. S. A.* **108**, 4417–4422 (2011).
114. Varadi, M. *et al.* AlphaFold Protein Structure Database: Massively expanding the structural coverage of protein-sequence space with high-accuracy models. *Nucleic Acids Res.* **50**, D439–D444 (2022).
115. Jumper, J. *et al.* Highly accurate protein structure prediction with AlphaFold. *Nature* **596**, 583–589 (2021).
116. Kuratani, M. *et al.* Structural basis of the initial binding of tRNAIle lysidine synthetase TilS with ATP and L-lysine. *Structure* **15**, 1642–1653 (2007).
117. Nakanishi, K. *et al.* Structural basis for translational fidelity ensured by transfer RNA lysidine synthetase. *Nature* **461**, 1144–1148 (2009).
118. Broderick, J. B., Duffus, B. R., Duschene, K. S. & Shepard, E. M. Radical S - Adenosylmethionine Enzymes. *Chem. Rev.* **114**, 4229–4317 (2014).
119. Bork, P. & Koonin, E. V. A P-loop-like motif in a widespread ATP pyrophosphatase domain: Implications for the evolution of sequence motifs and enzyme activity. *Proteins Struct. Funct. Bioinforma.* **20**, 347–355 (1994).
120. Fellner, M., Hausinger, R. P. & Hu, J. A structural perspective on the PP-loop ATP pyrophosphatase family. *Crit. Rev. Biochem. Mol. Biol.* **53**, 607–622 (2018).
121. Lipinski, P. *et al.* Induction of iron regulatory protein 1 RNA-binding activity by nitric oxide is associated with a concomitant increase in the labile iron pool: Implications for DNA damage. *Biochem. Biophys. Res. Commun.* **327**, 349–355 (2005).
122. Wehrspan, Z. J., McDonnell, R. T. & Elcock, A. H. Identification of iron-sulfur (Fe-S) cluster and zinc (Zn) binding sites within proteomes predicted by DeepMind's AlphaFold2 program dramatically expands the metalloproteome. *J. Mol. Biol.* **434**, 167377 (2022).
123. Bak, D. W. & Elliott, S. J. Alternative FeS cluster ligands: Tuning redox potentials and chemistry. *Curr. Opin. Chem. Biol.* **19**, 50–58 (2014).
124. Caserta, G. *et al.* Unusual structures and unknown roles of FeS clusters in metalloenzymes seen from a resonance Raman spectroscopic perspective. *Coord.*

Chem. Rev. **452**, 214287 (2022).

125. Chenna, R. *et al.* Multiple sequence alignment with the Clustal series of programs. *Nucleic Acids Res.* **31**, 3497–3500 (2003).
126. Robert, X. & Gouet, P. Deciphering key features in protein structures with the new ENDscript server. *Nucleic Acids Res.* **42**, 320–324 (2014).
127. Liu, Y., Long, F., Wang, L., Söll, D. & Whitman, W. B. The putative tRNA 2-thiouridine synthetase Ncs6 is an essential sulfur carrier in Methanococcus maripaludis. *FEBS Lett.* **588**, 873–877 (2014).
128. Mueller, E. G. & Palenchar, P. M. Using genomic information to investigate the function of ThiI, an enzyme shared between thiamin and 4-thiouridine biosynthesis. *Protein Sci.* **8**, 2424–2427 (1999).
129. Nakanishi, K. *et al.* Structural basis for lysidine formation by ATP pyrophosphatase accompanied by a lysine-specific loop and a tRNA-recognition domain. *Proc. Natl. Acad. Sci. U. S. A.* **102**, 7487–7492 (2005).
130. You, D., Xu, T., Yao, F., Zhou, X. & Deng, Z. Direct evidence that thil is an ATP pyrophosphatase for the adenylation of uridine in 4-thiouridine biosynthesis. *ChemBioChem* **9**, 1879–1882 (2008).
131. Baek, M., McHugh, R., Anishchenko, I., Baker, D. & DiMaio, F. Accurate prediction of nucleic acid and protein-nucleic acid complexes using RoseTTAFoldNA. *bioRxiv* 2022.09.09.507333 (2022) doi:10.1101/2022.09.09.507333.
132. Mobley, D. L. *et al.* Predicting absolute ligand binding free energies to a simple model site. *J. Mol. Biol.* **371**, 1118–1134 (2007).
133. Deng, Y. & Roux, B. Calculation of standard binding free energies: Aromatic molecules in the T4 lysozyme L99A mutant. *J. Chem. Theory Comput.* **2**, 1255–1273 (2006).
134. He, N. *et al.* A subclass of archaeal U8-tRNA sulfurases requires a [4Fe–4S] cluster for catalysis. *Nucleic Acids Res.* **50**, 12969–12978 (2022).

Acknowledgements

I would like to appreciate my supervisor, Emeritus Professor Min Yao, who trained in my bachelor's, master's, and doctoral programs even after her retirement. She respected my initiative and provided me with various opportunities, allowing me to enjoy science and acquire expertise in structural biology. She also taught me presentation skills for various domestic and international conferences and scientific writing skills. I will work harder in Germany from April 2023 and come back to Japan to repay your kindness.

I would also like to express my gratitude to my supervisor, Professor Toyoyuki Ose. His useful advice on experimental techniques and discussions at lab meetings have greatly advanced my research. He taught me not only the theory of crystallography, but also the importance of applying the best approaches depending on research questions.

I wish to thank Professor Yoshikazu Tanaka (at Tohoku University) for a lot of support including reviewing our papers. He also gave me an opportunity to enter the Ambitions Leader's Program (ALP), which widen my comprehensive perspective, including QM/MM simulations and MD simulations. I am grateful to my collaborator, Associate Professor Masaki Horitani (at Saga University) for EPR experiments. When I had trouble with the results, he always responded sincerely to my questions.

For the establishment of the foundation of the TtuA project, I would like to express my respect and gratitude to my predecessors, Dr. Minghao Chen and Mr. Shun Narai. I have also learned countless things from them in terms of experimental techniques, analysis methods, and even their research attitude. I would also like to thank Associate Professor Koji Kato (at Okayama University) and Specially Appointed Associate Professor Jian Yu (at Osaka University) for teaching me how to use various software for X-ray crystallography. I also thank the beamline staff at the Photon Factory and SPring-8 for their support. This work was supported by the Japan Society for the Promotion of Science (JSPS), ALP, and the Nitobe School at Hokkaido University.

Thanks to the support of all members of my laboratory and friends, I was able to continue my research and successfully complete my doctoral program. Finally, I would like to thank my family, especially my parents, with all my heart for their continuous dedication and support throughout the past 27 years.